UNIVERSIDADE FEDERAL DE SANTA CATARINA
CENTRO TECNOLÓGICO
PROGRAMA DE PÓS-GRADUAÇÃO EM ENGENHARIA DE ALIMENTOS

Ana Augusta Salvador

Mathematical modeling and computational simulation of multiphase transport and structural deformation in porous food during microwave vacuum drying

Florianópolis
2023

Ana Augusta Salvador

Mathematical modeling and computational simulation of multiphase transport and structural deformation in porous food during microwave vacuum drying

Tese de doutorado submetida ao Programa de Pós-graduação em Engenharia de Alimentos na Universidade Federal de Santa Catarina como requisito para obtenção do título de Doutor.

Orientador: Prof. Dr. Bruno A. M. Carciofi
Coorientadores: Prof. Dr. Ashim K. Datta e Prof. Dr. Jhony T. Teleken

Florianópolis
2023

Ficha de identificação da obra elaborada pelo autor,
através do Programa de Geração Automática da Biblioteca Universitária da UFSC.

Salvador, Ana Augusta
Mathematical modeling and computational simulation of multiphase transport and structural deformation in porous food during microwave vacuum drying / Ana Augusta Salvador ; orientador, Bruno Augusto Mattar Carciofi, coorientador, Ashim Kumar Datta, coorientador, Jhony Tiago Teleken, 2023.
115 p.

Tese (doutorado) - Universidade Federal de Santa Catarina, Centro Tecnológico, Programa de Pós-Graduação em Engenharia de Alimentos, Florianópolis, 2023.

Inclui referências.

1. Engenharia de Alimentos. 2. alimentos. 3. simulação. 4. micro-ondas. 5. deformação. I. Carciofi, Bruno Augusto Mattar. II. Datta, Ashim Kumar. III. Teleken, Jhony Tiago IV. Universidade Federal de Santa Catarina. Programa de Pós Graduação em Engenharia de Alimentos. V. Título.

Ana Augusta Salvador

Mathematical modeling and computational simulation of multiphase transport and structural deformation in porous food during microwave vacuum drying

O presente trabalho em nível de Doutorado foi avaliado e aprovado, em 14 de julho de 2023, pela banca examinadora composta pelos seguintes membros:

Prof. Dr. Neyval Costa Reis Junior
Departamento de Engenharia Ambiental
Universidade Federal do Espírito Santo

Prof. Dr. Sérgio Luciano Avila
Departamento de Engenharia Elétrica
Instituto Federal de Santa Catarina

Prof. Dr. Sergio Yesid Gómez González
Departamento de Engenharia Química e Engenharia de Alimentos
Universidade Federal de Santa Catarina

Prof. Dr. João Borges Laurindo
Departamento de Engenharia Química e Engenharia de Alimentos
Universidade Federal de Santa Catarina

Prof. Dr. Jhony Tiago Teleken
Presidente
Faculdade de Minas e Meio Ambiente
Universidade Federal do Sul e Sudeste do Pará

Certificamos que esta é a versão original e final do trabalho de conclusão que foi julgado adequado para obtenção do título de Doutor em Engenharia de Alimentos.

ICP-Edu
Documento assinado digitalmente
Jaciane Lutz Ienczak
Data: 05/09/2023 13:25:52-0300
CPF: ***.280.630-**
Verifique as assinaturas em https://v.ufsc.br

_____
Prof.(a) Dr.(a) Jaciane Lutz Ienczak
Coordenadora do Programa de Pós-Graduação

ICP-Edu
Documento assinado digitalmente
Bruno Augusto Mattar Carciofi
Data: 05/09/2023 13:47:23-0300
CPF: ***.515.208-**
Verifique as assinaturas em https://v.ufsc.br

_____
Prof. Dr. Bruno Augusto Mattar Carciofi
Orientador

Florianópolis, 2023.

This work is dedicated to my parents, Ilson and Dirlene.

ACKNOWLEDGMENT

I would like to express my gratitude to the following individuals and institutions who have played a crucial role in the successful completion of my doctoral:

First, I am grateful to the Graduate Program in Food Engineering at the Federal University of Santa Catarina for providing me with the opportunity to pursue my doctorate. I am also thankful to CAPES-Proex and CAPES-Print for the generous scholarships that have supported my research.

I extend my sincere appreciation to the Departments of Food Engineering, Chemical Engineering, Mechanical Engineering, and Electrical Engineering and their Professors for offering the diverse range of disciplines that have greatly contributed to the development of my thesis proposal.

I am deeply thankful to Cornell University, specifically the College of Agriculture and Life Science, for welcoming me during my association.

I would like to express my gratitude to the Laboratory of Physical Properties of Food (PROFI) and its team for their collaboration, sharing valuable materials and methods that were essential for the successful execution of my experiments.

I am honored and grateful to Professors Neyval Junior, Sergio Avila, Sergio González, João Laurindo, and Jhony Teleken for accepting the responsibility of being part of my thesis evaluation panel and for their contributions.

Special thanks to my advisor, Prof. Bruno Carciofi, for this opportunity, belief in my abilities, and the tremendous support he has provided throughout my doctoral. I am truly grateful for his patience and assistance manly during the difficult times.

I would like to express my appreciation to Prof. Ashim Datta for graciously welcoming me and for his support and encouragement, particularly during the challenging times of the pandemic.

I extend my heartfelt gratitude to Prof. Jhony Teleken for his wealth of knowledge, dedication to teaching, care, encouragement, and for being a friend whenever needed. Thank you for being there at the worst moments.

I am grateful to Prof. Sergio Avila and Prof. João Laurindo for their contributions that helped me during the progress of my thesis in various ways.

I would like to acknowledge all my colleagues at PROFI and Professor Datta's Laboratory, for their assistance during laboratory experiments and simulation tests. I am also thankful to Mayuri for our productive discussions on the model and simulations, always a pleasure.

I am deeply indebted to my family members, especially my parents, for their emotional and financial support throughout these past few years. I am grateful to Amadeo and Colleen for their belief in me and for welcoming me into their lives. I would also like to express my appreciation to Paulo and Angela for their constant presence and support, and to Luci and Ivo for their patience and encouragement. Thank you, Nona Augusta, for all the prayers. Lastly, I am grateful to Tata and Keko for their unconditional affection.

Finally, my gratitude to God for the gift of life.

Thank you all for your contributions and support.

RESUMO

Existem diversos métodos para preparar alimentos utilizando calor, como fritura, cocção, secagem solar, fornos com diferentes fontes de energia (gás, lenha, elétrico), secagem com convecção forçada e micro-ondas. A escolha do método mais adequado depende dos produtos desejados, além de considerações de viabilidade. Neste trabalho, nos concentramos em um método discutido na literatura há mais de 50 anos e que tem sido aplicado nos setores industriais de alimentos e farmacêuticos há mais de 20 anos: o processo de secagem por micro-ondas a vácuo (MWVD). O método oferece vantagens se comparado a métodos convencionais. Devido à aplicação do vácuo, a temperatura de secagem é reduzida, e, o tempo de aquecimento é menor em razão das características das ondas eletromagnéticas. As temperaturas mais baixas e o tempo de exposição ao calor reduzido ajudam a preservar o sabor, as cores e até mesmo certas vitaminas nos alimentos. Após selecionar o método a ser estudado, definiu-se que o mesmo seria investigado por meio de simulações computacionais. Portanto, o objetivo deste trabalho foi prever a evolução do estado de uma matriz alimentícia porosa durante MWVD, por meio de simulação numérica, validada experimentalmente, e embasada em um modelo matemático composto por distribuição de ondas eletromagnéticas em uma cavidade e as transferência de calor e massa com mudança de fase acoplada a mecânica dos sólidos. Apesar das várias tentativas de investigar a deformação de diferentes produtos alimentícios sob diversos processos e condições de secagem, ainda faltam estudos que analisem os efeitos combinados do Eletromagnetismo, Transporte Multifísico com mudança de fase e Mecânica dos Sólidos em um meio poroso durante MWVD. Com o intuito de preencher essa lacuna, foram realizados experimentos em bancada de laboratório e simulações computacionais. Os experimentos foram realizados em triplicata, utilizando a batata como matriz porosa e um micro-ondas doméstico adaptado com uma câmara de vácuo. A partir destes experimentos, foram coletados dados de potência absorvida na cavidade, temperatura e deformação inicial e final do alimento, e variação da umidade do alimento ao longo do tempo. As simulações foram realizadas utilizando o software comercial COMSOL Multiphysics. Os dados obtidos foram comparados com os resultados dos experimentos. O modelo e a simulação numérica demonstraram que os gradientes de pressão são responsáveis pelas deformações de expansão na estrutura do alimento. Enquanto os gradientes de concentração formados durante a perda de água, tiveram o maior efeito na deformação, causando o encolhimento inelástico da amostra. O estudo ressalta a influência das condições de contorno, propriedades físicas e mecânicas, bem como seus efeitos subsequentes na dinâmica da secagem, proporcionando uma melhor compreensão dos mecanismos envolvidos no processo. Essas descobertas fornecem informações valiosas sobre o comportamento do teor de umidade, temperatura, pressão e deformação durante o processo MWVD e podem ser úteis na otimização do processo, no desenvolvimento e melhoramento de produtos e no design de novos equipamentos.

Palavras-chave: micro-ondas, simulação, deformação, alimentos.

RESUMO EXPANDIDO

Introdução

A secagem é um dos métodos de conservação mais amplamente utilizados na indústria alimentícia. Geralmente, é usada para transformar uma colheita em uma mercadoria de prateleira, reduzir a embalagem, diminuir os custos de armazenamento e transporte, pois reduz o peso e elimina a necessidade de armazenamento refrigerado, além de oferecer a possibilidade de adicionar valor aos alimentos processados. Entre os métodos de secagem, o aquecimento por micro-ondas a vácuo (MWVD) é especialmente usado para desidratar alimentos sensíveis a altas temperaturas e à presença de oxigênio. Devido ao uso do vácuo, as temperaturas de secagem são reduzidas e não há oxigênio, tornando possível preservar as propriedades nutricionais do alimento. Nas etapas finais da secagem por micro-ondas à vácuo, a temperatura pode atingir 80°C, mas os danos térmicos neste período ainda são relativamente baixos, porque a sensibilidade ao calor diminui com a redução do teor de água. Além disso, as mudanças de pressão durante a secagem geram um produto com textura e formas únicas, devido às deformações e mudanças na porosidade da fruta. Em geral, a distribuição de temperatura e as diferenças de pressão nos alimentos durante a secagem provocam mudanças na textura, porosidade e deformação do alimento, e todas essas modificações também influenciam diretamente na concentração de nutrientes do produto. A melhor maneira de compreender todos os fenômenos envolvidos em um método de secagem após experimentação é a simulação do processo. A simulação numérica de processos de produção de alimentos vem auxiliando na elucidação da interação entre fenômenos complexos envolvidos, propicia economia de tempo, pois diminui o número de experimentos de bancada, viabiliza o estudo de propriedades intrínsecas mais detalhadamente, como a tortuosidade e a permeabilidade. Isso pode ser feito com a criação de modelos que representam a realidade dos fenômenos, ou seja, modelos validados experimentalmente e capazes de prever as consequências de possíveis mudanças no processo.

Objetivos

Este trabalho tem como objetivo prever a evolução da umidade, pressão, temperatura e deformação sólida em um alimento poroso durante o processo de secagem por micro-ondas a vácuo por meio de simulação numérica, com base em um modelo matemático mecanicista que descreve a propagação de ondas eletromagnéticas, fenômenos de transferência de calor e massa, e deformação sólida. Os objetivos específicos deste estudo incluem o desenvolvimento de um modelo matemático abrangente que descreve o processo de secagem por micro-ondas a vácuo, considerando os aspectos fundamentais da propagação e aquecimento de ondas eletromagnéticas, transferência de calor e massa, fluxo de líquido e vapor, bem como deformações mecânicas sólidas em um meio poroso, com base em princípios mecanicistas. Além disso, pretende-se implementar esse modelo no software COMSOL Multiphysics para obter uma solução numérica que represente as tendências do processo de secagem, abrangendo o aquecimento eletromagnético, perfis de pressão de gás e água, concentração de gás e água, evaporação e condensação, bem como mudanças nas proporções de área e volume e tensões. Outro objetivo é realizar um estudo paramétrico variando as propriedades intrínsecas, como a permeabilidade, a constante de evaporação e o coeficiente de encolhimento volumétrico, a fim de avaliar seu impacto no processo de secagem e nos perfis de umidade, pressão, temperatura, evaporação e deslocamento no espaço e no tempo. Por fim, realizar uma comparação entre a solução numérica obtida e resultados experimentais de secagem, analisando a evolução

temporal do teor de umidade e as mudanças na temperatura superficial e área superficial de uma batata antes e após o processo de secagem.

Metodologia

A metodologia foi dividida em Experimentos de Laboratório, Modelagem Matemática e Implementação Computacional. Os experimentos de laboratório abrangeram várias etapas: preparação da amostra em formato cilíndrico de 2,5 cm de altura e 3,5 cm de diâmetro e armazenada a temperatura de 20 ˚C; o MWVD como a técnica central de secagem, com experimentos de 16 min aplicando potencia de 50%; as análises gravimétricas de umidade, envolvendo a determinação da curva cinética inicial seguida de medições de umidade antes e depois da deformação; ensaios de temperatura com câmera termográfica, capturando as mudanças na temperatura da superfície superior antes e depois da deformação e ensaios de deformação, nos quais o foco era avaliar a área antes e depois da deformação com o auxílio de uma câmara fotográfica. Os experimentos foram realizados em triplicata em um micro-ondas doméstico adaptado com uma câmara de vácuo, utilizando uma batata como matriz porosa. A modelagem matemática foi desenvolvida com base em elementos-chave: suposições, que definiram o escopo do modelo e considerações fundamentais; os parâmetros tanto para a amostra quanto para a estrutura do forno; as equações governantes descrevendo cada fase da amostra e a distribuição da onda; e as condições iniciais e de contorno. Por fim, a implementação computacional ocorreu em duas etapas, a primeira focada na distribuição da onda e a segunda envolvendo transferência de calor e massa acoplada com deformação. As simulações foram realizadas no software comercial COMSOL Multiphysics em um computador de 128 GB de memória RAM divididas em 16 processadores. Cada simulação apresentou um estudo inicial de independência de malha e teve os dados comparados aos experimentos.

Resultados e Discussão

Foi desenvolvido um modelo matemático abrangente que descreve o processo de secagem por micro-ondas a vácuo, incluindo a propagação e o aquecimento das ondas eletromagnéticas, fenômenos de transferência de calor e massa, fluxo de líquido e vapor, e deformação mecânica sólida em um meio poroso com base em princípios mecanicistas. As equações definidas neste modelo matemático foram implementadas com sucesso no software comercial COMSOL Multiphysics, obtendo uma solução numérica que descreve as tendências para a secagem por micro-ondas a vácuo de meios porosos. Essa solução numérica foi comparada com resultados experimentais de secagem, avaliando a evolução temporal do teor de umidade e os resultados antes e depois da secagem, incluindo a temperatura superficial e a área superficial de uma batata. Notou-se que a diminuição na área superior correspondeu às descobertas experimentais, enquanto a redução lateral refletiu a contração sem a presença de bolhas. No estudo, foram identificados pontos cruciais no processo de secagem por micro-ondas a vácuo. A potência de micro-ondas absorvida pela amostra diminui gradualmente durante a secagem. O aumento do coeficiente de encolhimento volumétrico resulta em deformações mais acentuadas na amostra, gerando gradientes mais pronunciados de pressão e concentração de água. As amostras exibem deslocamentos mais significativos nas bordas em comparação com o centro do meio poroso, atribuídos à deformação. A principal alteração na relação de volume da amostra é causada pela perda de água e pode levar ao fenômeno de puffing, dependendo dos gradientes de pressão. Durante o processo de secagem, a porosidade de gás e as propriedades mecânicas da amostra aumentam à medida que ela perde água, ao contrário das propriedades dielétricas. A escolha da condição de contorno na parte inferior do sistema tem um impacto significativo na deformação da amostra, podendo aumentar a pressão interna (quando a parte inferior está fechada) ou

controlar o deslocamento (com a parte inferior aberta ou fechada). O modelo matemático desenvolvido é eficaz na representação do encolhimento da amostra e pode ser ajustado levando em consideração os efeitos do aquecimento. Ademais, realizou-se um estudo paramétrico das propriedades com diferentes valores para o coeficiente de encolhimento volumétrico e permeabilidade intrínseca na solução numérica, avaliando seus impactos no processo de secagem por micro-ondas a vácuo e no perfil de umidade, pressão, temperatura, evaporação e deslocamento ao longo do espaço e do tempo. Com o aumento do coeficiente de encolhimento, verificou-se que tanto o deslocamento quanto a pressão interna da amostra aumentaram, sem observação de variação na temperatura superficial. Em resumo, esses achados proporcionam valiosos insights sobre o comportamento do teor de umidade, temperatura e pressão durante o processo de MWVD, destacando a influência das condições de contorno, propriedades físicas e mecânicas, e fornecendo uma compreensão mais profunda desses mecanismos complexos.

Considerações Finais

O modelo acoplado proposto para o transporte multifásico, deformação e transição de fase durante a secagem por micro-ondas a vácuo foi resolvido com sucesso por meio de uma abordagem numérica usando métodos de elementos finitos. As descobertas fornecem informações valiosas sobre o comportamento do teor de umidade, temperatura e pressão durante o processo de MWVD. O estudo destaca a influência das condições de contorno, propriedades físicas e mecânicas e seus subsequentes efeitos na dinâmica de secagem, oferecendo uma melhor compreensão desses mecanismos complexos.

Palavras-chave: Micro-ondas, simulação, deformação, alimentos.

ABSTRACT

There are several methods for food preparation involving heat, including frying, cooking, solar drying, ovens with different energy sources (gas, wood, electric), forced convection drying, and microwave drying. The choice of the most suitable method depends on the desired food products and feasibility considerations. In this study, we focus on a method that has been discussed in the literature for over 50 years and has been applied in the food and pharmaceutical industries for more than 20 years: the microwave vacuum drying (MWVD) process. This method offers advantages compared to conventional methods. By applying a vacuum, the drying temperature is reduced, and the heating time is shortened due to the properties of electromagnetic waves. Lower temperatures and reduced heat exposure time help preserve the flavor, color, and even certain vitamins in the food. After selecting the method for investigation, it was decided to study it through computer simulations. Therefore, the objective of this work was to predict the evolution of a porous food matrix during MWVD through numerical simulation, based on a mathematical model that combines electromagnetic wave distribution in a cavity, heat and mass transfer with phase change, and solid mechanics. Despite several attempts to investigate the deformation of different food products under various drying processes and conditions, there is still a lack of studies that analyze the combined effects of Electromagnetism, Multiphysics Transport with phase change, and Solid Mechanics in a porous medium during MWVD. To address this gap, experiments were conducted on a laboratory bench and computer simulations were performed. The experiments, which involved using potatoes as the porous matrix and a domestic microwave adapted with a vacuum chamber, were carried out in triplicate. From these experiments, data were collected on the absorbed power in the cavity, temperature, initial and final deformation of the food, and variation of food moisture over time. The simulations were conducted using the commercial software COMSOL Multiphysics, and the obtained data were compared with the experimental results. The model and numerical simulation demonstrated that pressure gradients are responsible for expansion deformations in the food structure, while water loss, which had the greatest impact on deformation, caused shrinkage of the sample. The study highlights the influence of boundary conditions, physical and mechanical properties, as well as their subsequent effects on drying dynamics, providing a better understanding of the mechanisms involved in the process. These findings offer valuable insights into the behavior of moisture content, temperature, pressure, and strain during the MWVD process, which can be useful for process optimization, product development, and the design of new equipment.

Keywords: microwave, simulation, deformation, food.

LIST OF FIGURES

LIST OF TABLES

LIST OF SYMBOLS AND ABBREVIATIONS

	Electromagnetics
$\overrightarrow{B_s}$	Magnetic Flux Density vector [T]
$\vec{D}$	Electric Flux Density vector [C/m²]
$\vec{E}$	Electric field vector [V/m]
$\overrightarrow{E_s}$	Electric field vector (phasor form) [V/m]
E_0	Electric field amplitude at z=0 [V/m]
E^*	Conjugate Electric Field Vector [V/m]
f	Microwave frequency [Hz]
$\vec{H}$	Magnetic field vector [A/m]
$\vec{H_s}$	Magnetic field vector (phasor form) [A/m]
H_0	Magnetic field amplitude at z=0 [A/m]
$\vec{J}$	Conduction Current density vector (A/m²)
P^w	Microwave Real Power [W]
	Greek Symbols
α	Attenuation factor [Np/m]
β	Phase constant [rad/m]
γ	Propagation constant [Np/m]
δ	Penetration depth [mm]
ε	Electric Permittivity [F/m]
ε_0	Vacuum permittivity [F/m]
ε_r	Relative permittivity [F/m]
ε'	Dielectric Constant
ε''	Dielectric Loss
σ	Conductivity [S/m]
ρ_m	Volumetric Charge density [C/m³]
μ	Magnetic permeability [H/m]
μ_0	Vacuum permeability [H/m]
μ_r	Relative permeability [H/m]
λ	Wavelength [m]
ω	Angular frequency [rad/s]
	Transport
c_i	Mass volumetric concentration [mol/m³]
$C_{p,i}$	Specific Heat [J/kg K]
D_{self}	Self-Diffusivity [m²/s]
$D_{cap,i}$	Capillary diffusivity [m²/s]
D_{bin}	Binary Diffusivity [m²/s]
$\dot{I}$	Phase change [kg/m³s]
k_i	Thermal conductivity [W/m K]
k_{in}	Intrinsic Permeability [s-¹]
$k_{rel,i}$	Relative Permeability
K_{evap}	Evaporation rate constant [1/s]
M_a	Molecular weight of air [kg/mol]
M_v	Molecular weight of vapor [kg/mol]

M_w	Molecular weight of water [kg/mol]
m	Mass of raw sample [kg]
$\vec{n}_i$	Mass flux [kg/m²s]
p_c	Capillary Pressure of water [Pa]
p_{sat}	Saturation pressure [Pa]
$p_{v,eq}$	Equilibrium vapor pressure [Pa]
P, p	Total pressure and partial pressure, respectively [Pa]
Pr	Prandtl dimensionless number
$\dot{Q}$	Microwave-absorbed energy [W/m³]
R	Gas constant [J/mol K]
S_i	Saturation of a fluid phase
Sc	Schmidt dimensionless number
T	Temperature [K]
$\vec{v}_i$	Darcy's velocity [m/s]
V_i	Volume fraction of pores [m³]
$X_{d.b.}$	Dry basis moisture [kg/kg]
w_i	Phase mass fraction
	Greek Symbols
∅	Porosity
λ_{ev}	Latent Heat [J/kg]
τ	Tortuosity
ρ_i	Specific mass [kg/m³]
μ_i	Viscosity [Pa.s]
	Structural Deformation
E	Elastic modulus [N/m^2]
E_{el}	Green Lagrange strain tensor
F	Deformation gradient tensor
G	Shear modulus [N/m^2]
I	Identity tensor
J	Jacobian
K	Bulk modulus [N/m^2]
P_p	Pore pressure
S"	Piola-Kirchoff stress tensor, Pa
u	Displacement vector [m]
V	Volume [m^3]
$\overline{v_s}$	Solid velocity [m/s]
W	Strain energy
	Greek Symbols
ν	Poisson's ratio
$\bar{\sigma}$	Total stress tensor, [Pa]
σ	Stress, [Pa]
β_{vol}	Volumetric shrinkage coefficient [m^3/kg]
ϵ	Strain tensor
λ	Lame's parameter
φ	Volume fraction
	Subscripts
l, v, g, s, a	Liquid, vapor, gas, solid, air

t	Time [s]
(x,y,z)	Cartesians coordinates
G	Ground (stationary observer)
el	elastic
i	i-ish phase
0	Initial value, at time t=0
f	Final value

Mathematical Operators

$\overrightarrow{\nabla}$	Vector differential operator
∂	Partial derivative
j	Imaginary number

TABLE OF CONTENTS

1. INTRODUCTION

In recent decades mild food processing conditions have gained significant importance. These technologies aim to meet the growing consumer demand for food processing methods that have a reduced impact on nutritional content and overall food quality. The objective is to retain the nutritional qualities and sensory characteristics of the food product (GONZÁLEZ-CAVIERES et al., 2021). Among these technologies, microwave vacuum drying (MWVD) stands out as a suitable option, as it preserves a larger quantity of natural bioactive compounds and produces desirable sensory attributes (GUO et al., 2017; ANDO et al., 2019a, 2019b; MONTEIRO et al., 2018b). Furthermore, in addition to its scientifically proven benefits, microwave vacuum drying is already being utilized in the food industry for drying various products such as pasta, powders, and porous solids (EKEZIE et al., 2017; SUNJKA et al., 2004; TOPCAM; ERDOGDU, 2021).

The literature on microwave drying of food comprises a substantial body of research that delves into various aspects, including investigations into cavity analysis (BARRETO et al., 2019; CLARY et al., 2007; CLARY; WANG; PETRUCCI, 2005; GAO et al., 2019; HU et al., 2006a; JENI; YAPA; RATTANADECHO, 2010; KAENSUP; CHUTIMA; WONGWISES, 2002; MONTEIRO et al., 2015; SALVADOR et al., 2022; WRAY; RAMASWAMY, 2015; ZHOU; WANG; YANG, 2022), heat and mass transfer (ANTIPOV; ARAPOV; KAZARTSEV, 2020; GEEDIPALLI; RAKESH; DATTA, 2007; GULATI; DATTA; RANJBARAN, 2020; GULATI; ZHU; DATTA, 2016; MONTEIRO et al., 2022; RAKESH; DATTA, 2011; SONG et al., 2018; ZHANG; DATTA, 2003; ZHU et al., 2015), Multiphysics simulations on porous media (DHALL; DATTA, 2011; HALDER; DHALL; DATTA, 2007a; WARNING; ARQUIZA; DATTA, 2015), the Maxwell's equations or Lambert equation to describe the electromagnetic heating and wave propagation (AYAPPA et al., 1991; TELEKEN et al., 2020; ZHANG; DATTA, 2003), sample size and shape (cylinder, sphere and square) (BASAK; BHATTACHARYA; PANDA, 2016; BHATTACHARYA; BASAK, 2017; GULATI et al., 2016; HOSSAN; BYUN; DUTTA, 2010; TANG; LIANG, 1998; ZHU et al., 2015), properties (conductivity, dielectric constant, moisture) (ANDO et al., 2019b; BONDARUK; MARKOWSKI; BŁASZCZAK, 2007; GULATI; DATTA, 2013; HOLTZ et al., 2010; KROKIDA; MAROULIS, 1997; LIU; TANG; MAO, 2009; NELSON, 1991; RENSHAW et al., 2019), material type (one or two layers, homogeneous, isotropic, synthetic

or natural) (KLAYBORWORN et al., 2013; NI; DATTA; TORRANCE, 1999; YANG; SAKAI, 2001; ZHANG; DATTA, 2003), quality parameters (DEVAHASTIN; NIAMNUY, 2010; GULATI; DATTA, 2015; HUANG et al., 2012; ZHOU et al., 2021) mainly in microwave vacuum drying (CHONG et al., 2014; CUI et al., 2008; JIANG et al., 2017; MONTEIRO et al., 2018b; NOWACKA et al., 2019) and sample deformation microstructure and shrinkage or puffing effect (GULATI; ZHU; DATTA, 2016; RAKESH; DATTA, 2011; SAKAI; YANG; WATANABE, 2002; TSURUTA; TANIGAWA; SASHI, 2015). These studies present improvement alternatives for microwave technology, aiming to achieve products with better sensory and nutritional quality, as well as higher process efficiency. The abundance of experimental studies on microwave applications provides a solid foundation for exploring this method in various ways, including simulations and the development of new mathematical models.

Choosing an appropriate technology for drying food materials is as crucial as selecting the right parameters during food processing. Factors such as the irradiated power, cavity shape and internal pressure, sample quantity, and necessary pre-treatments play a significant role. To comprehend this process and its parameters, a variety of experimental practices can be employed, along with tools such as mathematical models and process simulation. These approaches involve creating models that accurately represent the real phenomena, meaning models that have been experimentally validated and can predict the outcomes of potential process changes. A thorough understanding of the underlying physics involved in food processing, specifically microwave vacuum drying, can greatly aid in predicting the state (temperature, composition, and shape) and the history (change of variables during time) of a food product, as well as ensuring its safety and quality (DHALL; DATTA, 2011). A research group, focused on microwave vacuum drying, at the Laboratory of Physical Properties of Food (PROFI) at Federal University of Santa Catarina (UFSC), had observed that foods dehydrated by this technology present different sensorial and physical characteristics, such as greater crunchiness (BARRETO et al., 2019; MONTEIRO et al., 2018b, 2020a; TELEKEN et al., 2020).

When discussing the multiphase transport in porous media in a microwave oven, the phenomena involved during drying are the transfer of momentum, heat, and mass and additional terms covering energy source types. Momentum conservation is mostly developed from Darcy's equation. The mechanisms in mass conservation equations represent the convection,

diffusion, and evaporation/condensation of water, considering phases of water, vapor, and air. The energy equations include the conduction, advection, and microwave heat source term (GULATI; DATTA; RANJBARAN, 2020; GULATI; ZHU; DATTA, 2016; KUMAR et al., 2018; ZHU et al., 2015). Additionally, to describe the deformation models, two different approaches are generally used: either the experimental shrinkage/puffing data is empirically fitted as a function of moisture content, or the sum of volumes of water and gas is used to predict deformation, considering a solid mechanics problem (DHALL; DATTA, 2011; JOARDDER et al., 2015; KATEKAWA; SILVA, 2006). The majority fraction of the food is the one that causes the greatest effect on the mechanical properties. For example, the mechanical properties of fatty foods are almost exclusively defined by the physical state and crystallinity of the lipid fraction (ROOS, 1995). In the same way, for a dried potato, the moisture content delimits the mechanical properties values during drying because as the food loses water, the properties change. The mechanical properties are considered one of the most important four parameters, which reflect the quality of the dried food material. In food processing, hardness can affect energy input, efficiency, and matter loss in dry and wet millings. Besides, it was found that taste can be related to mechanical properties such as viscoelastic parameters (HASSAN; ALHAMDAN; ELANSARI, 2005; QIAO et al., 2022). Understanding all these phenomena, modeling and simulation enable the definition of parameters to achieve the desired product and give new perspectives to process optimization.

In the last two and a half decades modelling of microwave drying of food has been studied by different perspectives. From years 1997 to 2007, heat and mass transfer were described by mechanistic models considering heat generation and water evaporation (GEEDIPALLI; RAKESH; DATTA, 2007; GIRI; PRASAD, 2007; NI; DATTA; TORRANCE, 1999; ORSAT et al., 2007; TULASIDAS; RATTI; RAGHA VAN, 1997). Throughout this period the last studies described the drying kinetics using fitting parameters and existing regression models (GIRI; PRASAD, 2007; SUTAR; PRASAD, 2007). Some authors were already developing models with finite elements discretization coupling the thermal and solid mechanics effects(RESSING; RESSING; DURANCE, 2007). During the following decade, 2007 to 2017, more models considering the food as a porous media appeared (RAKESH et al., 2012; RAKESH; DATTA, 2011, 2013). And now the models were coupling the electromagnetics, considering oven design, with heat generation, mass transfer and large deformation(GULATI; ZHU; DATTA, 2016; PITCHAI et al., 2012; ZHU et al., 2015). The

studies evaluated different viewpoints: experimental fitted model or mechanistic mathematical models cell scale or pore scale, shrinkage as consequence of water loss or puffing as effect of rapid evaporation (HALDER; DATTA, 2012; NAHIMANA; ZHANG, 2011; PITCHAI et al., 2012; TSURUTA; TANIGAWA; SASHI, 2015). And the last five years the main goal was to model alternatives to heating uniformity in microwave drying, with rotation devices, intermittent heating and machine learning (DASH; CHAKRABORTY; SINGH, [s.d.]; KUMAR et al., 2018; MIRAN; PALAZOĞLU, 2019). Also evaluating the influence and change on dielectric properties and moisture distribution in different food systems (ARBALLO; GOÑI; MASCHERONI, 2020; DUMPLER; MORARU, 2022; LIN; SUN, 2021; ZHOU et al., 2023). There were no study accounting the heat and mass transfer coupled with solid mechanics and electromagnetic wave distribution during microwave vacuum drying considering simultaneously effects of shrinkage and puffing in a food as a porous media.

The current work attempts to fill a gap in the literature by characterizing the structural deformation based on a multiphase transport with phase change on porous media during microwave vacuum drying. This thesis hypothesizes that the numerical simulation of a mechanistic mathematical model covering electromagnetic wave propagation, heat and mass transfer with evaporation, and solid deformation will predict the state evolution of porous food during microwave vacuum drying.

1.1 OBJECTIVES

1.1.1 Main Objective

This work aims to predict the moisture, pressure, temperature, and solid deformation evolution in a porous food during microwave vacuum drying process through numerical simulation, based on a mechanistic mathematical model for the electromagnetic wave propagation, heat and mass transfer phenomena, and solid deformation.

1.1.2 Specific Objectives

The specific aims of this study are:

a) Develop a mathematical model that describes the microwave vacuum drying process, including electromagnetic wave propagation and heating, heat and mass transfer phenomena,

liquid and vapor flow, and solid mechanical deformation in a porous media based on mechanistic principles.

b) Implement the discretized set of equations from the mathematical model into the commercial software COMSOL Multiphysics to obtain a numerical solution that describes the trends for microwave vacuum drying of porous media, regarding electromagnetic heating, gas and water pressure profiles, gas and water concentration, evaporation and condensation, changes in area, volume ratios and stresses.

c) Perform a parametric property study applying different values for intrinsic permeability, evaporation constant and volumetric shrinkage coefficient in the numerical solution to evaluate their effects on the microwave vacuum drying process and the profile of moisture, pressure, temperature, evaporation and displacement over space and time.

d) Compare the numerical solution with experimental drying results based on the temporal evolution of the moisture content and the before and after drying results of surface temperature and superficial area of a potato.

2. FUNDAMENTALS

This section reviews the scientific literature covering the theoretical foundation and observations related to this study. It begins with a review of previous studies on microwave vacuum drying (MWVD) application in food engineering analyzing oven cavities design and the technology importance in food. Next, it introduces key findings in the microwave vacuum drying of foods. Finally, it concludes with a review of mathematical modeling approaches that describe porous media characteristics, heat and mass transfer phenomena, and deformation in food systems.

2.1 MWVD LANDSCAPE APPLICATIONS FOCUSING FOOD ENGINEERING

2.1.1 Technology Applied in Food

MWVD is an advanced drying technique that utilizes microwave energy to rapidly heat food materials, leading to accelerated water evaporation. The high-speed heating is achieved through the interaction of the microwave energy with the food material (ANDO et al., 2019a; HU et al., 2006b; LI; WANG; KUDRA, 2011). The application of an oscillating electromagnetic field to food materials, agitates the water dipoles molecules, causing them to align in the direction of the applied electric field and follow electromagnetic field oscillations (ZIELINSKA; MARKOWSKI; ZIELINSKA, 2019). Because of that characteristic, the heat is not transferred but generated in the food tissue.

The combination of vacuum and microwave heating reduce the drying time in food system if compared to other technologies such as convective drying (CLARY et al., 2007; SUTAR; PRASAD, 2007; YANYANG et al., 2004; ZANG et al., 2023; ZIELINSKA; MARKOWSKI; ZIELINSKA, 2019). A vacuum allows water to vaporize at lower temperatures (20-31°C at 2.5-4.5 kPa), which helps preserve nutrients (NAHIMANA; ZHANG, 2011). Erle and Schubert (2001) dried apples and strawberries at 5 kPa, in which the vaporization point of pure water is 32.9°C, a low temperature compared to conventional methods. If enough water is in the tissue, this boiling point can only be exceeded minimally due to dissolved substances. In the final stages of microwave drying, the temperature may reach 80 °C, but thermal damage in this period is still relatively low because the heat sensitivity decreases with decreasing water content. Moreover, because air is excluded during drying,

oxidation reactions are minimized. MWVD is essential to products such as cranberry, where biologically active antioxidants are easily oxidized and degraded (WRAY; RAMASWAMY, 2015; ZIELINSKA; MARKOWSKI; ZIELINSKA, 2019).

Cui *et al*. (2008) microwave vacuum-dried carrots and observed that the reduction in carotene was only 5.3% against 29.4% dried with hot air. The same authors analyzed the degradation of vitamin C in apples, and the reduction was only 11% when dried with microwave vacuum drying and 36.3% when using hot air. These results show the benefits of using the microwave vacuum to dry fruits and vegetables. Some researchers have done the microwave vacuum drying of foods like cheese, milk, pork, beef, mushroom, pumpkin, banana, potato, garlic, wild cabbage, apple, pear, and grape, also showed that this technology results in better quality products (CLARY et al., 2007; CUI; XU; SUN, 2003; DUMPLER; MORARU, 2022; HU et al., 2006b; KROKIDA; MAROULIS, 1999; LIN et al., 2022; MONTEIRO et al., 2018a, 2020a, 2020b, 2022; PAWLAK et al., 2022; REN; LEI; SUN, 2023; SETIADY et al., 2009; SOUZA, 2021; YANYANG et al., 2004).

Researchers have employed MWVD to produce food with enhanced crunchiness and a pleasing puffing effect, resulting in positive consumer feedback. For instance, vacuum microwave drying has successfully created crispy pork snacks, when combined with a pre-treating of raw pork meat with proteases before drying (PAWLAK et al., 2022). The use of different thermal (blanching in steam or water) and non-thermal (osmotic solutions, sodium hydroxide solution, halving, slicing, and perforation) pretreatment methods before drying are used to modify the physicochemical properties of dried material as well as heat and mass transfer during drying. This dried-and-crisp structure has also been observed in vacuum microwave drying of pumpkin slices and potato chips (MONTEIRO et al., 2018a, 2020a).

The product shape and size during MWVD also need to be take into consideration. The most common uneven heating of microwaved foods is probably caused by the maxima of standing waves in foods, particularly when large-size (greater than the wavelength) foods are considered, especially for food with a low dielectric loss factor and a high dielectric constant. If the structures present edges and corners, the surface electric charges are accumulated more in these regions than in other places due to the geometric effect (ZHANG; DATTA, 2003). Edge heating results in extremely high temperatures resulting in over-drying and even scorching of the material near those locations affecting the final quality of the dried product (ZHU et al., 2015).

The absorption of microwaves by a sample also depends on its dielectric properties, which are correlated with the water content, temperature, and microwave frequency (ERLE; SCHUBERT, 2001; LIN et al., 2022; MUDGETT et al., 1980; NELSON, 1991; RENSHAW et al., 2019). It is known that the dielectric constant of water decreases as temperature increases (GULATI, DATTA, RANJBARAN, 2020), meaning that the dielectric properties of food decrease while drying. Also, when water is lost during MWVD, the overall dielectric property is reduced for a rigid material. On the other hand, in a deformable material undergoing significant shrinkage during microwave drying, the volume shrinkage compensates for the volume of water lost (DEFRAEYE; RADU, 2018; DHALL; DATTA, 2011; TSURUTA; TANIGAWA; SASHI, 2015).

2.1.2 Dryer Design

Microwave technology has many current applications. It is handy for food processing, including domestic cooking, warming-up, industrial heating and drying. Generally, it heats faster than conventional applications; however, in most cases, it results in non-uniform temperature distribution.

This section aims to highlight the significance of cavity characteristics in heat distribution during the microwave drying of food products. It presents cavity design and process optimization studies conducted over the past 25 years. Microwave cavities are used in various applications, such as microwave resonators, waveguides, and components like filters, circulators, and cavities for microwave amplifiers.

Microwave ovens present big cavities that work in batches (REMYA and SWAIN, 2019; SANTOS *et al*., 2018) or continuous form (CHENG *et al*., 2015; ZHANG *et al*., 2019), using constant or variable power sources (KAENSUP *et al*., 2002; BARRETO *et al*., 2019) with different cavities shape for the most diverse purposes (GAO *et al*., 2019, ALBANNAY *et al*., 2019; HALIN and SWITHENBANK, 2019). The designs can present one (GAO *et al*., 2019; WRAY and RAMASWAMY, 2015) or more magnetrons (JENI *et al*., 2010; HU *et al*., 2006) with different power, with or without rotation cavity systems (KAENSUP *et al.,* 2002; JENI *et al*., 2010; MONTEIRO *et al*., 2015; BARRETO *et al*., 2019), and in small (MONTEIRO *et al*., 2015; GAO *et al*., 2019; WRAY and RAMASWAMY, 2015) or big (HU *et al*., 2006; CLARY et al., 2007; BARRETO *et al*., 2019) vacuum cavities.

Some oven cavities-related studies available in the literature are present in **Table 2.1**.

Table 2.1: Literature studies on microwave dryer's cavities for drying foods.

Food Product	**Objective**	**External cavity [work volume] (m^3)**	**Pressure (atm)**	**Power (W) [number of magnetrons]**	**Ref.**
Chilli	Drying Kinetics	0.0342 [0.0212]	0.08, 0.21, 0.34	800 [1]	KAENSUP *et al*., 2002
Edamames	Process efficiency and food quality	NI	0.93	1400 [3]	HU *et al*., 2006
Grapes	Food quality	NI	0.02	3000 [1]	CLARY *et al*., 2007
Tea leaves	Process feasibility	0.13 [0.035]	0.51;0.70	800;1600 [2]	JENI *et al*., 2010
Cranberries	Drying Kinetics and food quality	0.022 [0.0016]	0.06	1000 [1]	WRAY and RAMASWAMY, 2015
Banana, grape, tomato, and carrot slices	Low-cost, flexible and ease-to-assemble device	0.045 [0.0106]	0.1	1000 [1]	MONTEIRO et al., 2015
Potato slices	Production of oil-free potato snacks	0.174 [0.122]	0.03	300; 1500; 2700 [1]	BARRETO *et al.,* 2019
Water film	Guidance for the design and scaling-up	0.028 [0.00006]	NI	100 [1]	GAO *et al*., 2019
Whole liquid egg	Optimization cavity geometry for industrial continuous flow	0.210 [0.000203]	NI	2500 [8]	(TOPCAM; ERDOGDU, 2021)
Potato	Developed a method to design a multiport microwave oven	0.157 [0.0136]	0.1	1000 [12]	(SALVADOR et al., 2022)

*NI = not informed

Clary et al. (2007) developed a microwave vacuum dryer that used temperature to control the emitted power, with microwave power adjusted based on the product surface temperature measured by an infrared temperature sensor, enabling control from 0 to 3 kW. This equipment featured a cylindrical vacuum cavity of 0.76 m^3. Barreto *et al*. (2019) worked with a cavity of

0.122 m³ to produce oil-free potato chips, while Hu *et al*. (2006) dried edamame in a hexagonal cavity of 0.91 m³ with 6 triangular sample holders. These structures were developed to dry high quantities of materials, more than 1 kg.

Kaensup et al. (2002) designed a cavity to combine microwave, vacuum, and rotary drum to dry chili, analyzing moisture content vs. drying time and drying rate vs. moisture content. Jeni et al. (2010) investigated the feasibility of using a microwave double-feed vacuum drier for drying biomaterials under various conditions, including microwave radiation time, microwave power level, vacuum level, and the microwave feeding process. Gao et al. (2019) evaluated the influence of different design parameters on microwave heating performance by coupling the electromagnetic and heat transfer equations.

Commercial domestic microwave ovens typically operate at frequencies of 2.45 GHz. The waves are distributed through waveguides in the TE_{10} mode, with power ranging from 1 kW to 2 kW. The microwave oven utilized in this study differs from many others described in the literature, as it is specially designed with unique features (MONTEIRO *et al*., 2015; TELEKEN *et al*., 2020). It is a domestic microwave vacuum oven adapted for drying bananas, grape tomatoes, and carrots. The equipment, with a volume of 0.045 m³ volume externo, incorporates a polypropylene rotatory cavity of 0.0106 m³, capable of withstanding a vacuum pressure of 4 kPa.

When designing a microwave cavity some process features have a greater impact in the temperature distribution inside the food. For instance, in addition to utilizing vacuum, adjusting the magnetron duty cycle (power on/off times) and regulating power density (applied watts per gram of sample material) can decrease the food temperature (ORSAT et al., 2007). Power cycling also allows better redistribution of the temperature and moisture profile within the product during power-off periods, as can be verified in the MWVD of cranberries by Sunjka et al. (2004) and ginseng Zang et al. (2023).

The physics phenomena involved in microwave vacuum drying and how they are represented mathematically are described in the following section.

2.2 MATHEMATHICAL MODELING OF WAVE DISTRIBUTION

Wave equations are a fundamental tool for study of microwave cavities due to their ability to describe and predict the behavior of electromagnetic waves within these confined

structures. Based in these equations is possible to understand wave propagation, field distribution and wave penetration in food systems.

Understanding a cavity with electromagnetic waves leads to comprehending any microwave oven cavity, the electromagnetic waves and heat distribution, the dielectric properties, and the types of excitations. The electric field distribution inside an oven cavity is obtained by solving Maxwell's equation presented in the point form (SADIKU, 2018):

$$\vec{\nabla} \times \vec{H} = \vec{J} + \frac{\partial \vec{D}}{\partial t} \tag{2.1}$$

$$\vec{\nabla} \times \vec{E} = -\frac{\partial \vec{B}}{\partial t} \tag{2.2}$$

$$\vec{\nabla} . \vec{B} = 0 \tag{2.3}$$

$$\vec{\nabla} \vec{D} = 0 \tag{2.4}$$

As presented, ampere's law states that an electric current (either conduction $(\vec{J})$ or displacement $(\vec{D})$ produces a magnetic field $(\vec{H})$. Faraday's law states that a time-varying magnetic flux $(\vec{B})$ produces an induced electromotive force $(\vec{E})$. The negative sign expresses Lenz's Law, which states that the electric field produced would tend to generate a current that opposes the initial variation of the magnetic flux. Gauss's law of magnetism states that the total magnetic flux across any closed surface is zero. Finally, Gauss's law states that the electric flow through a closed surface is equal to the charge contained within the surface, which, in the case of the microwave oven, is zero.

Besides Maxwell's equations, the constitutive relations are needed to characterize the material medium with electric permittivity ε, magnetic permeability μ, and conductivity σ.

$$\vec{D} = \varepsilon \vec{E} \tag{2.5}$$

$$\vec{B} = \mu \vec{H} \tag{2.6}$$

$$\vec{J} = \sigma \vec{E} \tag{2.7}$$

The permittivity ε is defined as:

$$\varepsilon = \varepsilon_0 \varepsilon_r \tag{2.8}$$

Here, ε_r is the relative permittivity or dielectric constant, and ε_0 is the permittivity of free space.

The permeability is defined as:

$$\mu = \mu_0 \mu_r \tag{2.9}$$

μ_r is the relative permeability and μ_0 the permeability of free space.

The electromagnetic wave propagation equation is described according to SADIKU (2018) as:

$$\vec{\nabla} \times \left(\vec{\nabla} \times \overrightarrow{E_s}\right) = -j\omega\mu(\sigma + j\omega\varepsilon)\overrightarrow{E_s} \tag{2.10}$$

in a medium characterized by ε, μ and σ, with a wave frequency of ω. It is the wave equation for the electric field obtained by manipulating Equations 2.1-2.7.

The propagation constant, γ, is another important definition for understanding how waves propagate in a medium.

$$\gamma = \alpha + j\beta \tag{2.11}$$

This constant carries the attenuation factor (α) and the phase constant (β). The attenuation factor measures the spatial rate of the wave's decay in a medium, and the phase constant measures the phase shift per length. Both terms are presented below (SADIKU, 2018).

$$\alpha = \omega \sqrt{\frac{\mu\varepsilon}{2}\left[\sqrt{1 + \left(\frac{\sigma}{\omega\varepsilon}\right)^2} - 1\right]} \tag{2.12}$$

$$\beta = \omega \sqrt{\frac{\mu\varepsilon}{2}\left[\sqrt{1+\left(\frac{\sigma}{\omega\varepsilon}\right)^2}+1\right]} \tag{2.13}$$

The attenuation factor enables the determination of penetration depth, which is the distance that an electromagnetic wave can penetrate in a dielectric until the wave amplitude decrease by a factor e^{-1} (about 37%) of its initial value at the sample surface.

$$\delta = \frac{1}{\alpha} \tag{2.14}$$

The power absorbed per unit volume in the material is obtained from the Poynting Theorem. The net power flowing out of a given volume is equal to the lime rate of decrease in the energy stored within the volume minus the conduction losses:

$$Q(x,y,z,t) = \frac{1}{2}\,\omega\varepsilon_0\varepsilon''(\vec{E}\cdot E^*) \tag{2.15}$$

In which E^* is the conjugate electric field vector.

The heat source term in the energy conservation equation is described as a potential function (**Equation (2.16)**) (RAKESH; DATTA, 2011), based on the Lambert equation (**Equation (2.17)**) (DATTA; NI, 2002; TELEKEN et al., 2020) or as Poynting Theorem for microwave power according to aforementioned (ZHANG; DATTA, 2003).

$$Q = 1.5\times 10^7\left(\frac{M_0}{M}\right)^{-1.17} \tag{2.16}$$

where M_0 is the initial and M actual moisture content.

$$Q = \frac{F_{mic,s}}{\delta}\exp\left(-\int_0^x \frac{dx}{\delta}\right) \tag{2.17}$$

The $F_{mic,s}$ is the microwave flux at the surface, x is the sample thickness, and δ is the penetration depth based on the dielectric properties (RAKESH et al., 2012).

The dielectric loss factor ε'' is defined from the loss tangent and the dielectric constant ε' of the medium as (SADIKU, 2018):

$$\tan\theta = \frac{\sigma}{\omega\varepsilon} = \frac{\varepsilon''}{\varepsilon'} \tag{2.18}$$

For lossless dielectrics, $\tan\theta \ll 1$; for good conductors, $\tan\theta \gg 1$; and for lossy dielectrics, $\tan\theta$ is of the order of unity.

The ability of microwave energy to heat a product is dictated by the product's dielectric properties (ε', ε''), which are positively correlated to its water activity. It can, in effect, impose a self-regulatory aspect to microwave-based dehydration techniques because the portions of the sample containing more moisture tend to absorb more power, dry more quickly, and thus absorb less power later (ERLE; SCHUBERT, 2001; RENSHAW et al., 2019). It means that the sample will initially receive the electromagnetic waves in the same way, but during product drying, the heat absorb in each part will differ because of the moisture gradients. The equation of Landau, Lifhitz, and Looyenga was used successfully by many authors (GULATI; ZHU; DATTA, 2016; LIU; TANG; MAO, 2009; NELSON, 1991) to describe the dielectric properties change:

$$\varepsilon_c^{1/3} = (1-\emptyset)(\varepsilon_s' - j\varepsilon_s'')^{\frac{1}{3}} + S_l\emptyset(\varepsilon_l' - j\varepsilon_l'')^{\frac{1}{3}} + S_g\emptyset\left(\varepsilon_g' - j\varepsilon_g''\right)^{\frac{1}{3}} \tag{2.19}$$

where s, l, and g are the solid, liquid, and gas phases, respectively, $\emptyset$ and S_i depict porosity and percentage or saturation in the porous media.

2.3 MATHEMATICAL MODELING OF POROUS FOOD

A literature review was conducted to investigate the equations governing multiphase transport, phase transition and deformation during microwave drying. The objective was to understand the coupled effects of mass and heat transfer, including blowing, fluid flow in a porous medium, rapid evaporation, pressure development, and solid mechanics.

2.3.1 Porous Media Concept

Foods can be defined as deformable continuous media with liquid, vapor, and solid phases, **Figure 2.1**. The model for the porous medium can be based on the representative elementary volume (REV) theory, in which the properties are defined as spatial average (DATTA, 2007; WHITAKER, 1977).

Figure 2.1: Potato represented as a porous media composed of solid, liquid, and gas phases based on the Representative Elementary Volume (REV) concept. And the phenomena in each phase responsible for mass and heat transfer and solid deformation.

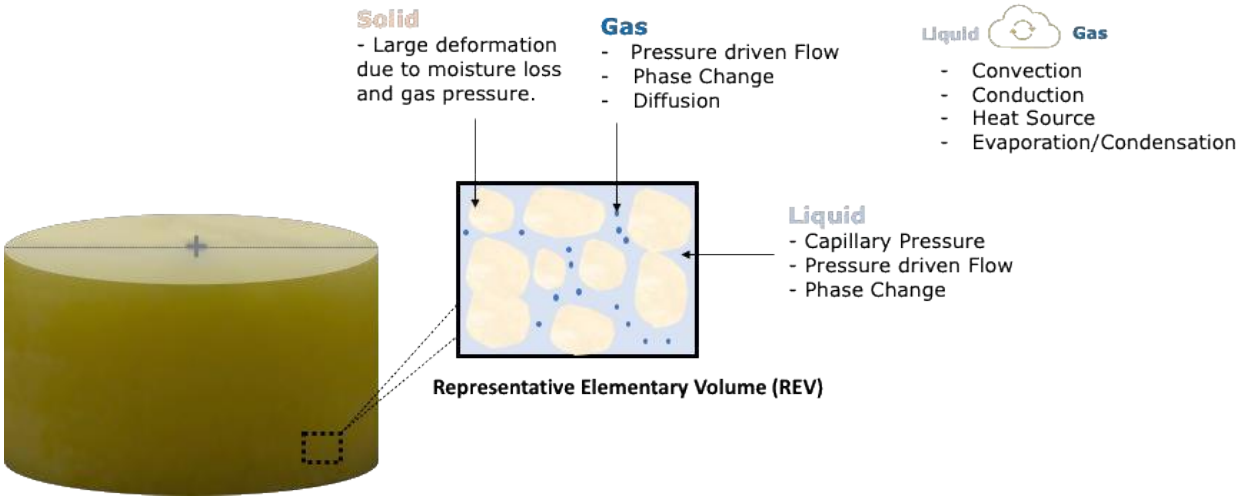

Source: Author

In **Figure 2.1**, the depicted phenomena in the gas phase include pressure-driven flow, where the gas is pushed outward and through the pores, and phase change, involving evaporation or condensation. Capillary flow in the liquid phase is driven by capillary forces within the pores. Also, binary diffusion in the gas phase occurs due to concentration gradients. Heat transfer in each phase is represented by conduction, advection, and additional source terms accounting for phase change and the microwave energy source. All phases are in thermal equilibrium.

2.3.2 Heat and mass multiphase transport

The momentum conservation is described with Darcy's law, where the different fluid phases (liquid and vapor water) arise due to gradients in gas pressure ($\vec{\nabla}P$).

$$\vec{v}_i = -\frac{k_{in,i} k_{rel,i}}{\mu_i} \vec{\nabla} P \tag{2.21}$$

in which $i = l, g$ denotes the liquid water and gas phases, respectively, intrinsic permeability $k_{in,i}$, relative permeability $k_{rel,i}$, and μ_i is the fluid viscosity. In general, Darcy's law is valid in vegetables since the pore structure is not well developed and the Reynolds number for vapor flow is at the order of 10^{-5} (NI, 1997). Both velocities are written as relative since the solid phase is moving due to deformation.

Fluid permeability is described as a product of intrinsic permeability, which depends on structural parameters such as porosity and relative permeability, which, in turn, depend upon the fluid phases' relative saturation (ZHU et al., 2015). The magnitude of the intrinsic permeability of different food products can be seen in **Figure 2.2**. The experimentally determined intrinsic permeability value in the raw potato is very low (around 1×10^{-18} m^2) and applies to potatoes with a void air space fraction of around 0.11 (DATTA, 2006). Apples are in the same magnitude of intrinsic permeability as potatoes, rice depends on the treatment of the grain, and meat presents intrinsic permeability around 1×10^{-19} m^2.

Figure 2.2: Range of water intrinsic permeability of different food products.

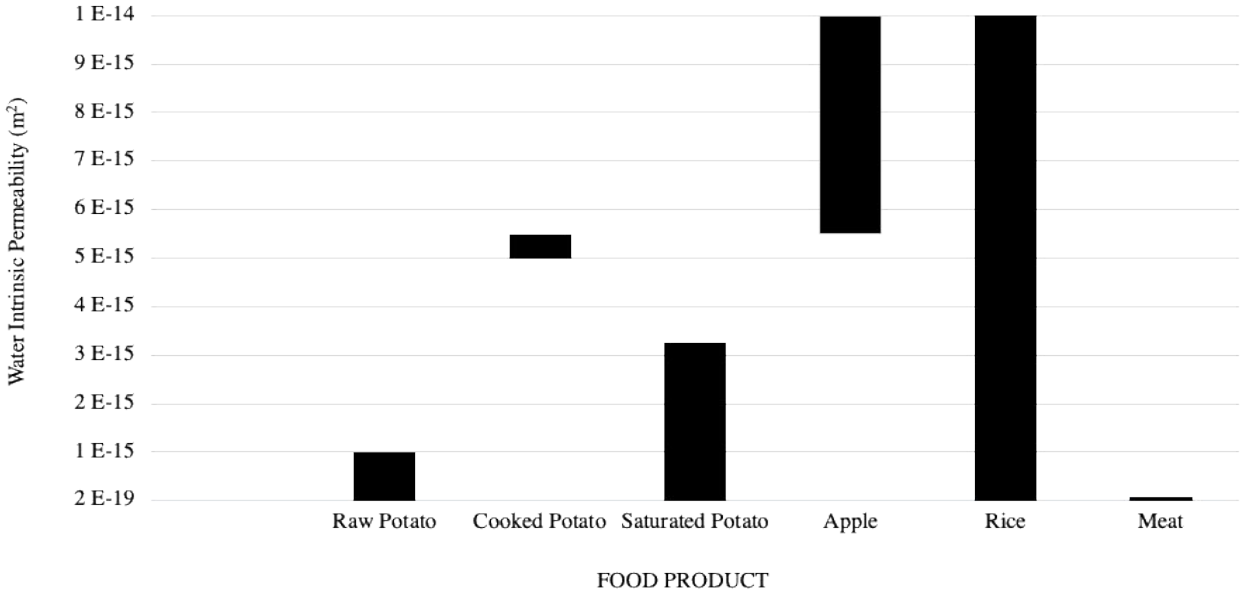

Source: Author based on (DADMOHAMMADI et al., 2020; DATTA, 2006; NI; DATTA, 1999; OROSZVÁRI et al., 2006; WARNING; ARQUIZA; DATTA, 2015)

The predicted water permeability at a swelling index of 1.05 is within one order of magnitude of directly measured data, 4×10^{-18} m^2 (the average of eight measurements of two Russet potato samples) (DADMOHAMMADI et al., 2020). It is important to mention that the intrinsic permeability for the gas phase differs from that of liquid water and is calculated from liquid water permeability via the Klinkenberg correction factor (TANIKAWA; SHIMAMOTO, 2009).

Mass conservation equations are presented for liquid water and water vapor in **Equations (2.22)** and **(2.23)**, respectively.

$$\frac{\partial c_l}{\partial t} + \vec{\nabla} \cdot \vec{n}_{l,G} = -\dot{I} \tag{2.22}$$

$$\frac{\partial c_g}{\partial t} + \vec{\nabla} \cdot \vec{n}_{g,G} = \dot{I} \tag{2.23}$$

Where $c_l = \rho_l S_l \emptyset$ and $c_g = \rho_g S_g \emptyset$ are the mass volumetric concentration of the liquid phase (l) and gas phase (g), respectively, considering density (ρ_i), saturation (S_i), total porosity ($\emptyset$) and $\dot{I}$ denotes the phase change that will be explained with more details later.

If the gas phase is composed of air and water vapor, another equation for vapor phase (v) is needed:

$$\frac{\partial c_v}{\partial t} + \vec{\nabla} \cdot \vec{n}_{v,G} = \dot{I} \tag{2.24}$$

The liquid water flux ($\vec{n}_{l,G}$), vapor water flux ($\vec{n}_{v,G}$) and gas flux ($\vec{n}_{g,G}$) are defined concerning the ground frame, i.e., considering the movement of the solid. The vapor and air concentration are related to gas phase concentration by their mass fraction $w_v + w_a = 1$, so $c_v = c_g w_v$ and $c_a = c_g w_a$.

The $\dot{I}$ denotes the non-equilibrium formulation for phase change, leading to evaporation/condensation, defined through **Equation (2.25)** (HALDER; DHALL; DATTA, 2007a):

$$\dot{I} = K_{evap}(\rho_{v,f} - \rho_{v,0}) S_v \emptyset \tag{2.25}$$

In which K_{evap} is a material and process-dependent parameter reciprocal of equilibration time, $\rho_{v,f}$ is the final vapor density after the equilibration time and $\rho_{v,0}$ is the initial vapor density. Considering a representative elemental volume inside the pores, the phase change occurs in a non-equilibrium evaporation rate as given by **Equation (2.27)**. The ideal gas law is used to relate gas phase density and pressure, **Equation (2.26)**:

$$\rho_i = p_i \frac{M_i}{RT} \tag{2.26}$$

$$\dot{I} = K_{evap}\left(p_{v,eq} - P\right)\frac{M_v}{RT} S_v \emptyset \tag{2.27}$$

in which P is the partial pressure of the vapor phase obtained from Darcy's law, $p_{v,eq}$ is the equilibrium vapor pressure of the food material obtained by the product of saturation pressure (p_{sat}) **Equation (2.28)** and moisture sorption isotherm, **Equation (2.29)**, as a function of moisture, X_{db} (WANG; BRENNAN, 1991):

$$p_{v,eq} = A_w p_{sat} \tag{2.28}$$

$$A_w = e^{-0.094-\left(3.15e^{-23.44X_{db}}\right)} \tag{2.29}$$

For porous materials having an average pore diameter of 25 μm, such as potatoes, the equilibration time has been estimated to be about 10^{-5}s (HALDER; DHALL; DATTA, 2011). It leads to a K_{evap} value of 100,000 s^{-1}. However, during numerical implementation, it was found that for K_{evap}= 1000 s^{-1} and above, the solution has little changes, for example, temperature and moisture values. For drying processes, equilibrium almost always exists between instantaneous vapor density and saturation vapor density, and this can easily be achieved in **Equation (2.27)** by keeping the evaporation rate constant high enough that the solution process is no longer affected by the value of K_{evap}.

It is important to mention that as the value of the constant K_{evap} increases, the time for phase change is reduced, i.e., for infinitely large K_{evap} values, the phase change occurs

instantaneously. A very high value of K_{evap}, however, complicate the convergence of the numerical solution (HALDER; DATTA, 2012).

The saturation S_i of a specific phase denotes the fraction of volume occupied by the phase, V_i , concerning the pore space volume, V_f, as in **Equation (2.30)**:

$$S_i = \frac{V_i}{V_f} \tag{2.30}$$

$$S_l + S_g = 1 \tag{2.31}$$

The summation of the saturation equation must lead to unity (**Equation (2.31)**). S_l and S_g are obtained from mass conversation equations.

The potato liquid saturation assumed values from 0.99 to 0.09, the last being the irreducible saturation, S_{ir}. Darcy's law holds when $S_{ir} < S < 1$, but there is no water flow when $0 < S < S_{ir}$ (ILIC; TURNER, 1989).

The total porosity ($\emptyset$) is the fraction of volume occupied by the fluid phases, or void space.

$$\emptyset = \frac{V_f}{V} \tag{2.32}$$

The fluxes in mass conservation equations are defined concerning a ground frame of reference. Adding a flux arising due to the movement of the solid phase, material deformation is considered. The flux relative to the ground frame ($\vec{n}_{i,G}$) is equal to flux relative to deforming solid ($\vec{n}_{i,s}$) added to a flux due to solid movement ($c_i\overline{v_s}$) as:

$$\vec{n}_{i,G} = \vec{n}_{i,s} + c_i\overline{v_s} \tag{2.33}$$

The $\vec{n}_l$ and $\vec{n}_g$ are the mass flux of liquid and gas, respectively and were specified according to the Equations **(2.34)** and **(2.35)**:

$$\vec{n}_l = -\rho_l \frac{k_{in,l} k_{rel,l}}{\mu_l} \vec{\nabla}(P - p_c) \tag{2.34}$$

$$\vec{n}_g = -\rho_g \frac{k_{in,g} k_{rel,g}}{\mu_v} \vec{\nabla} P \tag{2.35}$$

in which it is possible to identify the gradient of gas pressure ($\vec{\nabla}P$), capillarity pressure (p_c) resulting from the interaction of forces between pore walls.

In addition to gas pressure, the liquid water inside the pores experiences an attractive force in terms of capillary pressure (p_c). This water flux was described with a capillary diffusivity, $D_{cap,l}$, by HALDER, DHALL, and DATTA, 2007a, and it is the definition used:

$$D_{cap,l} = -\rho_l \frac{k_{in,l} k_{rel,l}}{\mu_l} \frac{\partial p_c}{\partial c_l} \tag{2.36}$$

$$\vec{n}_l = -\rho_l \frac{k_{in,l} k_{rel,l}}{\mu_l} \vec{\nabla} P - D_{cap,l} \vec{\nabla} c_l \tag{2.37}$$

As mentioned before, the net flux of liquid and vapor need to be defined concerning the ground frame, so the solid velocity is added $\overrightarrow{v_s}$:

$$\vec{n}_{l,G} = -\rho_l \frac{k_{in,l} k_{rel,l}}{\mu_l} \vec{\nabla} P - D_{cap,l} \vec{\nabla} c_l + c_l \overline{v_s} \tag{2.38}$$

$$\vec{n}_{g,G} = -\rho_v \frac{k_{in,v} k_{rel,v}}{\mu_v} \vec{\nabla} P + c_v \overline{v_s} \tag{2.39}$$

In cases where the air needs to be considered, an additional equation is presented in the model:

$$\vec{n}_{v,G} = -\rho_v \frac{k_{in,v} k_{rel,v}}{\mu_v} \vec{\nabla} P - \frac{c_g^2}{\rho_g} M_v M_a D_{bin} \nabla x_v + c_v \overline{v_s} \tag{2.40}$$

The equation for vapor concentration changes with a binary diffusion term, where M_v is the molar mass of vapor, M_a is the molar mass of air, D_{bin} binary diffusivity and x_v mole fraction of vapor. The gas diffusivity is defined according to (MILLINGTON; QUIRK, 1961):

$$D_{bin,\,g} = \frac{2.13}{P}\left(\frac{T}{273.15}\right)^{1.8} S_g \emptyset \tag{2.41}$$

The energy conservation equation includes heat conduction, $\vec{\nabla}\left(k_{ef}\vec{\nabla}T\right)$, convection of fluid phases, $(\vec{n}_{l,G}C_{p,l} + \vec{n}_{g,G}C_{p,g}) \cdot \vec{\nabla}T$, evaporative cooling, $\lambda_{ev}\dot{I}$, and microwave heat source, $\dot{Q}$. The three phases are assumed to be in thermal equilibrium.

$$\rho C_{p,ef}\frac{\partial T}{\partial t} + (\vec{n}_{l,G}\, C_{p,l} + \vec{n}_{g,G}\, C_{p,g}) \cdot \vec{\nabla}T = \vec{\nabla}\left(k_{ef}\vec{\nabla}T\right) - \lambda_{ev}\dot{I} + \dot{Q} \tag{2.42}$$

The properties of the porous media are obtained by averaging those of pure components, weighted by either their mass or volume fractions:

$$\rho C_{p,ef} = (1 - \emptyset_0)\rho_s C_{p,s} + \emptyset\left(S_l\rho_l C_{p,l} + S_g\rho_g C_{p,g}\right) \tag{2.43}$$

$$k_{ef} = (1 - \emptyset_0)k_s + \emptyset\left(S_l k_l + S_g k_g\right) \tag{2.44}$$

where ρ, C_p, k are the density, specific heat and thermal conductivity of each phase, respectively.

Regarding the boundary conditions, to model microwave drying different phenomena can be considering depending on process specifications. The external convection at the boundary is a phenomenon that requires attention. During drying the water and gas will move from surface in different rates depending on the process, and these rates are defined with the help of mass (h_m) and heat transfer (h_t) coefficients. The coefficients assume in the literature for different process considering microwave are presented in the **Table 2.2**:

Table 2.2: Heat and mass transfer coefficients used in simulation papers with microwave drying.

	Process	Coefficient Value	Source
h_t	Microwave	10 W/m^{2}K	(RAKESH et al., 2012)
	Microwave puffing	20 W/m^{2}K	(NI; DATTA; TORRANCE, 1999)
	Microwave with forced convection	1.5-6.6 W/m^{2}C	(VERBOVEN et al., 2003)
h_m	Microwave	0.008 m/s	$\frac{h_t}{h_m} = \rho_v c_{p,v} (Sc/Pr)^{2/3}$
	Microwave puffing	0.01 m/s	(NI; DATTA; TORRANCE, 1999)
	Microwave with forced convection	0.0063 m/s	(VERBOVEN et al., 2003)

The heat loss due to evaporation of water, removal of water and vapor can also be added to boundary condition with heat and mass transfer coefficients. The values for heat and mass transfer are very low at the beginning of drying because of the small difference between the product temperature and the ambient temperature, but they increase with time.

One of the Chilton-Colburn correlations is presented in **Table 2.2**. It is based in the analogy between heat and mass transfer for a specific geometry, where heat and mass transfer ratios are interchangeable. This mean that the numbers Nusselt and Sherwood are, in general, proportional to Prandtl (Pr) and Schmidt (Sc). The analogy can be used to determine a convective coefficient, i.e., h_m, from knowledge of the other coefficient. The same relationship can be applied to the mean coefficients and be employed in turbulent flows as well as in laminar flows (INCROPERA et al., 2013).

2.3.3 Structural deformation in Porous Media

Mathematical models to describe deformations of fruit and vegetables during drying are presented in literature in microscopic (DEFRAEYE; RADU, 2018; FANTA et al., 2014; LI; THOMAS, 2016; RANJBARAN; DATTA, 2019) or macroscopic (GULATI; DATTA; RANJBARAN, 2020; RESSING; RESSING; DURANCE, 2007; ZHU et al., 2015) scales; large (AREGAWI et al., 2013; CHESTER; ANAND, 2010; GULATI; DATTA, 2016) or small deformation; and with various drying process as air drying (LLAVE et al., 2016; YANG; SAKAI, 2001), microwave drying (GULATI; ZHU; DATTA, 2016; RAKESH; DATTA, 2011)

and combining techniques (KROKIDA; MAROULIS, 1999; TULASIDAS; RATTI; RAGHA VAN, 1997). Modelling of deformation had also been performed empirically using empirical equations relating the deformation to the moisture content of a specific material undergoing a specific drying process (KROKIDA; MAROULIS, 1997; TULASIDAS; RATTI; RAGHA VAN, 1997; YANG; SAKAI, 2001). And in these cases, different correlations can be used to describe how the initial volume (V_0) change during time depending on moisture (X_{db}) and temperature (T) gradients leading to a final deformed volume *(V)* (DEVAHASTIN; NIAMNUY, 2010):

$$\frac{V}{V_0} = f(X_{db}, T) \tag{2.45}$$

This type of correlation can assume linear, nonlinear or polynomial forms. In case of vacuum drying and superheated steam drying (PANYAWONG; DEVAHASTIN, 2007) or samples with lower moisture contents (KATEKAWA; SILVA, 2006) the pores formation during drying needs to be considerate and in these cases the linear models are not adequate.

The food deformation can result in shrinkage, puffing or swelling in a specific direction or at all directions, depending on the sample characteristics, mass and heat transfer involved, as represented in **Figure 2.3**.

Figure 2.3: Scheme with food deformation considering the Jacobian value and deformation gradient changed.

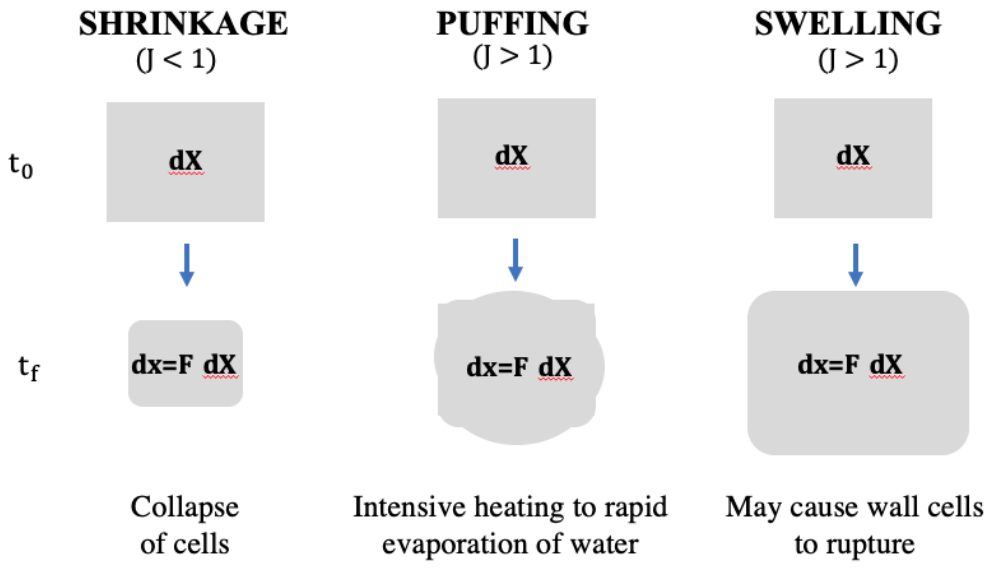

Source: Author

Regarding the **Figure 2.3**, when a sample undergoes deformation, it causes a change in the Jacobian (J), also known as the volume ratio. Initially, the Jacobian has a value of 1. However, if the final volume of the sample increases, the Jacobian becomes greater than 1, indicating expansion. On the other hand, if the sample undergoes shrinkage, the Jacobian becomes less than 1. During deformation, a material element labeled as dX transforms into dx, where the transformation is governed by the deformation gradient F. These elements, namely the Jacobian and the deformation gradient, will be further discussed.

Shrinkage is one of the major physical changes that occur during the drying process and is the result from the collapse of cells during water evaporation (FANTA et al., 2014), and according to majority of drying methods if no mechanical restrictions were presented, shrinkage would be linearly proportional to the volume of water removed (DEVAHASTIN; NIAMNUY, 2010; DHALL; DATTA, 2011; KATEKAWA; SILVA, 2006). Puffing refers to intensive heating of food materials to obtain low moisture ready-to-eat products with altered structural characteristics (RAKESH; DATTA, 2011). The intensive heating leads to rapid evaporation of water to vapor resulting in large pressure development (GULATI; DATTA, 2016). The microwave heating is considering a puffing mechanism that depends on optimum moisture content, heating rates and cavity environment (RAKESH; DATTA, 2011; RESSING; RESSING; DURANCE, 2007). The last one swelling, during swelling the fruits and vegetables absorb water and swell many times their original size, what may cause wall cells to rupture (DUDA; SOUZA; FRIED, 2010; SILVA et al., 2012).

A simple but adequate approach, that may be used to model this type of material during drying involves alteration of a computational domain of the transport (heat and mass transfer) equations. The domain is updated at each computational time step, what is called moving boundaries. A moving boundary was implemented in COMSOL Multiphysics® using the Arbitrary Lagrange-Eulerian formulation that is capable to solve correlations as proposed for (DEVAHASTIN; NIAMNUY, 2010; SUVARNAKUTA; DEVAHASTIN; MUJUMDAR, 2007):

$$\frac{V}{V_0} = a\left(\frac{X}{X_i}\right)^2 + b\left(\frac{X}{X_i}\right) + c \tag{2.46}$$

Where initial volume (V_0) change during time depending on moisture content (X_i) leading to a final deformed volume (V).

It is well recognized that fruits and vegetables typically suffer nonuniform deformation during drying because of moisture gradients generating stresses inside the material, that for potatoes has been reported to be in the range of 1–1.12 MPa (GULATI et al., 2016; YANG; SAKAI, 2001). Because of this, Dhall and Datta (2011) proposed a study of porous mechanic deformation based in total stress tensor $\overline{\sigma}$ in the representative elementary volume (REV):

$$\overline{\sigma} = \frac{1}{V}\int_V \sigma \, dV \tag{2.47}$$

As the total volume can be written as a sum of volumes of the solid and the fluids present in the pores:

$$V = V_s + \sum_i V_i \tag{2.48}$$

The total stress tensor can also be express as a sum of average sum of individual phase volumes:

$$\overline{\sigma} = \frac{1}{V}\left[\int_{V_s} \sigma \, dV + \sum_i \left(\int_{V_i} \sigma \, dV\right)\right] = \varphi_s \overline{\sigma}_s + \sum_i (\varphi_i \overline{\sigma}_i) \tag{2.49}$$

Where φ_i is the volume fraction and $\bar{\sigma}_i$ is the volume-average stress of a phase i. As the shear stress in fluids can be negligible:

$$\overline{\sigma}_i = -p_i I \tag{2.50}$$

$$\overline{\sigma} = \varphi_s \overline{\sigma}_s - \sum_i (\varphi_i p_i I) \tag{2.51}$$

$$\overline{\sigma} = (1 - \emptyset)\overline{\sigma}_s - \emptyset \sum_i (S_i p_i I) \tag{2.52}$$

The first term on the right side is defined as effective stress on the solid skeleton ($\overline{\sigma'}$) and the second as pore pressure (P_p):

$$\overline{\sigma} = \overline{\sigma'} - P_p I \tag{2.53}$$

Considering the quasi-steady state assumption for deformation (acceleration is zero), the solid momentum balance led to divergence-free field of overall stress:

$$\vec{\nabla} \cdot \overline{\sigma} = 0 \tag{2.54}$$

The divergence of effective stress is equal to gradient of pore pressure:

$$\vec{\nabla} \cdot \overline{\sigma'} = \vec{\nabla} P_p \tag{2.55}$$

In case the pores are occupied by liquid water and vapor we have:

$$\vec{\nabla} \cdot \overline{\sigma'} = \vec{\nabla}(S_v P + S_l p_l) \tag{2.56}$$

The deformation considering two phenomena: moisture change, and gas pressure change presenting the following governing equation and constitutive law, respectively:

$$\vec{\nabla} \cdot \overline{\sigma''} = \vec{\nabla} P \tag{2.57}$$

$$\overline{\sigma''} = D \cdot \epsilon_m \tag{2.58}$$

Where $\overline{\sigma''}$ is the effective stress tensor due to mechanical load only, D is the stiffness fourth order tensor and ϵ_m is the mechanical strain.

Deformation at a material point of a body is characterized by changes of distances between any pair of material points within the small neighborhood. Since, through motion, a material element dX becomes dx = FdX, whatever deformation there may be at X, is embodied in the deformation gradient, F (LAI; RUBIN; KREMPL, 1993). For large deformation analysis,

a multiplicative split in deformation tensor can be used for accounting volume changes as affected by moisture loss, F_M, temperature effects, F_T, and elastic properties of the material, F_{el}. In case of microwave process only the moisture deformation gradient (F_M - any loss in volume is taken up by the solid phase) and the elastic deformation gradient (F_{el} – depends upon the mechanical properties of the material, Young`s modulus and Poison's ratio) will be consider. This because the temperature gradient during fruit and vegetable drying has a much smaller effect in deformation than moisture and pressure gradient.

$$F = F_M F_{el} \tag{2.59}$$

The deformation gradient is related to the Jacobian, J ,which is obtained as the ratio of total volume change and volume change due to moisture and temperature effects.

$$J = \det(F) \tag{2.60}$$

The solid momentum balance for drying process that presents gas pressure and moisture changes as driving mechanism are proposed by Dhall and Datta (2011) as:

$$\vec{\nabla} \cdot \sigma'' = \vec{\nabla} P \tag{2.61}$$

The Cauchy Stress Tensor σ'' and p_v is the gas pressure due to internal vapor generation during microwave process are calculated by the solid momentum balance written in Lagrangian reference with the Second Piola-Kirchoff stress tensor S'' and the elastic deformation gradient tensor F_{el}.

$$\vec{\nabla}_X \cdot (S'' F_{el}^T) = \vec{\nabla} P \tag{2.62}$$

The first one is related to Cauchy stress by:

$$S'' = J_{el} F_{el}^{-1} \sigma'' F_{el}^{-T} \tag{2.63}$$

Due to the large deformations, which the fruit undergoes during drying, (RAKESH; DATTA, 2011) linear elasticity should not be applied, and the moisture-induced shrinkage of the tissue needs to be modeled by nonlinear elasticity theory (DEFRAEYE; RADU, 2018).The fruits and vegetables are approached as isotropic hyperelastic materials, which was applied in other drying studies(DEFRAEYE; RADU, 2018; GULATI; ZHU; DATTA, 2016; RAKESH; DATTA, 2011). The viscoelasticity is not considered because the deformation is slow (GULATI; DATTA, 2015). Some authors classified the potatoes, eggplants, pears as viscoelastic material because the relationship between stress and strain depend on time (FANTA et al., 2014; LLAVE et al., 2016; SAKAI; YANG; WATANABE, 2002).

For hyperelastic materials the Second Piola-Kirchoff stress tensor, S" , is described as a function of Green Lagrange Tensor for elastic strain, E_{el}, using strain energy function, W.

$$S'' = \frac{\partial W}{\partial E_{el}} \tag{2.64}$$

The elastic Green-Lagrange strain tensor is defined as:

$$E_{el} = \frac{1}{2}\left(F_{el}^{T} F_{el} - I\right) \tag{2.65}$$

Where I is the identity tensor and F_{el} the elastic deformation gradient tensor. The Green-Lagrange strain gives the information about the change in the square length of elements.

In the mathematical description of material behavior, the response of the material is characterized by a constitutive equation which gives the stress as a function of the deformation history of the body. Different constitutive relations allow us to distinguish between a viscous fluid and a rubber or concrete. In a hyperelastic material the deformation is independent of the load path applied (BELYTSCHKO; LIU; MORAN, 2000). The Neo-Hookean material model is an extension of the isotropic linear Hooke's Law to large deformation and is being used to describe hyperelastic materials as abovementioned.

$$W = \frac{K}{2}(J_{el} - 1)^2 - \frac{G}{2}(\overline{I_1} - 3) \tag{2.66}$$

In which K and G are the bulk and the shear modulus, respectively. $\overline{I_1}$ is the first invariant of the Right-Cauchy Green tensor, for deviatoric part of elastic deformation gradient, $\overline{F_{el}}$, $F_{el} = J_{el}^{1/3}\overline{F_{el}}$.

To estimate elastic Jacobian, J_{el}, the moisture Jacobian also needs to be defined. According to Dhall and Datta (2011), if V is the REV volume at moisture volume fraction ($\emptyset_l$) the change in volume can be equaled to change in volume of moisture to be:

$$V - V_0 = \emptyset_l V - \emptyset_{l0} V_0 \tag{2.67}$$

$$J_M = \frac{V}{V_0} = \frac{1 - \emptyset_{l,0}}{1 - \emptyset_l} = 1 + \epsilon_m = 1 + \beta_{vol} M_l (c_l - c_{l,0}) \tag{2.68}$$

In which ϵ_m is the volumetric shrinkage strain, β_{vol} is the volumetric shrinkage coefficient and c_l is the moisture concentration (DEFRAEYE; RADU, 2018). Lu, Wang and Jiang (2015) reported a coefficient value of 1.26 x 10^{-2} for this parameter during convective drying of potato. Additional values can be found in the **Table 2.3**.

Table 2.3: Values for the volumetric shrinkage coefficient for food during different drying process.

Process	Value	Reference
Convective drying of rectangle-shape potato	0.0126	(LU; WANG; JIANG, 2015)
Convective drying of 38 potato cubes	0.1558	(FRIÁS; CLEMENTE; MULET, 2010)
Microwave vacuum drying of cylinder-shape potato	0.4729	(ISHIBASHI et al., 2022)
Convective drying of apple slices	0.672	(TOUJANI et al., 2014)
Vacuum drying of cheese with different thickness	0.017-0.004	(ERMOLAEV et al., 2021)

The volumetric shrinkage coefficient also mentioned as coefficient of hygroscopic swelling or moisture expansion coefficient is used as a constant value that correlates the deformation strain related to hygroscopic forces with the gain or loss of water during drying of food. Based on these studies is possible to observed that the coefficient will change with the food, food size and process applied (AREGAWI et al., 2013; DEFRAEYE; RADU, 2018;

ERMOLAEV et al., 2021; HOU; ZHOU; WANG, 2020; LU; WANG; JIANG, 2015; YUAN et al., 2019), with values from 0.004 to 0.672. The software COMSOL apply the **Equation (2.68)** abovementioned and to use the constant provide by other authors the units need to be check. In this case, the initial moisture content and dried mass of each sample should be considered.

The elastic Jacobian can be obtained by:

$$J_{el} = \frac{J}{J_M} \tag{2.69}$$

Because of deformation the food porosity changes with time according to:

$$\emptyset(t) = 1 - \frac{1 - \emptyset_0}{V(t)/V_0} = \frac{1 - \emptyset_0}{J(t)} \tag{2.70}$$

If the total porosity ($\emptyset$) of the material is changing with time, the liquid and gas permeability also change, because it alters the resistance flow of fluid phases through the material. To account these changes, the liquid and gas permeabilities are multiply for a porosity factor (**Equation (2.71)**) given by the Kozeny-Carman equation (BEAR, 1972):

$$f(\emptyset) = \left(\frac{\emptyset}{\emptyset_0}\right)^3 \left(\frac{1 - \emptyset_0}{1 - \emptyset}\right)^2 \tag{2.71}$$

The change in porosity, liquid saturation and evaporation is shown in **Figure 2.4**. According Ashim K. Datta (2021) during drying the size of the pore can decrease (shrinkage) or increase (puffing). If during the pore shrinkage not enough water is lost the liquid pore saturation increase, because the pore decreases in size but keep most of the water inside. When the pore is more saturated less void space is available which difficult the evaporation phenomenon to happen. In the opposite direction the pore liquid saturation decreases when puffing is observed during drying, what facilitates even more the evaporation.

Figure 2.4: Representation of change liquid saturation and evaporation of a pore during drying.

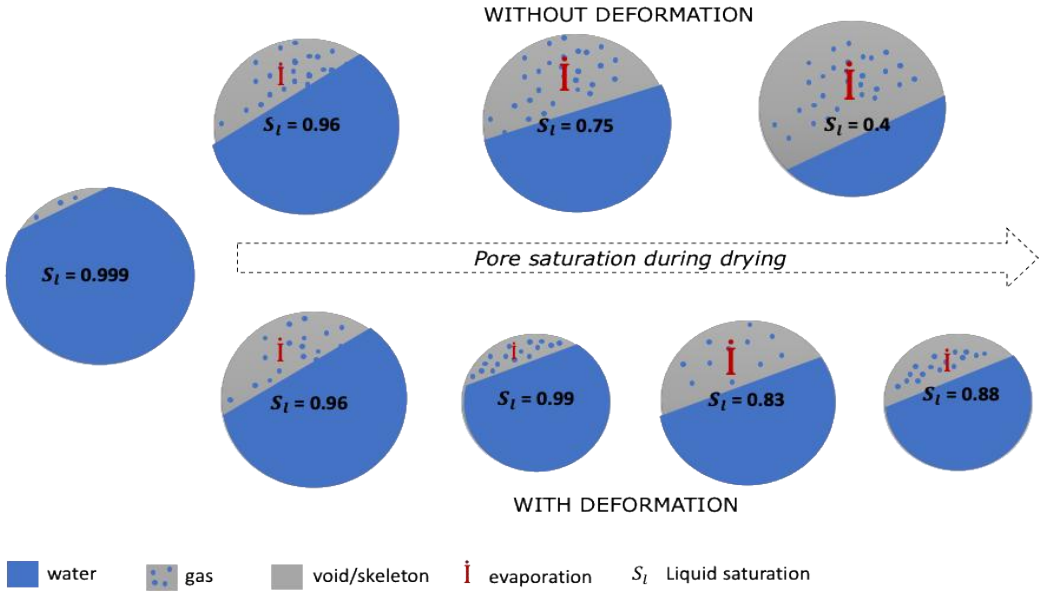

Source: Author, based in Ashim Datta (2021)

Another important phenomenon that occurs during drying is the rubbery–glassy phase transition of the material (GULATI; DATTA, 2015; KATEKAWA; SILVA, 2006). The glass transition changes the state of the material from soft and rubbery to hard and glassy. A state diagram, glass transition temperature (T_{gt}) versus the mass fraction of water, provides information about the states of the material. If the temperature of the material stays above T_{gt} curve, it is in a rubbery state. When the material achieves the glassy state, the stresses are higher what contributes to the development of textural attributes, as case-hardening (ACHANTA; OKOS, 1996). The **Equation (2.72)** adapted from (BENCZÉ DI; TOMKA; ESCHER, 1998) is used to predict the T_g temperatures based in the mass fraction of water (w_l) for a starch solution.

$$T_{gt} = 2652.5w_l^2 - 1570.3w_l + 518.65 \quad (2.72)$$

This rubbery–glassy phase transition together with flow and deformation play a major role in determining the final quality of the dried product and can explain the development of internal product microstructure (GULATI; DATTA, 2015; WANG; BRENNAN, 1995). Another way to determine the material state is using Poisson's ratio (ν), which is the ratio of

transversal strain (ϵ_d) to axial strain (ϵ_a), **Table 2.4**. It measures the deformation in the perpendicular direction of loading. Typical value for Poisson's ratio is 0.3 for steel and 0.5 for rubbery (LAI; RUBIN; KREMPL, 1993). During drying the Poisson's ratio for potato changes from 0.49 to 0.3, which means the transition between rubbery to glassy state, respectively.

Other important mechanical property is the Young modulus, or modulus of elasticity (E). It is the slope of material stress curve, stress (σ) versus strain (ϵ_a) of a material during deformation. Based in this curve the material is defined in linear elastic, hyperelastic or viscoelastic. The Poisson ratio and Young modulus give the based for material matrix and the mechanical properties as Lame parameter (λ), Bulk modulus (K) and Shear modulus (G) as can be seen in **Table 2.4**.

Table 2.4: Structural mechanic properties definition equations and common values for potato.

Parameter	Expression	Common Value for Food	Source
Poisson's ratio	$\nu = -\frac{\epsilon_d}{\epsilon_a}$	Potato: 0.49-0.5 Apple: 0.495 Eggplant: 0.492 Canned Ham: 0.49999	(DEFRAEYE; RADU, 2018; FINNEY; HALL, 1967; LLAVE et al., 2016; NOWAK; MARKOWSKI; DASZKIEWICZ, 2015)
Young's modulus	$E = \frac{\sigma}{\epsilon_a}$	Potato: 2.83 MPa Apple: 0.5 MPa Eggplant: 3.4 MPa Canned Ham: 0.1853 MPa	(DEFRAEYE; RADU, 2018; NOWAK; MARKOWSKI; DASZKIEWICZ, 2015; RUSSO; ADILETTA; DI MATTEO, 2013; YANG; SAKAI, 2001)
Lame's parameter	$\lambda = \frac{E\nu}{(1+\nu)(1-2\nu)}$	Potato 4.65×10^7 N/m^2	Calculated
Bulk modulus	$K = \frac{E}{3(1-2\nu)}$	Potato 4.594×10^5 N/m^2	(RAKESH; DATTA, 2011)
Shear modulus	$G = \frac{E}{2(1+\nu)}$	Potato 7.94×10^4 N/m^2	(RAKESH; DATTA, 2011)

3. MATERIAL AND METHODS

This Section explains the methodology employed to collect data on moisture, temperature, and visual images through laboratory experiments, as well as for solving the mathematical model using numerical simulation.

According to the flowchart, **Figure 3.1**, the methodology was divided in Laboratory Experiments, Mathematical Modeling, and the Computational Implementation. Laboratory experiments covered various steps: sample preparation (1), which included considerations for food system storage and shape; the MWVD (2) as the core drying technique; the moisture assays (3), involving determination of the initial kinetic curve followed by moisture measurements before and after deformation; temperature assays (4), capturing top surface temperature changes pre and post deformation; and deformation assays, in which the focus were to evaluate the area before and after deformation. The mathematical modeling was developed based in key elements: assumptions (1), that defined model scope and fundamental considerations; the parameters (2) for both sample and oven structure; the governing equations (3) describing each phase of the sample and the wave distribution; and the initial and boundary conditions (4). Lastly, the computational implementation happened in two stages, the first (1) focusing on wave distribution and the second (2) involving heat and mass transfer coupled with deformation.

Figure 3.1: Flowchart of Material and Methods employed for MWVD modeling

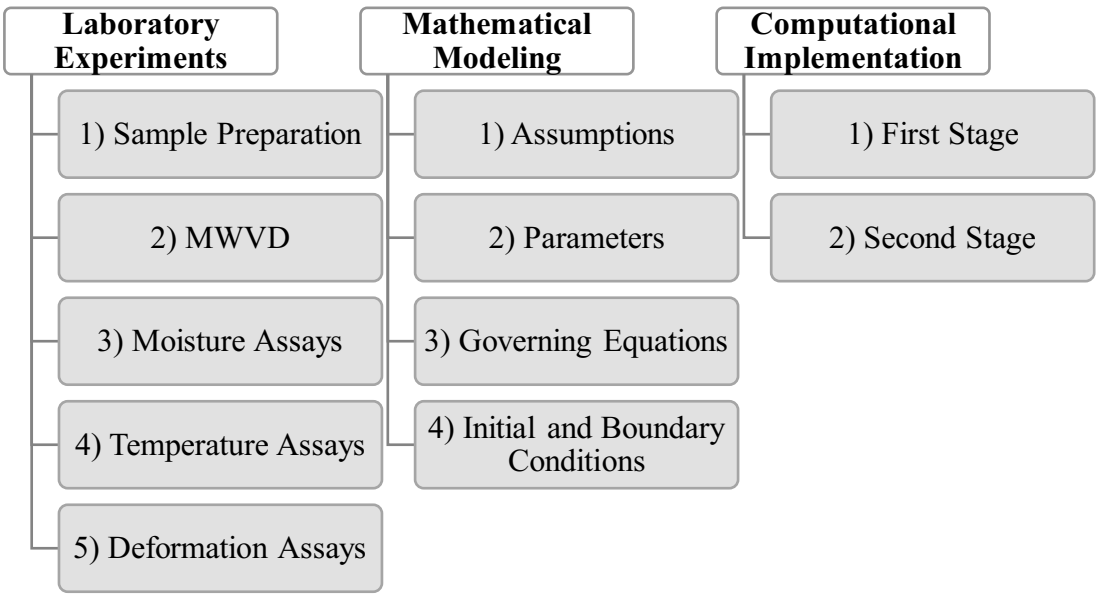

Source: Author

3.1 LABORATORY EXPERIMENTS

3.1.1 Sample Preparation

The food matrix utilized in this study was a potato (*Solanum tuberosum* cv Agata). The selection was based on the data available in the literature; potatoes present a simple structure and are a widely consumed dried product. It is worth to mentioning that potato material presents some advantages such as homogeneity, and isotropy of thermal-mass properties.

Before experimentation the vegetables were washed and stored in a refrigerator at (20 ± 2°C) for 24 h. After that time, they were peeled and cut into a cylinder shape 25 x 35 (h x r) mm. To swiftly cut the potato into cylindrical shapes, a customized stainless-steel cylinder with sharp edges was employed. This tool, along with a caliper rule, ensured consistent size patterns were maintained across all samples. Photographs of raw potato sample in cylindrical format are illustrated at **Figure 3.2**. The pictures present the superior and lateral view of potato placed on a base with pen marks. The marks, and the blue dot, were tools to ensure consistent positioning for each picture.

Figure 3.2: Photographs of the potato sample: Superior View (S) and Lateral View (L).

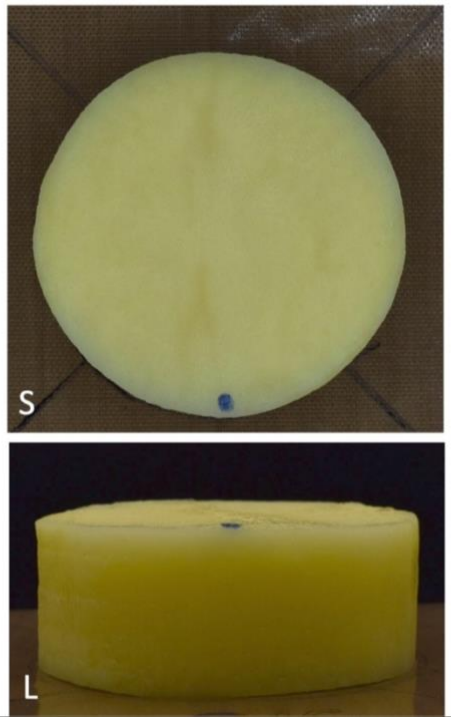

Source: Author

The potatoes presented initially 0.852 ± 0.002 kg/kg wet basis and water activity of 0.996 ± 0.002 at 25 °C.

3.1.2 MWVD System

The drying system was composed by an adapted microwave oven (1000 W, 2450 MHz, Electrolux, MEX55, Brazil), a propylene vacuum chamber, a vacuum pump (DVP, LC.305, Italy) and a standard digital vacuum gauge (Warme, WTP4010, Brazil). The domestic microwave oven equipped with variable power level settings (10–100%) and a propylene vacuum chamber, was adapted by Monteiro et al. (2015) at PROFI, **Figure 3.3**.

Figure 3.3: MWVD developed by Monteiro et al. (2015) in detail the inside of the oven cavity, the vacuum chamber, and the waveguide.

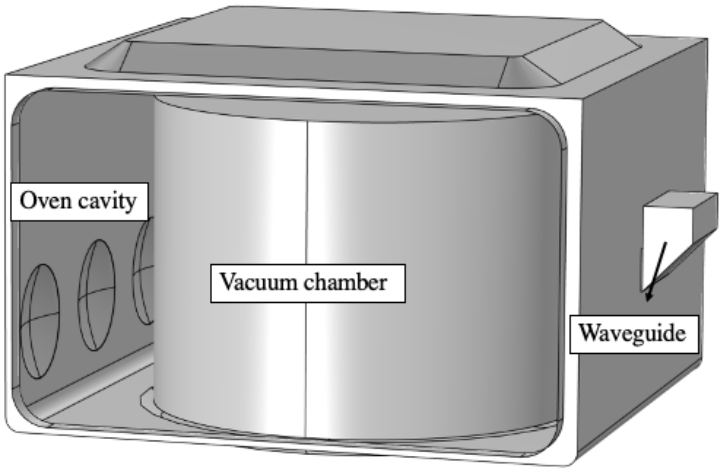

Source: Author

The pressure of 10 kPa were maintained through a vacuum pump and controlled using a standard digital vacuum gauge. Before starting the drying procedures, a power study was executed to ascertain the real power within the oven cavity according to IEC 60705/2010.

Following the sample and drying system definition the data collection of moisture, temperature and image could be performed. The **Figure 3.4** depicts the times selected to build the kinetic curve, and the pre and pos drying assays for moisture (X_{db}), surface temperature (T), and superior and lateral images. All these methods will be described with details in the next Sections.

Figure 3.4: Scheme of Laboratory Experiments realized to collect moisture (X_{db}), surface temperature (T), and superior and lateral images.

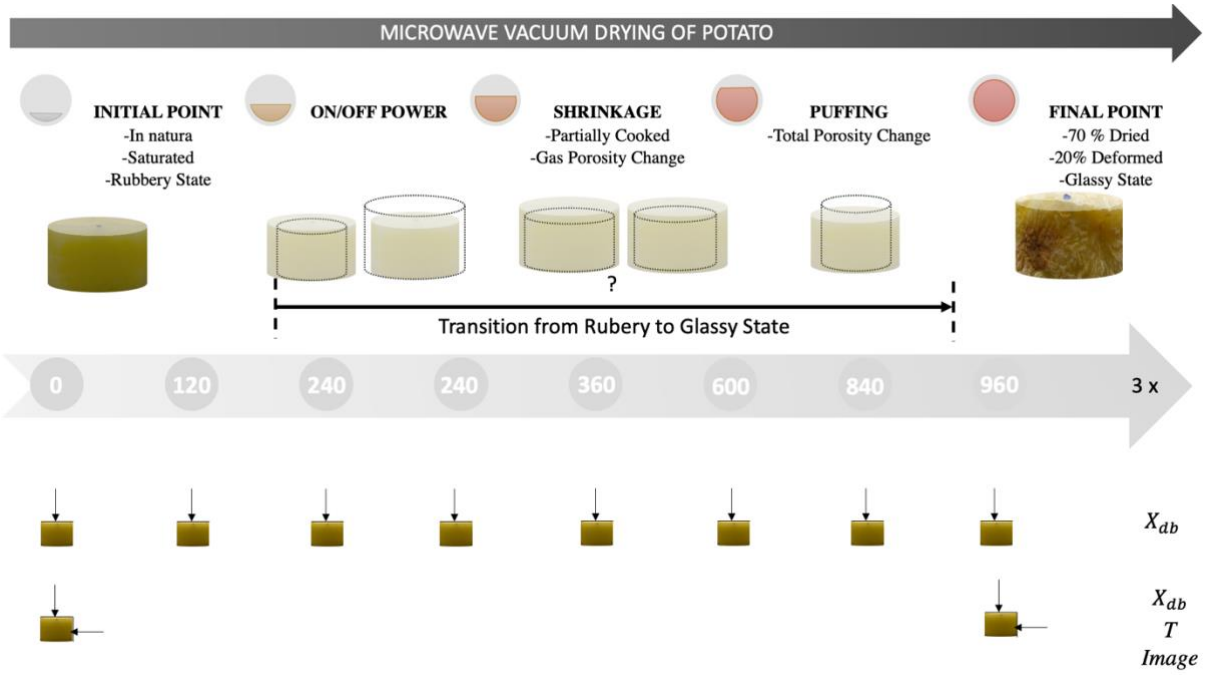

Source: Author

3.1.3 Kinetic curve and moisture measurements

Figure 3.5 is a scheme of mass measurement, where the pressure and power source during drying and weighing are presented. The dashed line indicates the pressure to which the potato was subjected during the drying process. When the pressure is at 10 kPa, the potato was inside the chamber, while the line reaching 100 kPa indicates that the sample was outside for mass measurement collection. The time intervals for mass measurements were chosen to ensure a more accurate representation of the kinetic curve. Before finalizing the triplicate measurements for the last kinetic curve, various time intervals were tested. The continuous gray line represents the Power Source applied by the microwave oven. The duty cycle occurred because the power was set in 50%, leading to an alternating ON/OFF operation cycle for the magnetron, which was the device responsible for generating the microwaves. When the magnetron was ON the curve is at 1×10^6 W/m^3, while it is set 0 W/m^3 when the magnetron is OFF.

Figure 3.5: Scheme of mass measurement of sample in a digital balance and the application of microwave power and vacuum during drying.

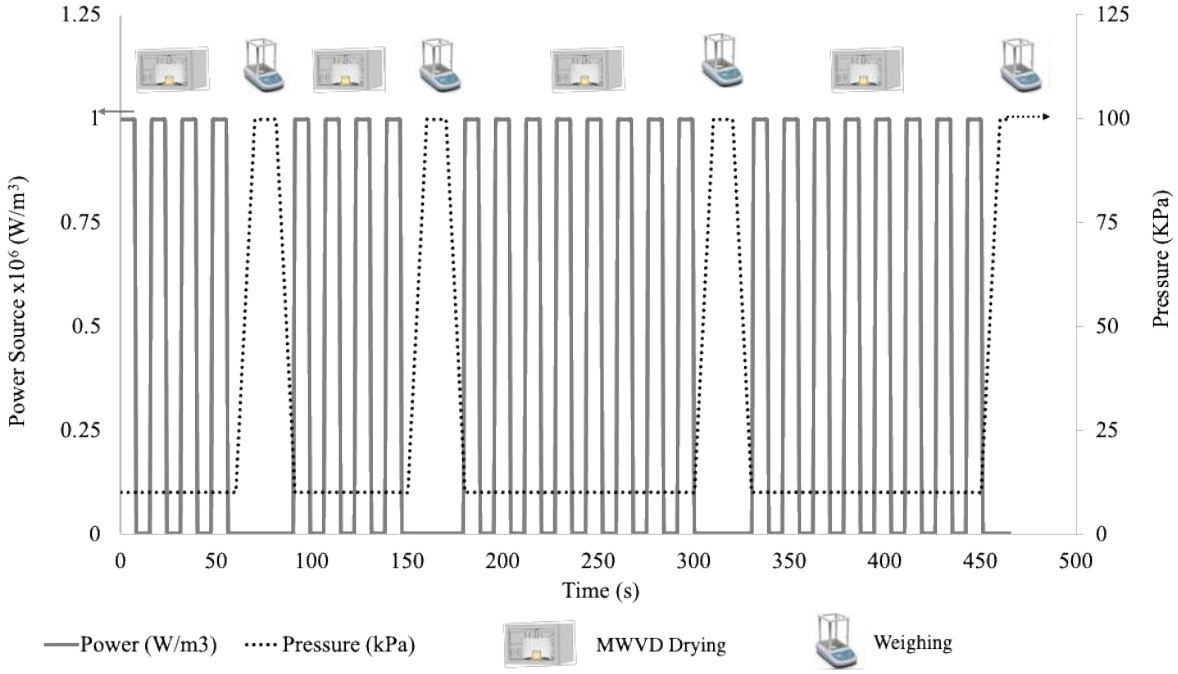

Source: Author

Moisture loss was measured using a digital weighing balance (Shimadzu, AY220, Philippines); 0.0001 g least count. Following the MWVD process, each sample was maintained at 105 ± 1 °C for 24-48 h. Afterward, the samples were reweighed, allowing for the calculation of the percentage of water lost in relation to the mass of solids.

3.1.4 Surface Temperature

Spatial temperature profiles were measured using an infrared thermal camera with accuracy of ± 2 °C (FLIR, model T360, Switzerland). The camera was placed outside a photograph chamber, where the sample was positioned. FLIR QuickReport 1.2 SP2 software was used to record and analyze surface temperature.

The infrared camera was calibrated as proposed by Albatici *et al.* (2013). The calibration required changing the emissivity value of the camera, room humidity and room temperature based in a hygrometer (Texto 610, Germany).

3.1.5 Deformation measurements

Deformation was determined by measuring changes in the surface area of initial and dried material. Snapshots of the sample were obtained using a digital camera (Nikon, D5500, Japan) in a photograph chamber.

The Images were analyzed using the software ImageJ (http://rsbweb.nih.gov//ij), with *Set Scale* and *Measure* tools for each surface. The measurement procedure involved image segmentation by converting color images to binary images to identify the surface area. **Figure 3.6** illustrates the classification of areas as superior and lateral; the measurements were conducted using a scale that was pre-established in the images. The superior area was matched to a circle, while the lateral area was matched to a rectangle. For the lateral area, two different measurements were taken: one without considering the bubbles formed during MWVD and the other considering them.

Figure 3.6: Diagram illustrating the methodology for measuring the superior and lateral areas.

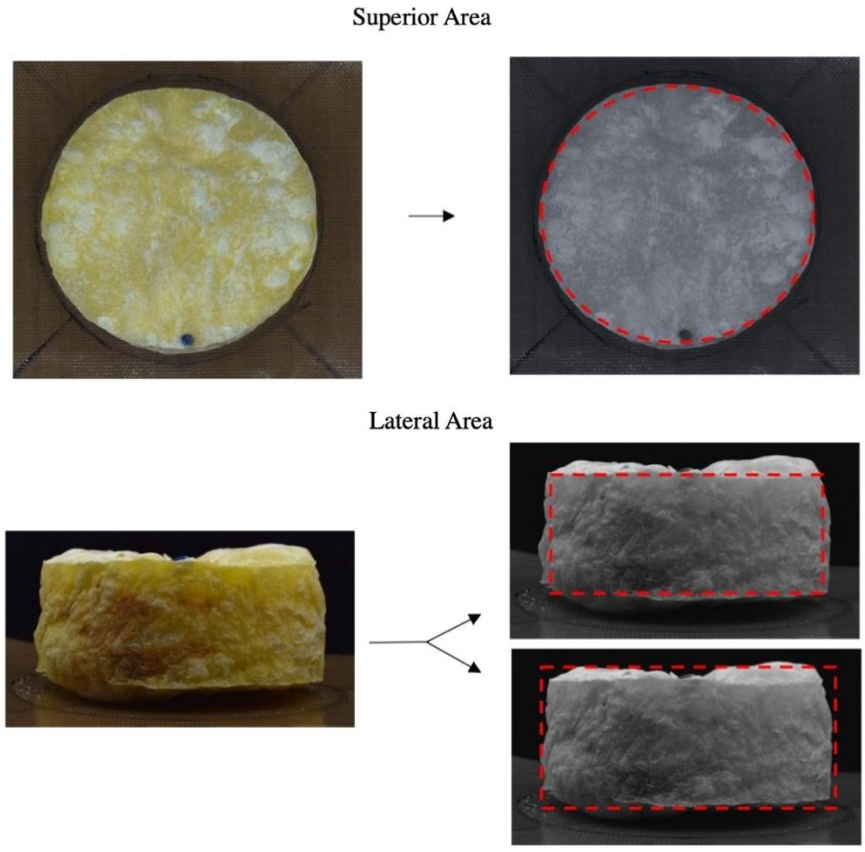

Source: Author

3.2 MATHEMATICAL MODELING

3.2.1 Model assumptions

The drying occurs as result of microwave heating in a vacuum cavity with porous media defined as representative elementary volume (REV) where the properties are defined as spatial average. The assumptions considered to mathematical modeling the food domain:

a) There were three phases (solid, liquid water and water vapor).
b) Gas phase followed ideal gas law.
c) Thermal equilibrium existed between all phases.
d) Regarding evaporation term, there was a non-equilibrium between water in the liquid phase and water vapor in the gas phase.
e) Evaporation/condensation (phase change) was distributed throughout the food domain.
f) Pressure-driven flow and capillary diffusivity were responsible for liquid transport.
g) Water loss and pressure gradient were considered factors for deformation.
h) The sample was in contact with the bottom of the vacuum chamber.
i) The sample was static inside the vacuum chamber, no rotation applied.
j) The sample was treated as a homogeneous cylinder, where symmetry could be applied.

Furthermore, the assumptions considered to mathematical modeling the wave distribution:

k) The oven walls were made of metal and considered perfect electrical conductors.
l) The vacuum chamber remained stationary without any rotation.
m) The waves propagated inside the entire system (microwave cavity, vacuum chamber, and sample), considering every structure detail.

3.2.2 Governing Equations

An illustrative chart in **Figure 3.7** explained all the phenomena and conditions used in the mathematical model in this study. Starting from the core of the diagram the modeled and

solved process is presented: MWVD of a deformable porous medium. Moving towards the outer areas of the core, the different phases presented in the porous medium are depicted: solid, gaseous, and liquid. In the blue rectangles, the four physical phenomena considered in the mathematical model are represented: Mass Transfer (1), Heat Transfer (2), Solid Mechanics (3) and Electromagnetism (4). Each rectangle is associated with specific structures, using mass transfer as an illustrative example. Linked to mass transfer, the initial and boundary conditions are found in the rectangle on the left with a solid line, representing, respectively, the initial conditions of sample moisture and predetermined fluid pressures and flows. Also related to mass transfer, in the dotted lines, are the properties that have the greatest impact on the simulation, such as density, viscosity, permeability and diffusivity. Finally, under each blue rectangle, the phenomena associated with each physics are indicated. In the case of mass transfer, these phenomena include pressure gradient, diffusion, and phase change. The other physics involved in the mathematical modeling and simulations were arranged in the diagram following the same logic.

Figure 3.7: The different physical phenomena, initial conditions, and boundary conditions associated with the microwave vacuum drying simulation.

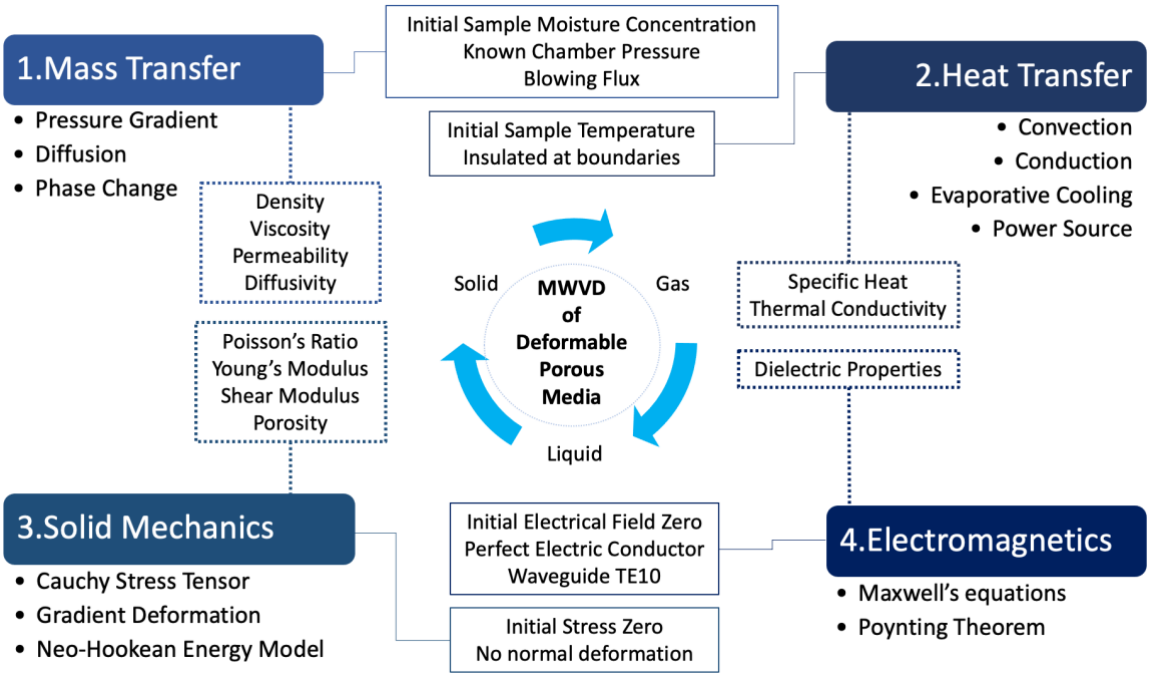

Source: Author

The equations used in the model are presented according to the abovementioned diagram where the Mass transfer (1), Heat Transfer (2), Solid Mechanics (3) and Electromagnetics (4) are shown with the phenomena involved in each of them, also the initial and boundary condition, and the main properties evaluated during simulation.

Mass conservation (1) equation for liquid water and water vapor was:

$$\frac{\partial c_l}{\partial t} + \vec{\nabla} \cdot \vec{n}_{l,G} = -\dot{I} \tag{3.1}$$

$$\frac{\partial c_v}{\partial t} + \vec{\nabla} \cdot \vec{n}_{v,G} = \dot{I} \tag{3.2}$$

Where $c_l = \rho_l S_l \emptyset$ and $c_v = \rho_v S_v \emptyset$ were the mass volumetric concentration of liquid phase (l) and vapor phase (v) respectively, considering density (ρ_i), saturation (S_i) and total porosity ($\emptyset$). The fluxes in mass conservation equations were defined with respect to a ground frame of reference. What means that flux was added arising due to movement of the solid phase deformation. The $\vec{n}_l$ and $\vec{n}_v$ were the mass flux of liquid and vapor water respectively and were specified according to the equations:

$$\vec{n}_{l,G} = -\rho_l \frac{k_{in} k_{rel,l}}{\mu_l} \vec{\nabla} P - D_{cap,l} \vec{\nabla} c_l + c_l \overline{v_s} \tag{3.3}$$

$$\vec{n}_{v,G} = -\rho_v \frac{k_{in} k_{rel,v}}{\mu_v} \vec{\nabla} P + D_{self} \vec{\nabla} c_v + c_v \overline{v_s} \tag{3.4}$$

In which is possible to identify the gradient of gas pressure ($\vec{\nabla}P$), capillarity diffusion ($D_{cap,l}$) and a gas self-diffusion term (D_{self}) that accounts the random movements of vapor molecules in the porous media.

The $\dot{I}$, in the mass conservation equation, denoted the non-equilibrium formulation for phase change, evaporation/condensation, defined through (HALDER; DHALL; DATTA, 2007a):

$$\dot{I} = K_{evap}\left(p_{v,eq} - P\right) \frac{M_v}{RT} S_v \emptyset \tag{3.5}$$

where, K_{evap} is a material and process-dependent parameter reciprocal of equilibration time, P is the vapor pressure obtained from Darcy's law, $p_{v,eq}$ is the equilibrium vapor pressure of the food material obtained by the product of saturation pressure (p_{sat}) and moisture sorption isotherm.

The saturation S_i and the total porosity ($\emptyset$) were defined as:

$$S_i = \frac{V_i}{\emptyset\, V} \tag{3.6}$$

$$\emptyset = \frac{\sum_{i=l,v} V_i}{V} \tag{3.7}$$

In which V_i is the volume occupied by a fluid.

The energy conservation equation (2) included heat conduction, $\vec{\nabla}(k_{ef}\nabla T)$, convection of fluid phases, $(\vec{n}_{l,G}C_{p,l} + \vec{n}_{v,G}C_{p,v}) \cdot \vec{\nabla}T$, evaporative cooling, $\lambda_{ev}\dot{I}$, and microwave heat source, $\dot{Q}$.

$$\rho C_{p,ef}\frac{\partial T}{\partial t} + (\vec{n}_{l,G}\, C_{p,l} + \vec{n}_{v,G}\, C_{p,v}) \cdot \vec{\nabla}T = \vec{\nabla}\left(k_{ef}\vec{\nabla}T\right) - \lambda_{ev}\dot{I} + \dot{Q} \tag{3.8}$$

The properties of the porous media were obtained by averaging those of pure components, weighted by their volume fractions:

$$\rho C_{p,ef} = (1 - \emptyset_0)\rho_s C_{p,s} + \emptyset\left(S_l\rho_l C_{p,l} + S_v\rho_v C_{p,v}\right) \tag{3.9}$$

$$k_{ef} = (1 - \emptyset_0)k_s + \emptyset(S_l k_l + S_v k_v) \tag{3.10}$$

Where ρ, C_p, k are the density, specific heat and thermal conductivity of each phase, respectively.

Regarding solid mechanics equations (3), a multiplicative split in deformation tensor, F, was used for accounting volume changes as affected by moisture loss, F_M, and elastic properties of the material, F_{el}.

$$F = F_M F_{el} \tag{3.11}$$

The deformation gradient was related to the Jacobian, J:

$$J = \det(F) \tag{3.12}$$

The solid momentum balance for drying process that presents gas pressure and moisture changes as driving mechanism were proposed by Dhall and Datta (2011) as:

$$\vec{\nabla} \cdot \sigma'' = \vec{\nabla} P \tag{3.13}$$

The Cauchy Stress Tensor σ'' and the gas pressure p_v were calculated by the solid momentum balance written in Lagrangian reference with the Second Piola-Kirchoff stress tensor S'' and the elastic deformation gradient tensor F_{el}.

$$\vec{\nabla}_X \cdot (S'' F_{el}^T) = \vec{\nabla} P \tag{3.14}$$

The first one is related to Cauchy stress by:

$$S'' = J_{el} F_{el}^{-1} \sigma'' F_{el}^{-T} \tag{3.15}$$

For hyperelastic materials the Second Piola-Kirchoff stress tensor, S'' , was described as a function of Green Lagrange Tensor for elastic strain, E_{el}, using strain energy function, W.

$$S'' = \frac{\partial W}{\partial E_{el}} \tag{3.16}$$

The elastic Green-Lagrange strain tensor was defined as:

$$E_{el} = \frac{1}{2}\left(F_{el}^T F_{el} - I\right) \tag{3.17}$$

Where I is the identity tensor and F_{el} the elastic deformation gradient tensor. The Neo-Hookean material model was used to describe hyperelastic materials:

$$W = \frac{K}{2}(J_{el} - 1)^2 - \frac{G}{2}(\overline{I_1} - 3) \tag{3.18}$$

where K and G are the bulk and the shear modulus, respectively. $\overline{I_1}$ is the first invariant of the Right-Cauchy Green tensor, for deviatoric part of elastic deformation gradient, $\overline{F_{el}}$, $F_{el} = J_{el}^{1/3}\overline{F_{el}}$.

To estimate elastic Jacobian, J_{el}, the moisture Jacobian was also defined:

$$J_M = \frac{V}{V_0} = \frac{1 - \emptyset_{l,0}}{1 - \emptyset_l} = 1 + \beta_{vol} M_w (c_l - c_{l,0}) \tag{3.19}$$

And then is easy to obtain:

$$J_{el} = \frac{J}{J_M} \tag{3.20}$$

The electric field distribution inside the oven cavity was obtained by solving the Maxwell's equation:

$$\overrightarrow{\nabla} \times \overrightarrow{H_s} = (\sigma + j\omega)\overrightarrow{E_s} \tag{3.21}$$

$$\overrightarrow{\nabla} \times \overrightarrow{E_s} = -j\varpi\overrightarrow{H_s} \tag{3.22}$$

$$\overrightarrow{\nabla} \times \overrightarrow{B_s} = 0 \tag{3.23}$$

$$\overrightarrow{\nabla} \times \overrightarrow{D_s} = 0 \tag{3.24}$$

In order to characterize the material medium some properties were defined: electric permittivity $\varepsilon = \varepsilon_0\varepsilon_r$ (F/m), magnetic permeability, $\mu = \mu_0\mu_r$ (H/m), and the conductivity

σ (S/m) characterized the material medium (SADIKU, 2014). Here, ε_r is the relative permittivity or dielectric constant, ε_0 is the permittivity of free space, μ_r is the relative permeability ($\mu_r = 1$) and μ_0 the permeability of free space.

The Power absorbed per unit volume in the material was obtained from the Poynting Theorem:

$$Q(x, y, z, t) = \frac{1}{2}\,\omega\varepsilon_0\varepsilon''\left|\vec{E}\right|^2 \tag{3.25}$$

To describe the dielectric properties change, the equation of Landau, Lifhitz and Looyenga was used:

$$\varepsilon_c^{1/3} = (1-\phi)(\varepsilon_s' - j\varepsilon_s'')^{\frac{1}{3}} + S_l\phi(\varepsilon_l' - j\varepsilon_l'')^{\frac{1}{3}} + S_g\phi\left(\varepsilon_g' - j\varepsilon_g''\right)^{\frac{1}{3}} \tag{3.26}$$

where, s, l and g are the solid, liquid and gas phases, respectively, $\emptyset$ and S_i depict porosity and percentage or saturation in the media.

Regarding the boundary conditions, as depicted in **Figure 3.8**, there was no mass and heat flow in the bottom of the media. For the gas phase conservation equation, the gas pressure on the sample surface was the vacuum chamber pressure (P^{ch}).

$$P = P^{ch} \tag{3.27}$$

An energy balance on the surface of the porous medium reveals that it is possible to assume a prescribed flow as a boundary condition for the conservation of energy, also the thermal conductivity is insignificant in the vacuum chamber ambient.

$$\vec{\nabla}T = 0 \tag{3.28}$$

For the liquid phase conservation equation, it was considered that liquid water can be pushed out of the porous medium when the internal pressure gradients are high enough to overcome capillary forces. When the internal product of the liquid phase velocity vector with the normal unitary vector of the surface is positive, the capillary mass flow is zero ($\vec{n}\cdot\vec{v}_{l,G} \geq$

0), in other words, water is transported out of the porous medium associated with the velocity field.

For solid mechanics the normal displacement of the bottom surface (lying on the chamber base) was set to be zero. The other boundaries are unconstrained and free to move.

Besides the boundary conditions used in the simulations, **Figure 3.8** also brings the system of coordinates applied in the 2D and 3D model. The 3D model was solved considering the microwave cavity, the vacuum chamber and the sample applying cartesian coordinates. The 2D model consider just the potato with an axisymmetric approach, applying cylindrical coordinates. More details about these two models will be explained in Section 3.3 of Computational Implementation.

Figure 3.8: Representation of MWVD and porous media geometry with the boundary conditions used in simulations.

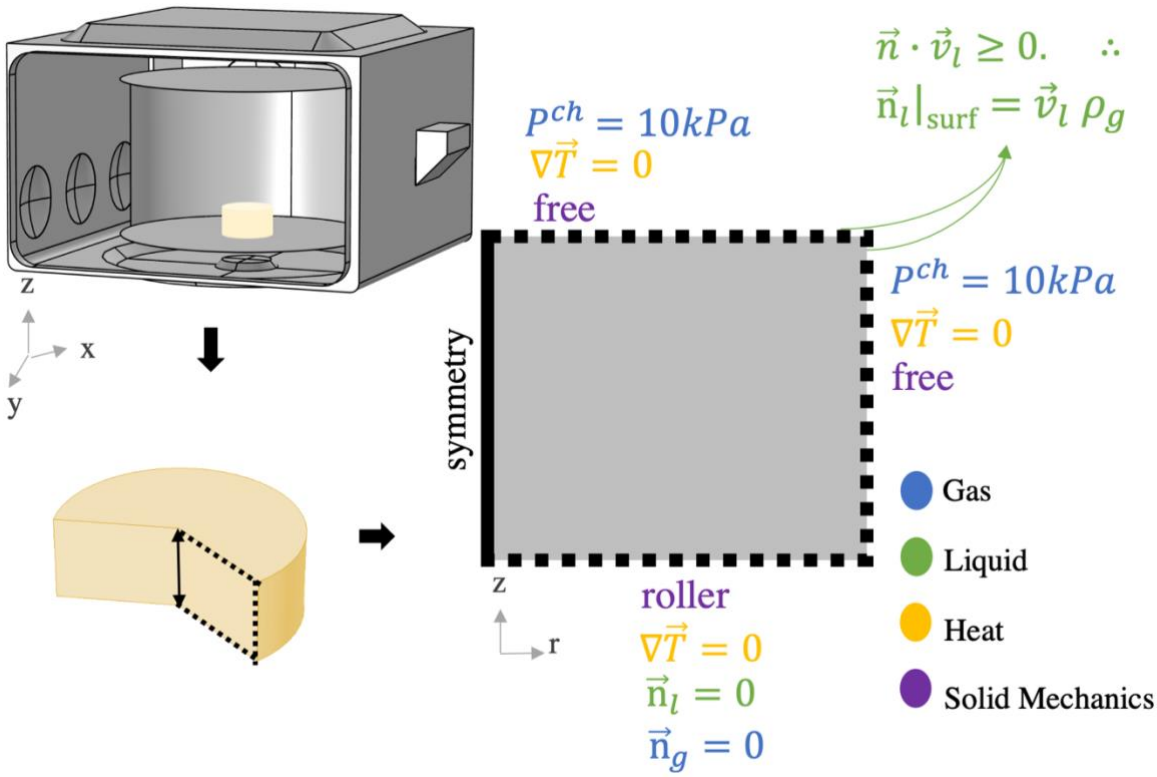

Source: Author

For the microwave cavity, the walls are assumed to be perfect electrical conductors ($\sigma \rightarrow \infty$) such that at the air–wall interface inside the oven cavity, the tangential component

of electric field is zero, the electromagnetic wave is completely reflected. The microwave source was described as a rectangular port with TE_{10} mode, excited with 767 ± 26 W power.

$$\vec{n} \times \vec{E} = 0 \tag{3.29}$$

The parameters applied in the model for numerical solution are presented in the **Table 3.1**.

Table 3.1: Parameters used in the model for numerical simulation

Parameter	Value	Reference
Sample – potato (m)	Cylinder (Height=0.025 x Diameter=0.035)	
Initial Conditions		
Temperature, T_0 (K)	293.15	
Pressure, P_0 (kPa)	10	
Saturation, S_0	0.999	Assumed
Electric Field, $\vec{E}$ (V/m^2)	$\vec{E} = 0$	
Displacement, u (m)	$u = 0$	
Electromagnetic		
Microwave Power Source, P^w(W)	767	Calculated
Microwave Frequency, f (GHz)	2.45	
Dielectric constant, ε'_i		
Water (1% salt)	75.004	(NELSON; DATTA, 2001)
Vapor	1	
Solid	4	(MUDGETT et al., 1980)
Dielectric Loss, ε''_i		
Water (1% salt)	21	(NELSON; DATTA, 2001)
Vapor	0	
Solid	0.2	(MUDGETT et al., 1980)
Transport		
Molar Mass, M_l (g/mol)	18	(BEJAN, 2013)
Specific Mass, ρ_i(kg/m³)		
Water	$1001.4 - 0.1276(T - 273) - 0.0029(T - 273)^2$	(MCCABE; SMITH; HARRIOTT, 1993)

Vapor	$\frac{M_l P}{RT}$	
Solid	1528	(FARKAS; SINGH; RUMSEY, 1996)
Viscosity, μ_i (Pa.s)		
Water	$2.74 \times 10^{-6} \exp\left(\frac{1735.5}{T}\right)$	(MCCABE; SMITH; HARRIOTT, 1993)
Vapor	$1.7096 \times 10^{-8} T^{1.1146}$	(PERRY; GREEN; MALONEY, 1997)
Intrinsic Permeability, $k_{in,i}$ (m²)		
Water	$f(\emptyset) \times 1 \times 10^{-15}$	(DADMOHAMMADI et al., 2020)
Vapor	$k_{in,l}\left[\frac{1 + 0.15(k_{in,l})^{-0.37}}{p_v}\right]$	(TANIKAWA; SHIMAMOTO, 2009)
Relative Permeability, $k_{re,i}$		
Water	$\begin{cases}\left(\frac{s_l - 0.09}{1 - 0.09}\right)^3 & s_l > 0.09 \\ 0 & s_l < 0.09\end{cases}$	BEAR, 1972; DATTA, 2006
Vapor	S_v	(WARNING et al., 2012)
Thermal conductivity, k_i (W/m K)		
Water	0.59	(BEJAN, 2013)
Vapor	0.025	(BEJAN, 2013)
Solid (potato)	0.21	(DONSÌ; FERRARI; NIGRO, 1996)

Specific Heat, $C_{p,i}$ (J/kgK)		
Water	4182	(BEJAN, 2013)
Vapor	2029	(BEJAN, 2013)
Solid (potato)	1650	(ZHU et al., 2015)
Capillary diffusivity, $D_{cap,i}$ (m²/s)	$10^{-8}e^{-2,8+2X_{db}}$	(HALDER; DHALL; DATTA, 2007a)
Gas self-diffusivity, D_{self} (m²/s)	$\frac{\emptyset}{\tau}\frac{2.13}{P}\left(\frac{T}{273.15}\right)^{1.8}$	(WARNING et al., 2012)
Evaporation Constant, K_{evap}(1/s)	100	(HALDER; DHALL; DATTA, 2007b)
Latent heat of evaporation λ_{ev}(J/kg)	$\frac{10^7}{2.385\times10^{-3}P^{0.4343}+4.034}$	(ELLIOTT; LIRA, 2011)
Equilibrium vapor pressure, p_{eq}(Pa)	$p_{sat}e^{-0.094-\left(3.15e^{-23.44X_{db}}\right)}$	(WANG; BRENNAN, 1991)
Water saturation pressure, p_{sat} (Pa)	$10^3e^{(16.3872-\left(\frac{3885.7}{230.170+T}\right)}$	(SMITH; NESS; ABBOTT, 2007)
Porosity, $\emptyset_0$	0.903	Calculated from (BLAHOVEC; LAHODOVÁ; ZÁMEČNÍK, 2012)
Correction function, $f(\emptyset)$	$f(\emptyset)=\left(\frac{\emptyset}{\emptyset_0}\right)^3\left(\frac{1-\emptyset_0}{1-\emptyset}\right)^2$	
Tortuosity, τ	$1-0.49\ln(\emptyset S_v)$	(DADMOHAMMADI et al., 2020)
Solid Mechanics		
Poisson's ratio, ν	0.49	(FINNEY; HALL, 1967)
Elastic modulus, E (N/m²)	$1.69\times10^7\exp(-0.522\,X_{db})\ X_{db}\geq1.2$ $5.23\times10^7\exp(-1.704\,X_{db})\ X_{db}<1.2$	(YANG; SAKAI, 2001)
Shear modulus, G (N/m²)	$G=\frac{E}{2(1+\nu)}$	

Bulk Modulus, K (N/m^2)	$K = \frac{E}{3(1-2\nu)}$	
Volumetric shrinkage coefficient, β_{vol} (m^3/kg)	1.4346×10^{-5}	(LU; WANG; JIANG, 2015)

*T is used in K in all equations.

3.3 COMPUTATIONAL IMPLEMENTATION

The previously detailed mathematical model was solved in two stages, as shown in **Figure 3.9**. In the first stage, the simulation geometry incorporated the microwave cavity, the vacuum chamber, and the food sample. In this case, the wave distribution was solved at steady state for different concentrations of water in sample independently. After solving these simulations, it was possible to obtain an average of the power dissipated in the sample dependent on the liquid saturation. A detailed discussion is presented in Section 4.1.1. The second stage accounted the Darcy's Law (vapor transport), Transport of Diluted Species (transport of liquids), Heat transfer in Fluids (heat transfer) and Solid Mechanics (hyperelastic model) as a axisymmetric coupled model. These physics were interrelated by key variables that change in every simulation time step, meaning that in each iteration a new set of parameters (the ones that depend on temperature or/and moisture) and variable were available for the next step. Furthermore, the interrelated variables communicate between physics, for instance, the Darcy's Law physics provided the gradient pressure to the Solid Mechanics physics as a source of deformation, while the Transport of Diluted Species provided the fluid velocity to the Heat transfer in Fluids.

Figure 3.9: Scheme explaining the strategy for the numerical solution implemented in COMSOL.

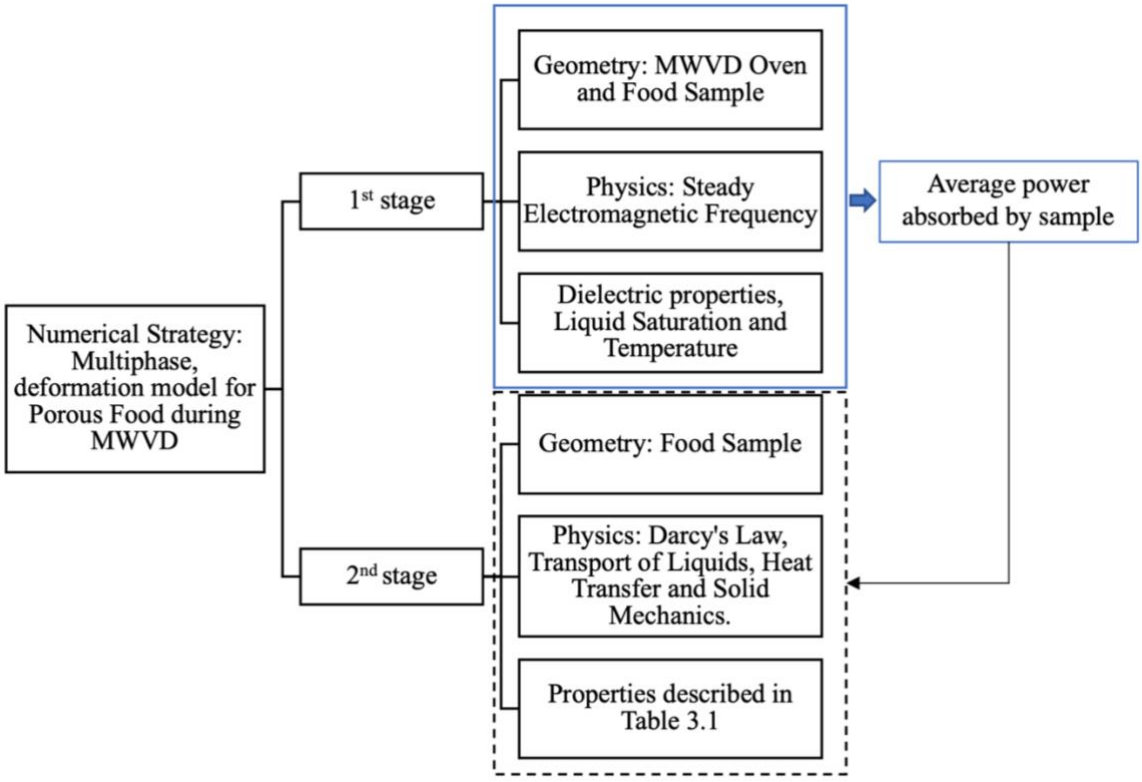

Source: Author

In addition to the two-stage approach, a simulation was conducted incorporating a constantly updated electromagnetic field that accounts for the changes occurring within the microwave cavity due to the sample. Initially, a preliminary study was performed without considering sample deformation, and the results are presented in **Appendix A-2**. Subsequently, a second study was conducted involving sample deformation; however, the numerical solution has not yet generated successful outcomes.

The governing equations for electromagnetics, multiphase transport in porous media and solid mechanics for large deformations were solved using the commercially available Finite Element software COMSOL Multiphysics 6.0 (COMSOL, Burlington, MA), using a 128 GB RAM Intel Core i9 computer. Mass, momentum, and energy conservation for various species were solved using the Transport of Diluted Species, Darcy's Law and Heat Transfer in Fluids modules, respectively, using the MUMPS direct solver. The transient solver automatically chose the time steps based on the solution variation between each step (maximum value of 0.1

s). Solid momentum balance was solved using the Non-linear Structural Mechanics module using the modified Neo-Hookean constitutive law for the deforming solid.

A mesh-independence study is always necessary to ensure that dependent variable did not change by more than 1% of the total change when the element size was reduced by half and is presented with more details in Section 4.1.2. The total number of degrees of freedom to be solved for varied between 200,000 to 1 million, and the computational time required to solve these degrees of freedom ranged from 8 hours to 70 hours, depending on the complexity of the problem and the computational resources available. The larger the number of degrees of freedom, the more computationally intensive the solution process becomes, resulting in longer simulation times. The range of degrees of freedom and computation times reflects the scale and complexity of the simulations undertaken in this study. The relative tolerance used in the simulations was 10^{-3}.

4. RESULTS AND DISCUSSION

This Section presents the results of the numerical solution obtained from the mathematical model. Initially, the electromagnetic power provided to the sample through microwaves was estimated, considering the entire MWVD system, without calculating heat and mass transfer or deformation. Following, a mesh-independence study was performed prior moving to a more complex model, aiming to select the most suitable mesh discretization. Subsequently a properties study was implemented to understand the impact of the volumetric shrinkage coefficient and the intrinsic permeability on the simulation results. Furthermore, the boundary conditions regarding the bottom of the sample and the sample size were altered and analyzed to propose a different perspective for understanding the mechanistic model. In the end, the simulation and experimental results were compared and discuss.

4.1 ESTIMATING ELECTROMAGNETIC POWER

The nominal power of the microwave oven was specified as 1000 W. However, experimental measurements revealed that the actual power output varied depending on the operation mode. When the magnetron was operating at full capacity, the calculated real power was found to be 767 ± 26 W. On the other hand, during the duty cycle of the magnetron, the real power was measured to be 337 ± 4 W. It is important to note that the real power corresponds to the power input set in the simulation at the magnetron port.

To accurately estimate the power delivered inside the oven cavity and absorbed by the porous media, a detailed 3D model of the oven design was utilized. This model considered the specific characteristics and geometry of the oven, allowing for a more precise estimation of the power distribution within the cavity. By integrating this information into the simulation, a more realistic representation of the microwave power absorbed by the porous media during the drying process could be obtained.

The simulation considered the properties of the oven and vacuum chamber as listed in the **Table 3.1**. The sample dimensions were chosen to match those used in the experimental setup. Additionally, the dielectric properties of the sample were determined using the Landau, Lifshitz, and Looyenga equation (**Equation 3.26**). This equation provided a means to calculate the dielectric properties based on the parametric sweep of liquid saturation. By incorporating the dielectric properties into the simulation and varying the liquid saturation parameter, the

effects of different moisture levels on the electromagnetic behavior of the sample could be analyzed. The results of this simulation were then imported into the 2D model to provide a more accurate source of microwave heat. A power curve was constructed based on the variation of water saturation in the sample, which is depicted in the **Figure 4.1**.

The domain of the simulation was discretized using tetrahedral elements. A second-order interpolation function was employed for the electromagnetic model, while first-order interpolation functions were applied for the transport models. For the electromagnetic model, COMSOL Multiphysics® software recommended using six elements with a second interpolation function order per wavelength to ensure accurate results independent of the mesh size. Consequently, in the air domain, the maximum element size was set to 2 cm, in the polypropylene chamber it was set to 1.3 cm, and in the porous medium, the software recommended using an extra fine mesh. This mesh refinement ensured a more precise representation of the intricate details within the porous medium.

Figure 4.1: The absorbed power depending on sample liquid saturation obtained from microwave oven heating

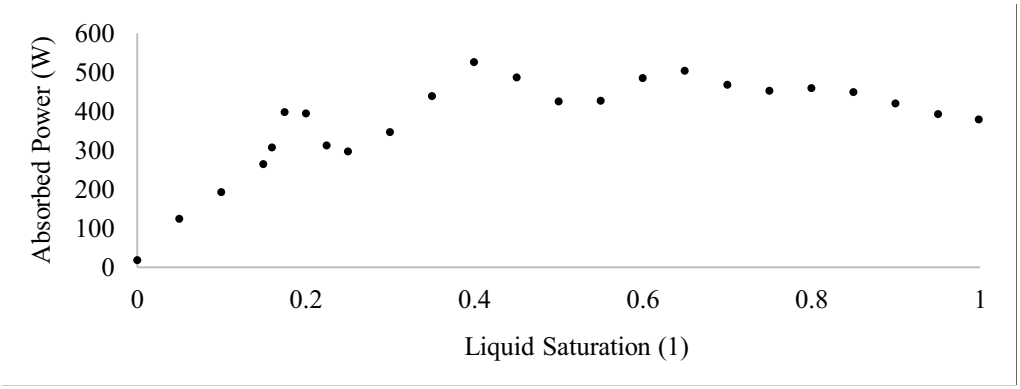

4.2 MESH-INDEPENDENCE STUDY

A study was conducted on meshing techniques, which consider element type, size, and discretization to solve the porous media model. In 3D models, tetrahedral elements are the default choice for most simulations in COMSOL, while triangular and quadrilateral elements are available for 2D models. Once the element type was chosen, the element size determines the mesh refinement, with smaller elements providing a more refined mesh at the cost of higher computational memory usage. The simulation also requires more memory as the shape function

order increases in element discretization. The shape function interpolates the solution within the elements and can be set to linear (first order), quadratic (second order), or cubic (third order). Finally, the mesh quality was assessed by plotting the quality of the elements, which determines the regularity of the mesh element shapes. The quality values ranged from 0 to 1, with 1 representing a perfectly regular element and 0 representing a degenerated element. The details of the tests are presented in the **Table 4.1**.

Table 4.1: Studies realized to guarantee the mesh-independence considering element size, type and order, number of elements, solution time and memory used.

Element type/order	Element size (mm)	Number of elements	Average quality of elements	Solution Time	Degrees of freedom	Memory used (GB)
Quadrilateral/2	0.25	10 000	1.0	5h 58 min 29s	202 005	5.62
	0.2	14 400	1.0	8h 41min 23s	290 405	6.91
	0.15	30 625	1.0	18h 36min 37s	616 005	10.26
Triangular/2	0.2	54 360	0.9653	13h 31min 11s	546 605	10.48

When the number of elements increased, the degrees of freedom also increased because there were more variables to calculate for the solution, resulting in longer solution times. The memory used by the computer to run the simulation depended on the number of degrees of freedom and the type of element. Triangular elements tended to use more memory. Furthermore, as the degrees of freedom increased, the memory usage also increased. All simulations were conducted on the same computer, an Intel Core i9 with 128 GB of RAM, since employing different computers altered the solution time.

The results of average moisture loss and average displacement over time from abovementioned studies were plotted in a two-axis graph as shown in **Figure 4.2**. The term "average" was employed because the results were computed as an average of the entire volume of the sample. No difference was noted in the moisture curves, just in the displacement curves for quadrilateral to triangular elements. Because the results do not depend on the size of the quadrilateral elements, they were chosen as the configuration to work with. And to guaranty the convergence even in more complexes cases the 0.2 element size was the one selected, that took almost 9h to solve each simulation.

Figure 4.2: Results of sample moisture and displacement for different element types (quadrilateral and triangular) and sizes used in the mesh discretization.

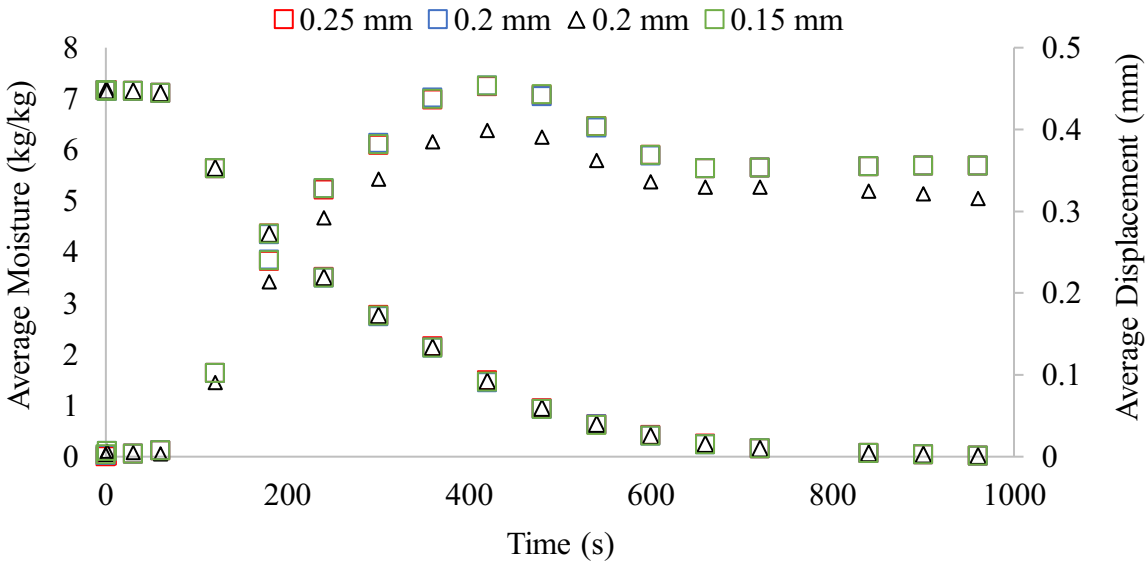

4.3 PROPERTIES STUDY

In this section, the results of a simulation of microwave vacuum drying (MWVD) of potatoes, with a duration of 960 seconds, is presented. The simulation provided insights into the behavior of moisture content, temperature, pressure, displacement over time, as well as spatial distribution of variables and the final 3D deformation. These findings helped understanding the phenomena described in the model. Additionally, intrinsic properties and deformation characteristics were also analyzed in this section. For further comprehension, the use of the term "average" indicates that the results were calculated as the mean value across the entire volume of the sample.

Figure 4.3 illustrates the moisture change on a dry basis throughout the drying process, with a specific focus on the later stages. As anticipated, the moisture content gradually decreased over time due to water loss via convection and diffusion. The driving force behind water removal was the pressure gradient generated during evaporation, which was facilitated by the temperature increase. The curve presented an initial points of sample heating (0-60 s), followed by a decrease of sample moisture with increase of sample temperature (600-660 s), until the water content in the sample significantly diminished (660-960 s).

Figure 4.3: Changes in the average moisture over time during MWVD with different values of the shrinkage coefficient (β_{vol}), detail for the later stages of the drying process.

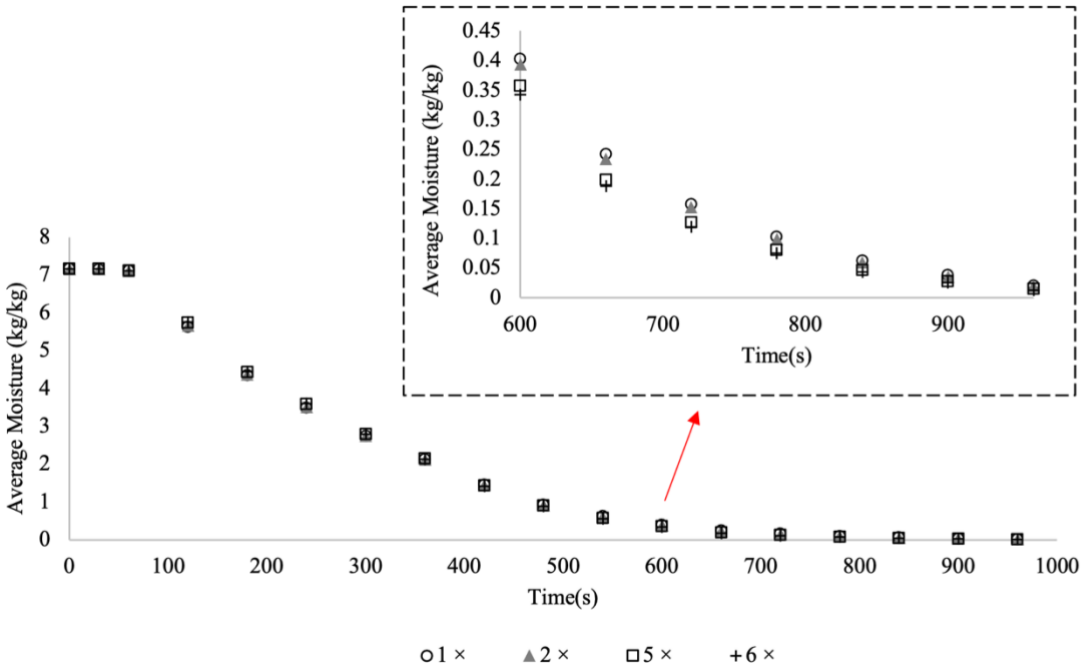

In the preliminary analysis, different values of the shrinkage coefficient (**Equation 3.19**) were applied, starting from β_{vol} =1.4346 x 10^{-5} m^3/kg (1×), and subsequently increased by two times this value (2×), five times (5×), and six times (6×). The moisture content exhibited difference only when a 5× increase was applied to the shrinkage coefficient, resulting in a noticeable difference observed at 600 s, where the sample size differed by 15%. This discrepancy arose due to the smaller sample size leading to increased internal pressure (**Figure 4.5**), facilitating water removal.

Figure 4.4 displays the surface temperature at the top surface of the sample during drying. The temperature rose by approximately 50°C within the first 120 s and remained within this range until around 400 s, indicating the removal of most of the water from the sample and the initiation of deformation. During this phase, the surface was being heated by the microwave while also being cooled by the evaporation of water migrating from the interior to the surface. In the next seconds, the temperature dropped due to the ongoing evaporation process coupled with a decrease in the energy input to the sample for two reasons: firstly, as the water saturation reduced, the absorption of electromagnetic power by the sample also decreased, as demonstrated on the **Figure 4.1**; secondly, since the microwave operated in duty cycle, there were intervals during which no power was being generated. After 600 s, the water saturation of

the sample dropped below 0.1, and the evaporation (**Figure 4.6**) was insufficient to effectively cool it down, causing the surface temperature of the sample to rose to 73°C ($1 \times \beta_{vol}$) and 86°C ($6 \times \beta_{vol}$).

Figure 4.4: Top surface temperature of the samples over time during MWVD using different values of the shrinkage coefficient (β_{vol}).

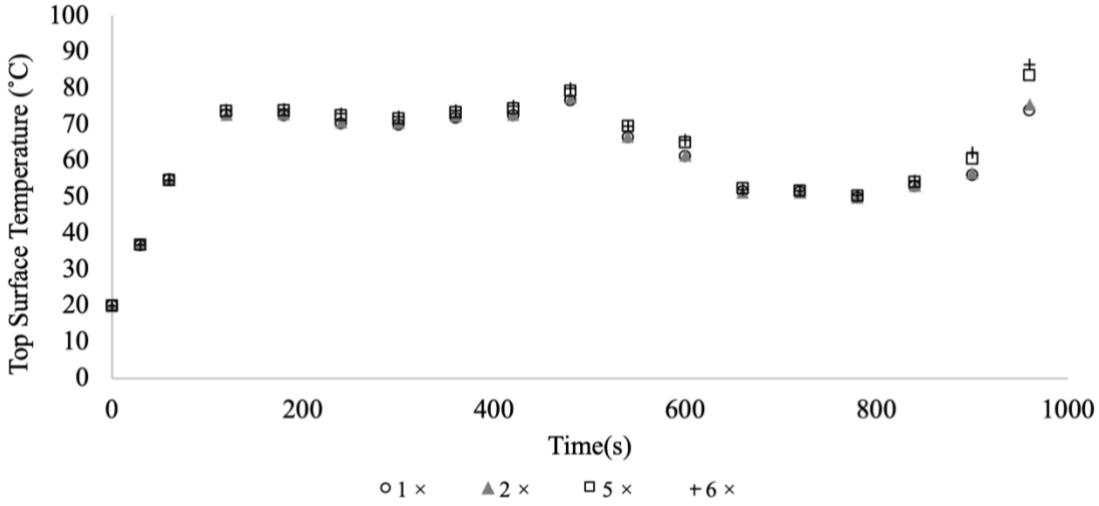

Figure 4.5 illustrates the average displacement and pressure within the sample throughout the drying process. As the shrinkage coefficient increased, both the displacement and internal pressure of the sample also increased. The evaporation of water leads to a rise in pressure, generating pressure gradients within the sample that drive the movement of vapor and water. As water is lost from the sample, concentration gradients intensify, resulting in increased strain.

Figure 4.5: Average displacement (left) and Average gas pressure (right) over time during MWVD using different values of the shrinkage coefficient (β_{vol}).

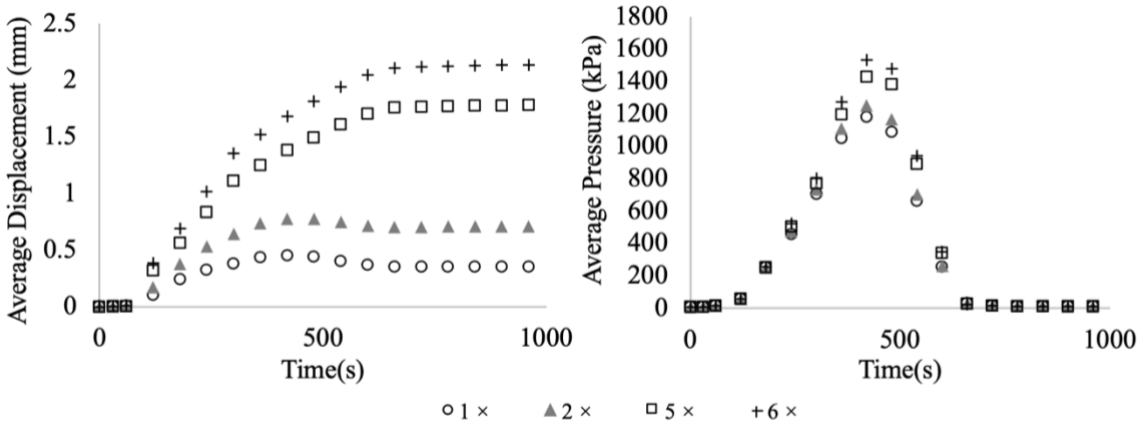

Figure 4.6 displays the spatial distribution of evaporation/condensation within the sample. This profile was calculated along a line extending from the center of the sample to the lateral end. Evaporation took place throughout the entire sample, with the highest rate occurring at the surface, reaching nearly 4 kg/m^{3}s. Inside the sample, water evaporates, leading to an increase in pressure, while at the surface, water quickly escapes into the surrounding environment. As expected for microwave heating a higher gas pressure was developed inside the food, what can be verified on **Figure 4.7**.

Figure 4.6: Evaporation in a longitudinal line from center to side of the sample with maximum deformation, each color represents one time.

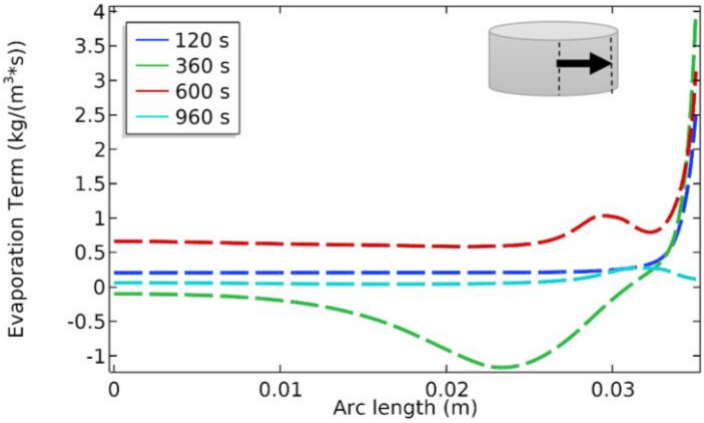

Evaporation exhibited fluctuations over time, with instances where the evaporation term values turned negative (360 s), indicating occurrences of condensation. This dynamic, in **Figure 4.6**, occurred due to the microwave oven duty cycle (ON/OFF) operation. When the energy is generated, ON period, heat is absorbed by the sample, what made the temperature increase and consequently enabled the evaporation. During the OFF period, no energy was generated, leading to the temperature of sample to decrease, which facilitated the condensation.

Despite the greater displacement observed when the shrinkage coefficient increased, the spatial profile of displacement in the samples remained consistent. The samples exhibited larger displacement vectors at the ends, while the displacement vector was null at the center. This pattern can be observed in **Figure 4.7**, where the 3D graphics are color-coded to represent displacement.

Figure 4.7: **a**, **b** - Potato 3D images of result of displacement from deformation at 960s (colorful scale). **c**,**d**,**e**,**f** - Potato 2D surface distribution of pressure (blue scale) and liquid velocity (blue arrows) at 480s e 600s for $1 \times \beta_{vol}$ and $6 \times \beta_{vol}$.

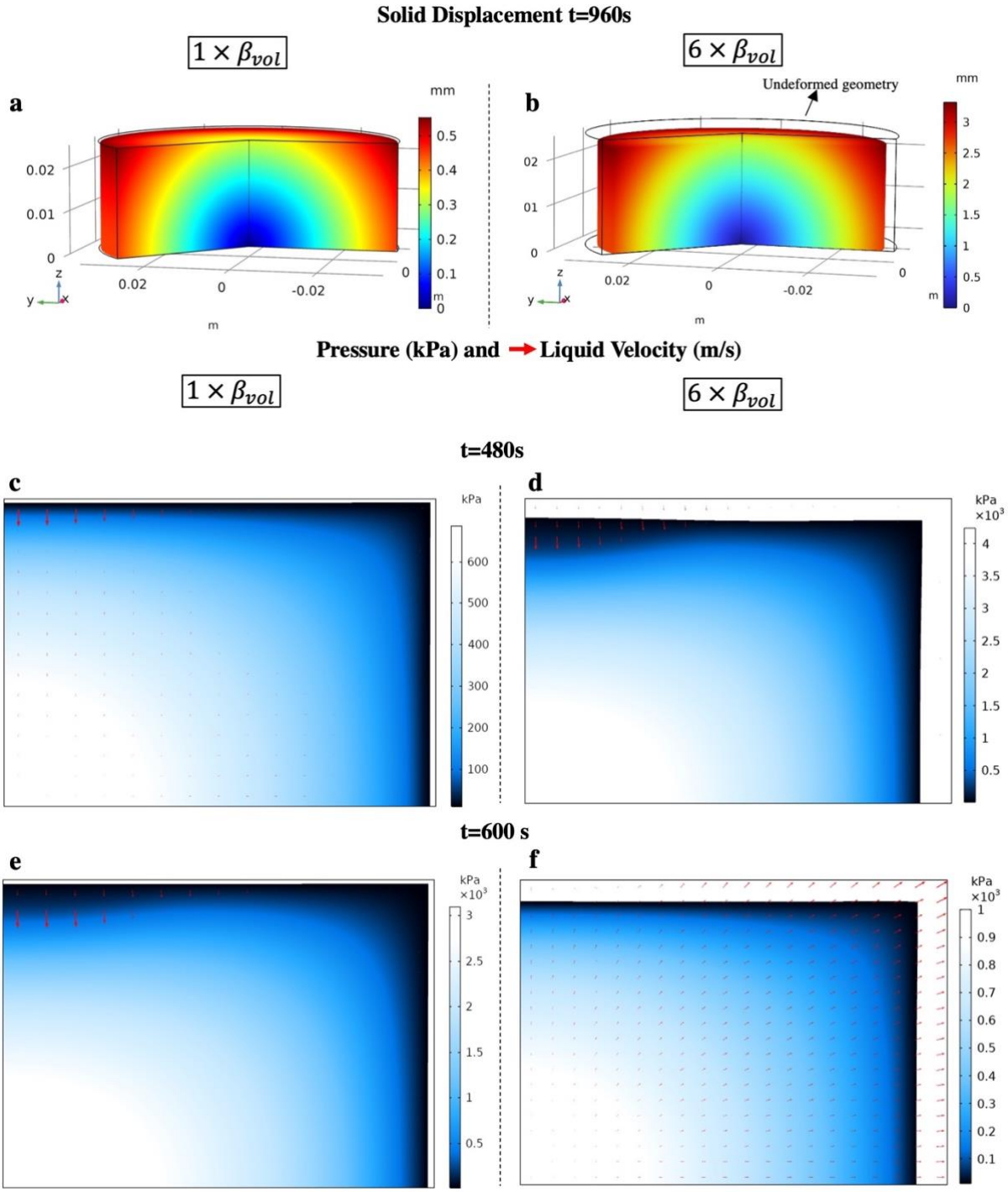

It is important to analyze in more detail some properties that are strongly related to deformation. **Figure 4.8** and **Figure 4.9** depict Jacobian (J), moisture Jacobian (J_M), gas porosity ($\emptyset_g$), liquid intrinsic permeability ($k_{in\text{-}l}$), and Young's modulus (E).

Figure 4.8 shows the variation of volume ratio (Jacobian), the moisture volume (Moisture Jacobian) ratio and de elastic volume ratio (Elastic Jacobian). The value of Jacobian was coincident with the value of Jacobian due to moisture loss, indicating volume change of the material was directly related to the amount of liquid water lost. The value of the Elastic Jacobian stayed near 1 because the value of Poisson used in the model was 0.49, rubbery state.

Figure 4.8: Jacobian, Elastic Jacobian and Moisture Jacobian change over time during MWVD for a sample with maximum deformation ($6 \times \beta_{vol}$).

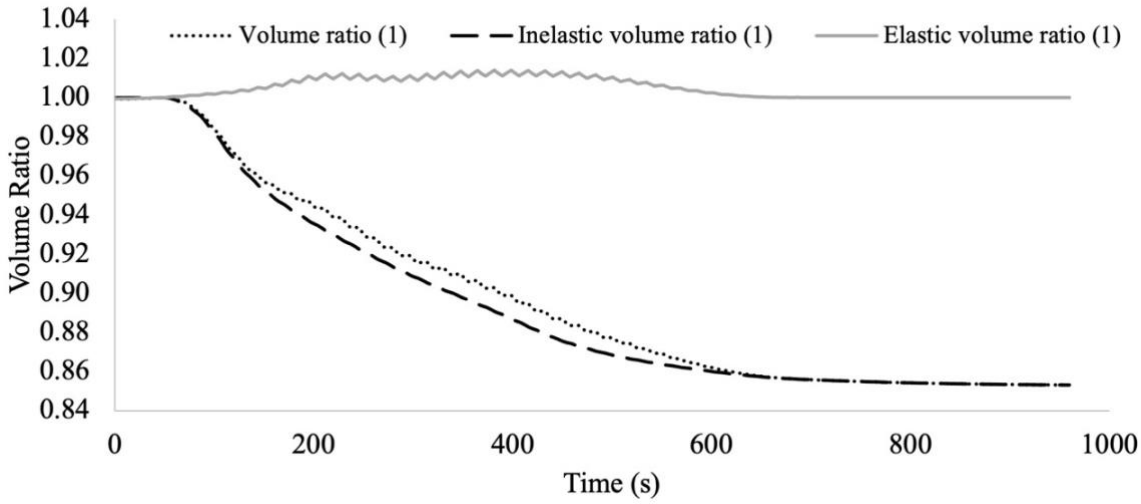

Figure 4.9 illustrates the average value of the elastic modulus, also known as the Young modulus, over time. The typical elastic modulus value for potato is 2.92 MPa. However, in this model, the correction proposed by Yang and Sakai (2001) based on the moisture content was applied. A higher elastic modulus corresponds to a steeper slope in the stress-strain curve, indicating that more force was required to deform the material, however changes in elastic modulus values did not affect shrinkage and moisture loss histories. The bulk modulus, shear modulus and Lame parameter also increase with time according to equations from **Table 3.1**.

Figure 4.9: Change in Young's Modulus over time during MWVD for a sample with maximum deformation ($6 \times \beta_{vol}$).

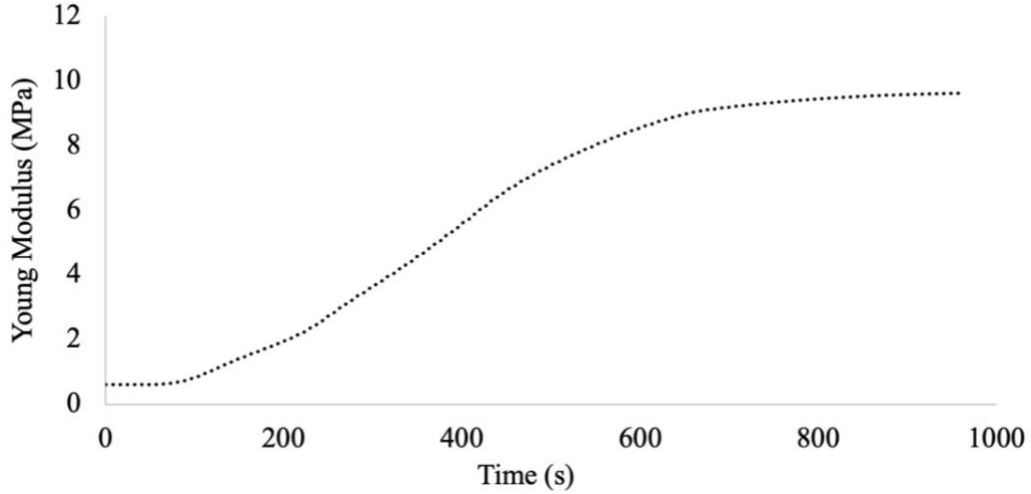

The change in the porosity is presented in **Figure 4.10**. As the sample dried, the porosity of the gas increased, as the vapor phase in the pores also increased ($\emptyset_g = S_v\emptyset$). However, the total porosity decreases, since the sample shrunk during drying. Gas porosity was lower for the shrunken material, if compared to the undeformed, since shrinkage is almost equal to the amount of water lost, the pores remain almost saturated with water with very little gas phase present in them, as explain in **Figure 2.5** before. Regarding dielectric properties, the less water present in the food, the lower the value of these properties, which results in a decrease in the efficiency of electromagnetic heating.

Figure 4.10: Change in the gas porosity (left) and dielectric permittivity (right) over liquid saturation.

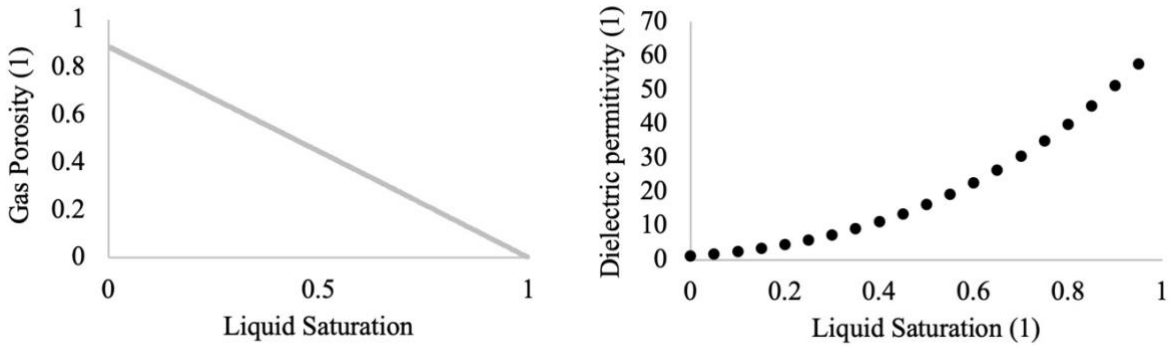

Given the variability of some of the parameters, a parametric sensitivity analysis is carried out to gain confidence in the model predictions. In this case, the parameter analyzed was the water intrinsic permeability that varied from 10^{-15} to 10^{-18}, as presented in **Figure 4.11** and **Figure 4.12**. The interest was to determine how these values affect moisture loss, mainly in the beginning of simulations build up.

Figure 4.11: Moisture loss over time using different values for water intrinsic permeability

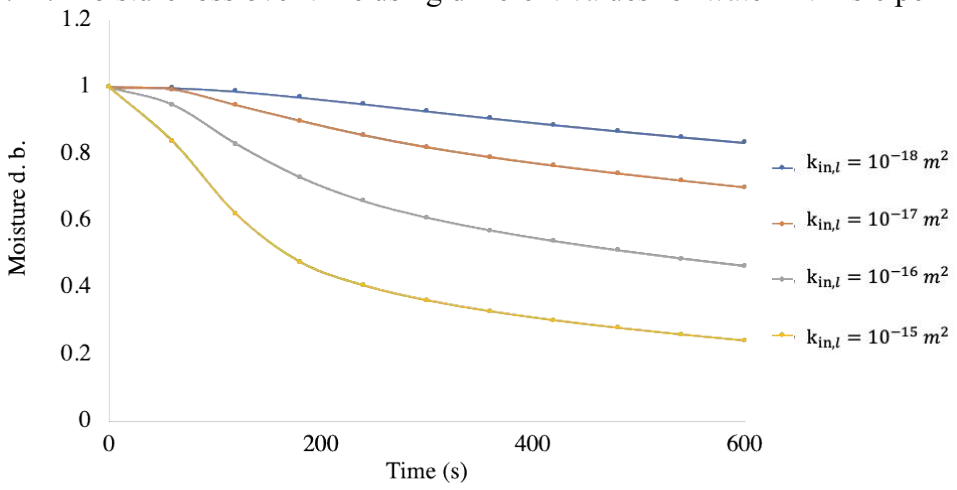

Figure 4.12: Average Temperature over time using different values for water intrinsic permeability.

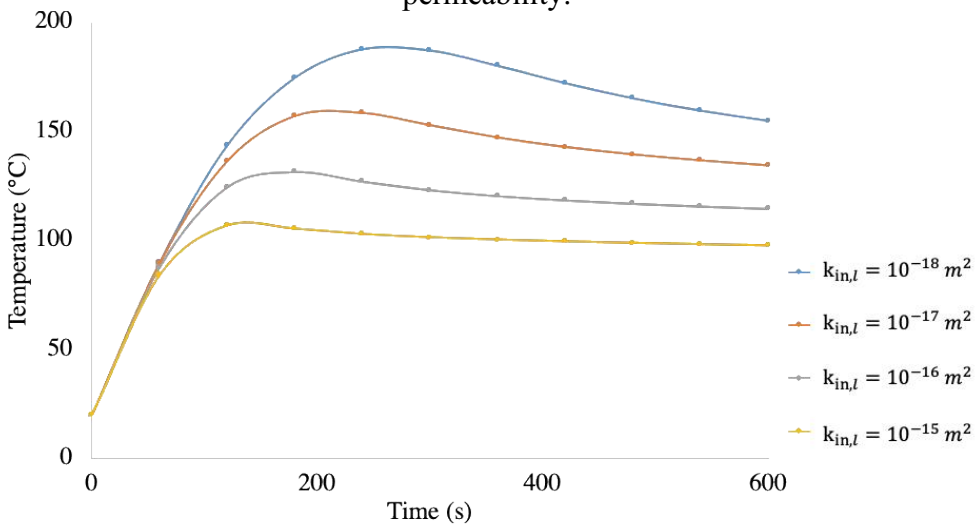

4.4 IMPACT OF BOUNDARY CONDITIONS

Two studies were conducted to evaluate the boundary conditions on the bottom of the sample. In the first study, the impact of allowing or restricting the passage of water and steam through this base was analyzed. In the second study, the roller boundary condition in solid mechanics was replaced with a fixed base boundary condition, resulting in zero displacement in any direction. The results of the first study are presented in **Figures 4.13** and **4.14**, while the responses to the modification in the second study are shown in **Figure 4.15**. These tests hold significance because, in the MWVD experiments, the sample remained stationary at the bottom of the chamber. Thus, it was assumed that the base would remain immobile, preventing the passage of fluids. However, upon observing the final deformation of the sample, the question arose if the sample suffered any deformation at the base allowing the passage of fluid.

According to the graphs in **Figure 4.13**, when the bottom of the sample was closed for mass transport, the moisture decreases only slightly faster. This occurs because the bottom was not primarily responsible for the significant loss of water. Instead, water and vapor preferentially exited the sample structure through the lateral and top borders, as shown in **Figure 4.14**. The blue arrows representing the liquid flux and the red arrows indicating the pressure gradient demonstrate the fluid movement towards the top and lateral sides during the period of highest pressure.

Figure 4.13: The average values for moisture, temperature, pressure, and displacement during MWVD for sample treated with two different boundary conditions: bottom open and bottom closed for water and vapor transfer.

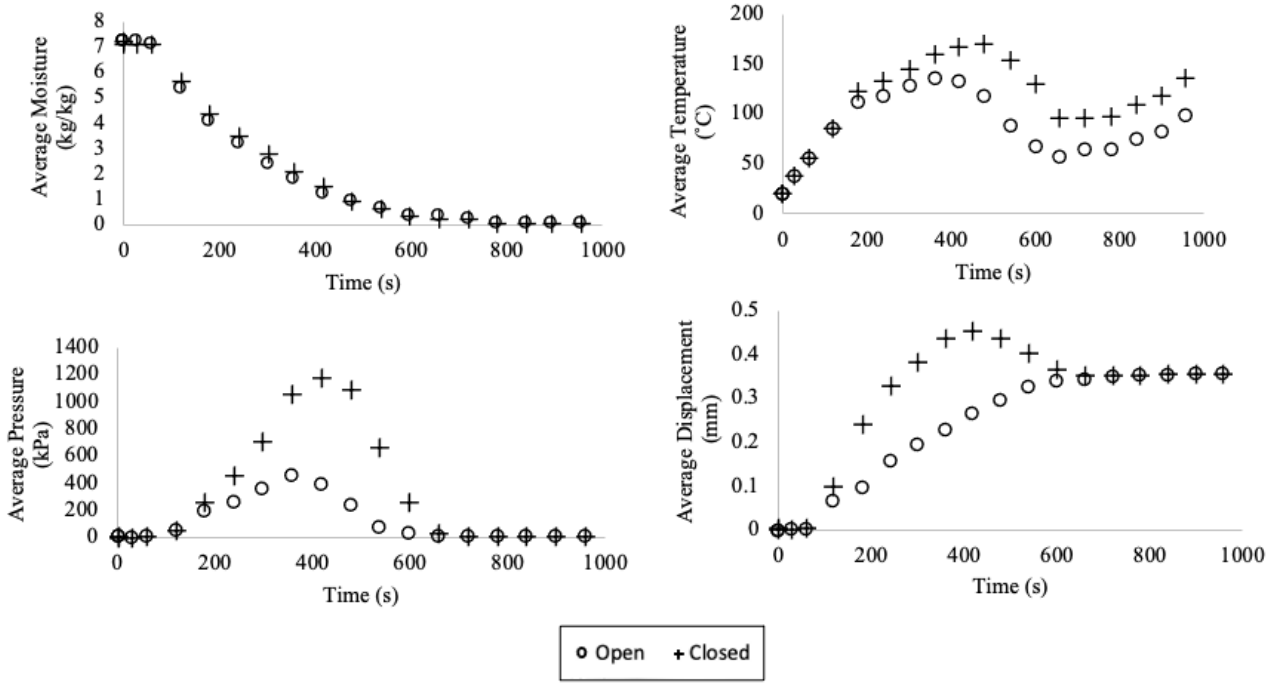

The higher pressure for open bottom was 452 kPa and 1181 kPa for the closed bottom. When the bottom was open, the gas pressure was lower because the boundary pressure was fixed at 10 kPa, creating a gradient that allowed the blowing of water and gas. In both cases, the gas pressure inside the sample reached its peak at around 400 s. At the same time, the displacement of the sample was at its maximum, which can be explained by the pressure gradient pushing the water out of the sample. As the water exits the sample, the sample undergoes deformation. The model suggests that deformation occurs with significant pressure gradients and is more sensitive to water loss.

Figure 4.14: Displacement, Liquid flux and Gas gradient pressure distributed in the sample for 360s and 600s.

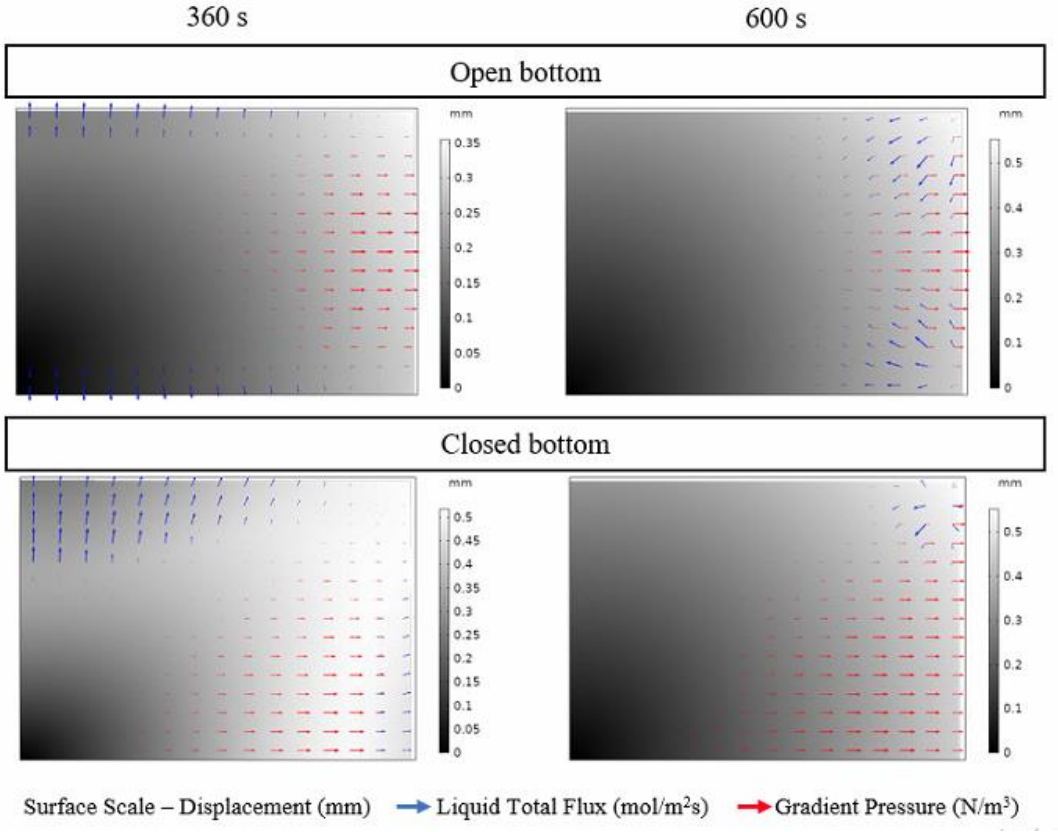

In **Figure 4.15** the results of the second study on roller and fixed boundary conditions are presented. Displacements were plotted at three sample borders: top (1), side (2), and bottom (3). A detailed observation revealed that when the boundary is fixed, the base of the potato remained in the same position, while the rest of the lateral surface decreased in the radial direction. Additionally, there was a reversal in the boundaries with greater displacement. When the roller condition was used, the lateral boundary exhibited the greatest displacement. However, when the fixed condition was applied, the top boundary became more susceptible to displacement. This occurred because the side surface is connected to the base, and if the base remains immobile, it hinders the movement of the side surface.

Figure 4.15: Surface displacement in the sample considering the A-roller and B-fixed boundary condition (red arrow showing the undeformed bottom) in the end of the process. The displacement for each borderline during MWVD for C-roller and D-fixed conditions.

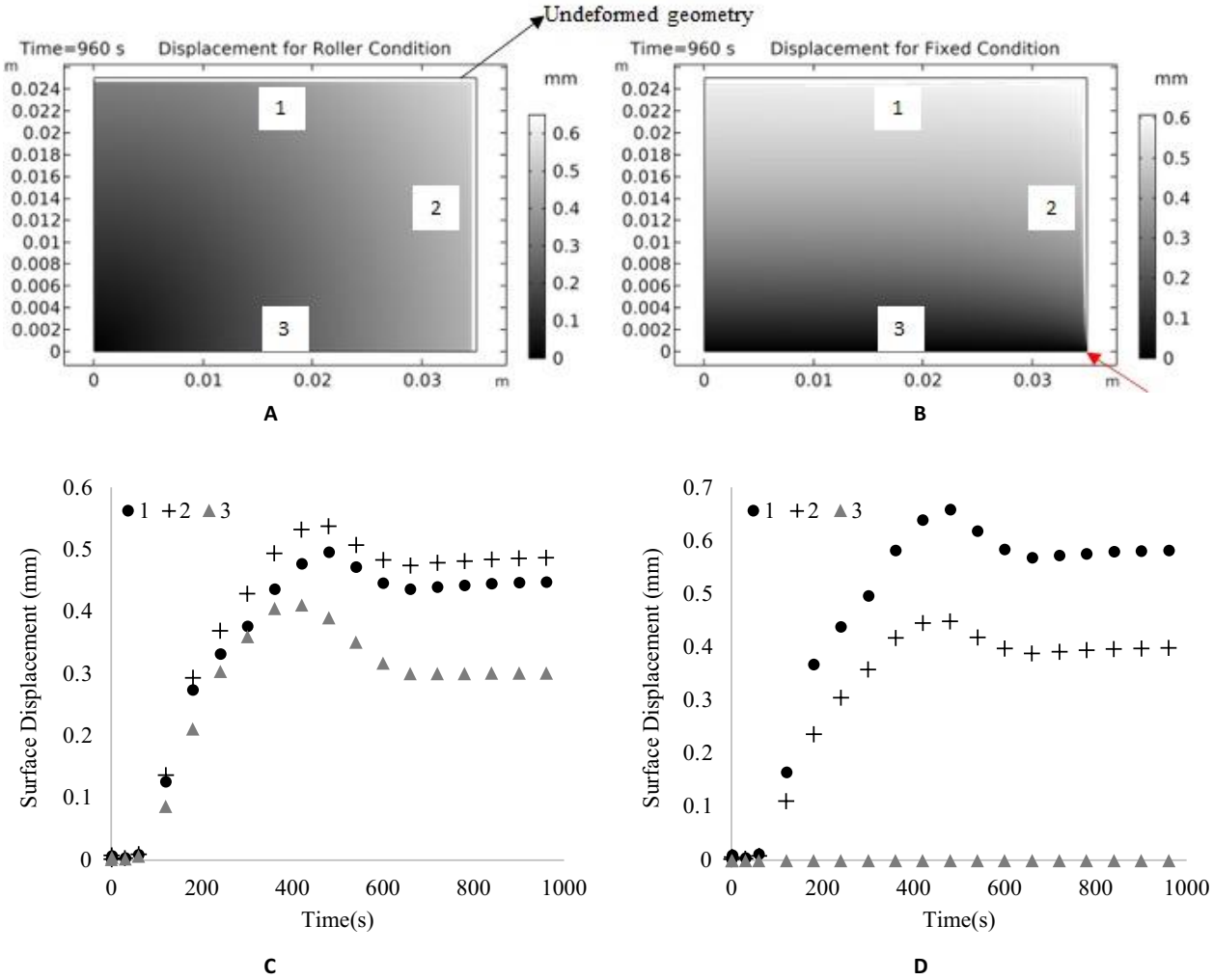

4.5 CHANGE IN THE SIZE OF THE SAMPLE

A study was conducted to investigate the effects of varying sample sizes on the simulations results. The aim was to understand how these changes would influence the moisture content, temperature profiles, or any other relevant variables.

The sample size used in this study, referred to as case "**a**", was selected as the standard size for this investigation. In "**b**" scenario, a height was selected to ensure equal top and lateral areas, resulting in a value of 38.48 cm^3. In the third scenario, "**c**", the sample exhibited an increase in height while maintaining the same value for radius, both set at 35 mm. **Figure 4.16**

illustrates a schematic representation of each configuration. The computational simulations considered the two-stage strategy and a shrinkage constant of $5 \times \beta_{vol}$.

Figure 4.16: Schematic representation for each configuration for different size of samples, **a** - actual size, **b** - same lateral and top area, **c** - same radius and height.

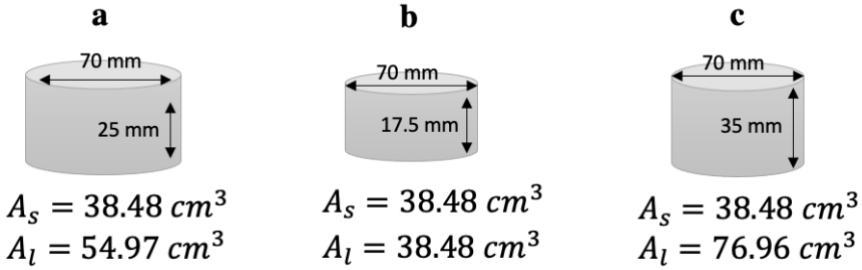

The results portraying the variations in temperature, pressure, top surface temperature, moisture, and the elastic Jacobian and Jacobian for each configuration are presented in **Figure 4.17**. The **Figure 4.18** illustrated the displacements, water and vapor fluxes in the top and lateral surface of the sample during the MWVD. A visualization of the final deformation structure and the average body load for each case studied are presented in **Figure 4.19**. Some variables showed responses in non-continuous curves because of the microwave ON/OFF cycle.

Analyzing **Figure 4.17**, at the beginning of simulation, the average temperatures of samples **a** and **b** were close. After 300 s, the temperature of sample **a** continued to increase, while the temperature of sample **b** begun to decrease (**Figure 4.17**). This can be explained by the fact that, at that moment, sample **b** already had less water than sample **a**, which can be confirmed by the water flow graphs (**Figure 4.18**). The greatest top and lateral water fluxes occurred before 200 s and then decreased radically, while the water fluxes of samples **a** and **c** remained almost constant.

Following the same idea, on **Figure 4.17**, while the temperature and amount of water were lower in sample **b**, the evaporation rate was also lower, generating less pressure compared to the other samples (~ 500 s). During this period, when the samples gained more temperature, evaporation increased, and the pressure raised. In the case of sample **a**, after 500 s of drying, it experienced a decrease in moisture content, resulting in a drier state. As the sample became drier, the electromagnetic field took longer to heat because the reduced moisture. Additionally, with less water available for evaporation, there was a decrease in the generation of gas pressure.

Considering **Figure 4.17,** the surface temperature of the sample is greatly influenced by the evaporation that occurs at the surface. In the first 100 s of drying, the sample is gaining

temperature. When evaporation starts to increase (with higher values at the surface, as shown in **Figure 4.6**), the temperature at the surface stabilizes (the cooling energy of the water evaporating and leaving the surface equals the energy provide to the surface). If the supply of water at the surface ceases, then the temperature increases, as the case with sample **a** at ~400 s and **b** at ~500 s.

Figure 4.17: Temperature, pressure, top surface temperature, moisture, and the elastic Jacobian and Jacobian for each configuration.

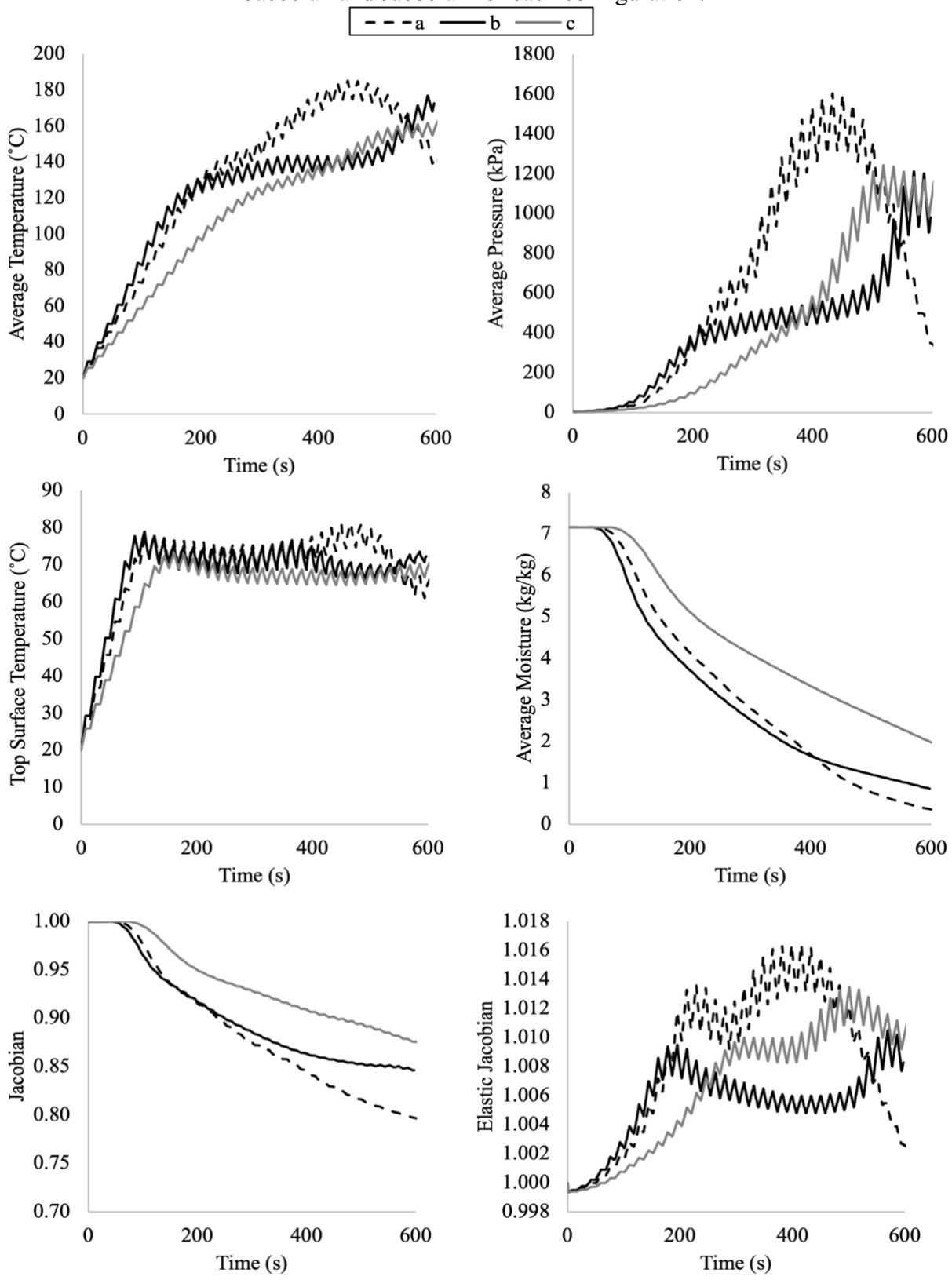

Figure 4.18: Displacements, water and vapor fluxes in the top and lateral surface of the sample during the MWVD.

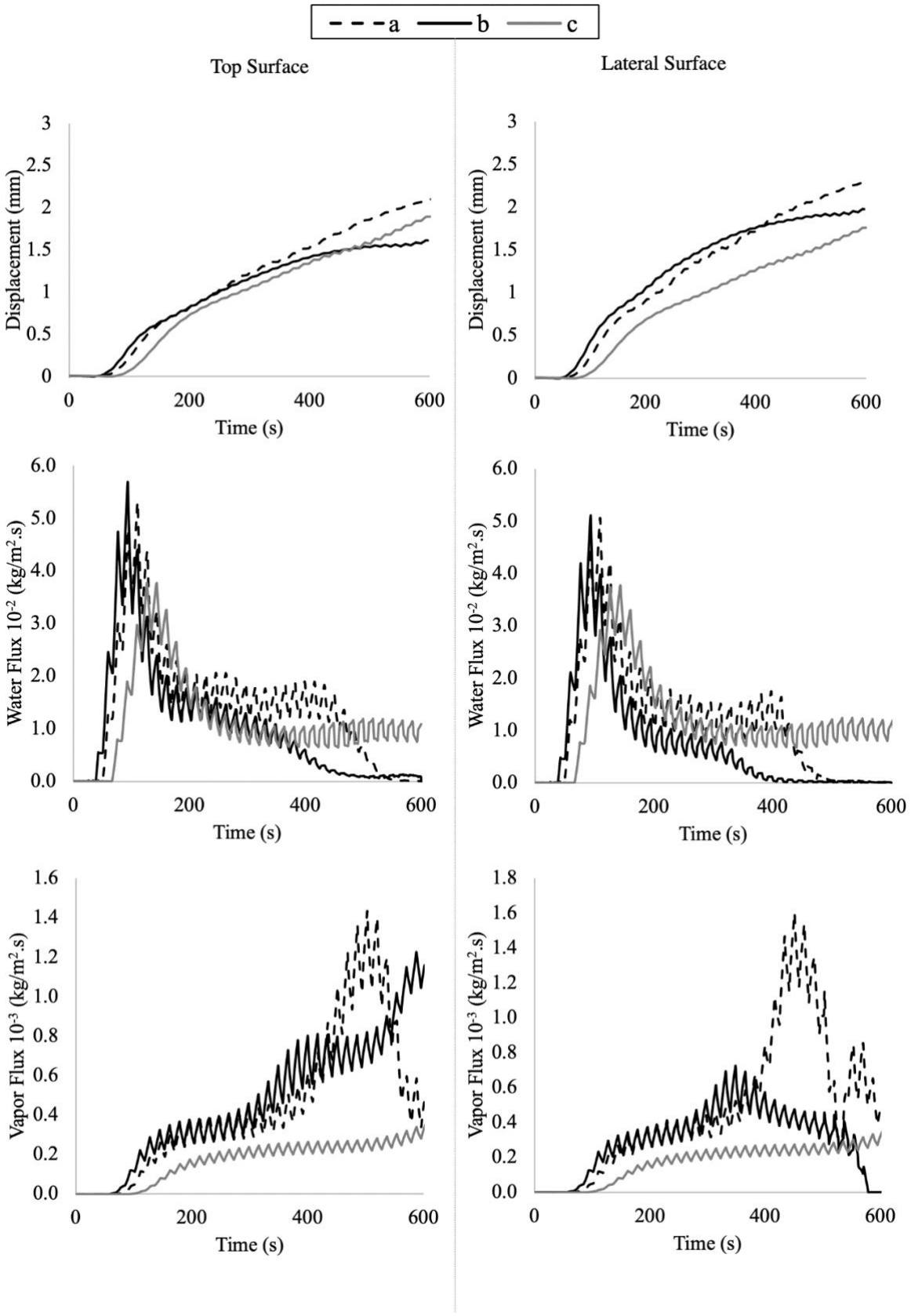

Figure 4.19: Surface displacement for cases **a**, **b** and **c** on 600s and Body load due to gas pressure in R direction and Z direction over time.

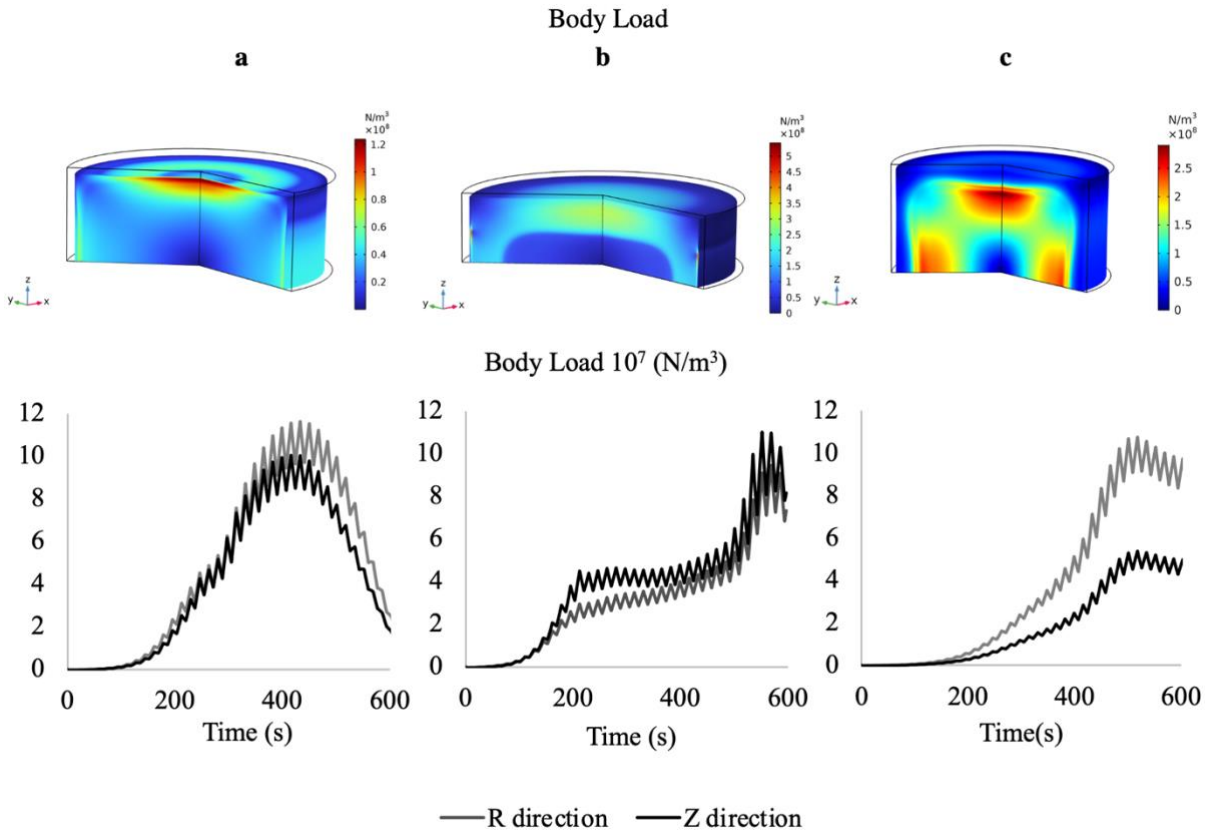

According to the moisture graph from **Figure 4.17** the sample **c** lost water slower than **a** and **b**, mainly because this sample was the biggest one. This can be confirmed in the water fluxes in the **Figure 4.18**, where this sample presented the higher flux of water in the end of simulation. Sample **b**, just after 400 s, showed a change in the behavior of the drying curve, as at that moment, there was a decrease in the flow of water leaving the surface of this sample (**Figure 4.18**), probably because the water was inside and not yet reached the surface. In **Figure 4.17**, it is observed that the pressure increases at this same moment, also due to the increase in temperature.

Changes in the Jacobian are related to water loss and changes in the Elastic Jacobian with changes in pressure. Comparing the graphs of moisture loss, Jacobian (**Figure 4.17**) with lateral and top displacement (**Figure 4.18**), it was noted that changes in the behavior of the curves always occurred at the same points for all samples. For example, if there was stabilization in moisture loss, there was also delay in the displacement and stabilization o f the

Jacobian. Similarities can be observed between the elastic Jacobian graph of the samples and the average pressure within the sample.

The body load, that is the force that generates the elastic deformation, due to gas pressure, is depicted in the R direction and in the Z direction in **Figure 4.19**. In the case where both lateral and superior area were the same for the sample, the body load was practically the same and presented the same behavior in both directions. As higher the area exposed to 10 kPa, higher will be the body load in that direction. For example, if the lateral area of a cylinder is bigger than the superior area, then the body load in R direction will be bigger than the Z direction for a case of MWVD.

The findings of this study contribute to a better understanding of the relationship between sample size and drying behavior, which can be valuable in optimizing drying processes, determining appropriate sample sizes for specific applications, and enhancing the overall efficiency and quality of the drying operation.

4.6 COMPARISON BETWEEN EXPERIMENTAL AND SIMULATION RESULTS

This Section presents the results obtained from the bench experiments. Two sets of experiments were conducted, as explained in detail in Section 3.1. The first set of experiments focused on the changes that occur between the initial point (0 s) and the final point of drying (960s), examining variations in moisture, surface temperature, and deformation at these two time points. Following that, the moisture curve was analyzed, which tracked the changes in the sample's moisture at different time intervals.

Figure 4.20 and Figure 4.21 depict the deformation of the potato. The first figure consists of illustrative photos, while the second figure presents the results obtained from Image J analysis. In the **Figure 4.20**, by comparing the superior areas in pictures S0 and S960, it was evident that the radius decreased, as indicated by the circular pen mark at the base. Comparably, when examining the images of the lateral area L0 and L960, an enlargement of the extremities can be observed, indicating the formation of bubbles, puffing effect. Additionally, the dried material exhibited a brown color on the left side, indicating the presence of a hot spot.

Figure 4.20: Potato sample before (S0 – superior view; LO – lateral view) and after (S960 – superior view; L960 – lateral view) MWVD.

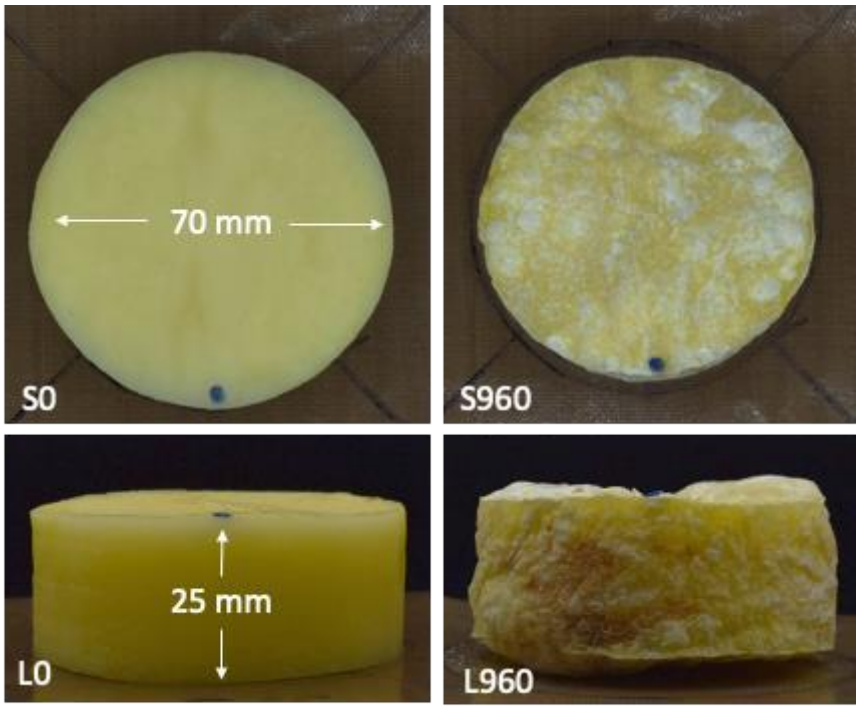

The **Figure 4.21** illustrates the changes in the top and lateral areas of the sample after a drying time of 16 minutes, comparing experimental results with simulation. As a result of radial shrinkage during drying, it was evident that the top area decreased. However, the lateral area presented two different scenarios: if considered the bubbles formed on the surface of the sample, the area increased by approximately 2 cm^2, whereas if the bubbles were disregarded, the area decreased by 3 cm^2. When comparing the results with the simulation, it can be observed that the decrease in the top area aligns with the experimental findings, while the lateral decrease corresponds to shrinkage without the presence of bubbles.

Figure 4.21: Simulated and measured area of the top and side surfaces of the sample of the beginning (0 s) and the final stage (960 s) of MWVD.

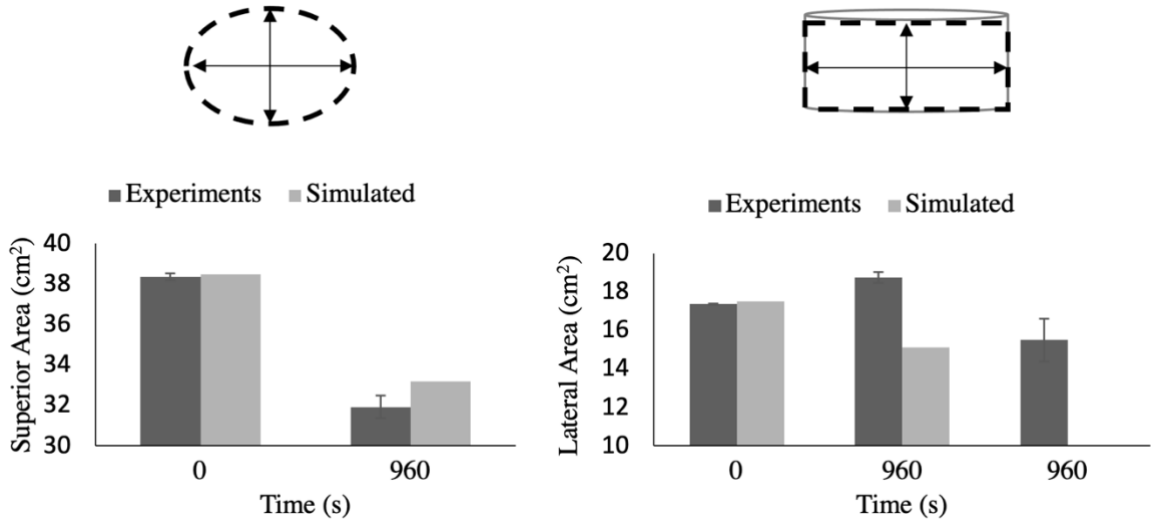

Another crucial analysis to consider when studying food deformation is the fracture stress. The fracture stress represents the maximum stress level that a material can withstand before it experiences a complete failure or fracture. According to Yang and Sakai (2001), the fracture stress curve is a useful information to prevent the food stress cracking. **Figure 4.22** illustrates the evolution of effective stress within the material along with the corresponding failure stress of the material.

Figure 4.22: Effective Stress and Fracture Stress into sample over time during MWVD

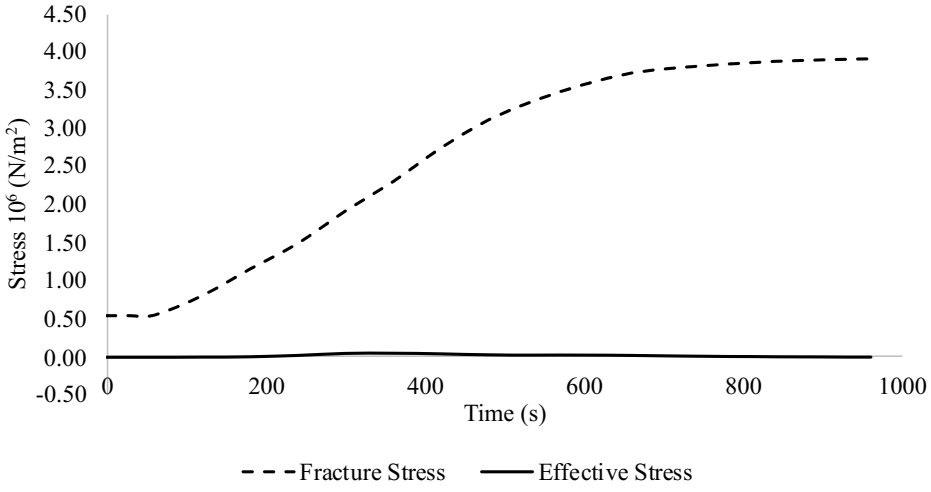

The effective stress exhibited an increase as the moisture content decreases. This increase in stress is attributed to the rise in strain levels that occurs when the material undergoes

shrinkage because of moisture loss. As the moisture content decreases, the spaces between the particles of the material become smaller, leading to a reduction in volume and an increase in strain. Consequently, the effective stress experienced by the material intensifies, reflecting the internal forces exerted within the material. It is important to note that the effective stress remained significantly below the fracture stress at all moisture levels, thereby preventing any initiation of cracks. This observation was confirmed experimentally, as no evidence of crack formation was observed in the material.

The distribution of surface temperature on the top surface of the sample is depicted in **Figure 4.23**. The presence of a hot spot was evident in these infrared images. Despite attempts to incorporate a more realistic heating distribution in the simulation by utilizing dielectric properties and an imported power, the final temperature did not align with the experimental results. This discrepancy arises from the fact that in the 3D cavity, where wave distribution occurred, water saturation was the only change considered, and the electric field was not influenced by sample temperature or deformation. The observed pattern in the simulation results revealed a higher temperature in the middle of the sample compared to the surface. This phenomenon can be attributed to two factors: firstly, during a significant portion of the drying process, the sample retained more moisture in its middle section, making it more conducive to microwave heating; secondly, at the surface, evaporation-induced cooling was occurring, leading to lower temperatures in this region.

Figure 4.23: Experimented and Simulated results of Surface temperature distribution on the top surface of the sample of the beginning and the final stage of MWVD.

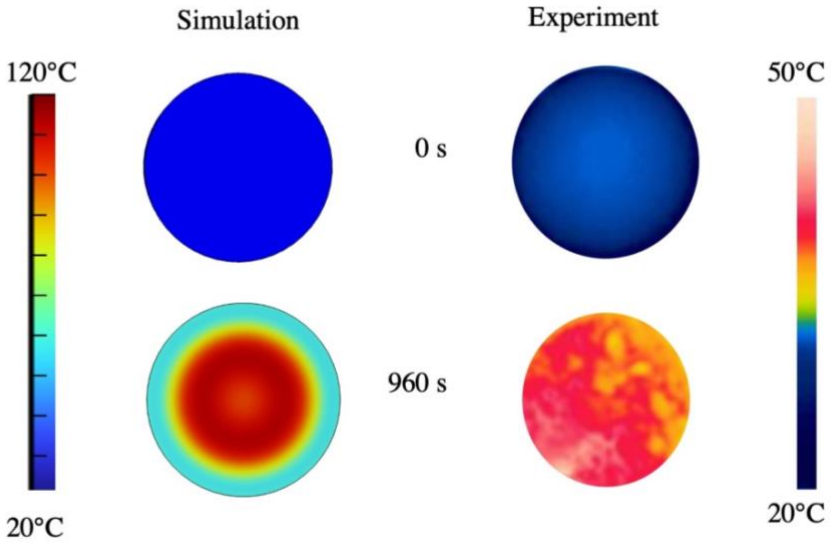

Figure 4.24 illustrate the change of temperature over time based in simulation results and the surface temperatures with minimum, average and maximum values observed. The temperatures ranged from minimum of 20.2 °C to maximum of 48.9°C, after 16 min drying, low temperatures if compare with convective drying methods. The predicted and observed temperature data at the surface of the potato differed as already mentioned. The experimental values were lower than the simulations because the electric field actualization was not being accounted.

Figure 4.24: Change of temperature over time based in simulation results and the experimental measurement for surface temperatures with minimum (green), average (blue) and maximum (orange) values.

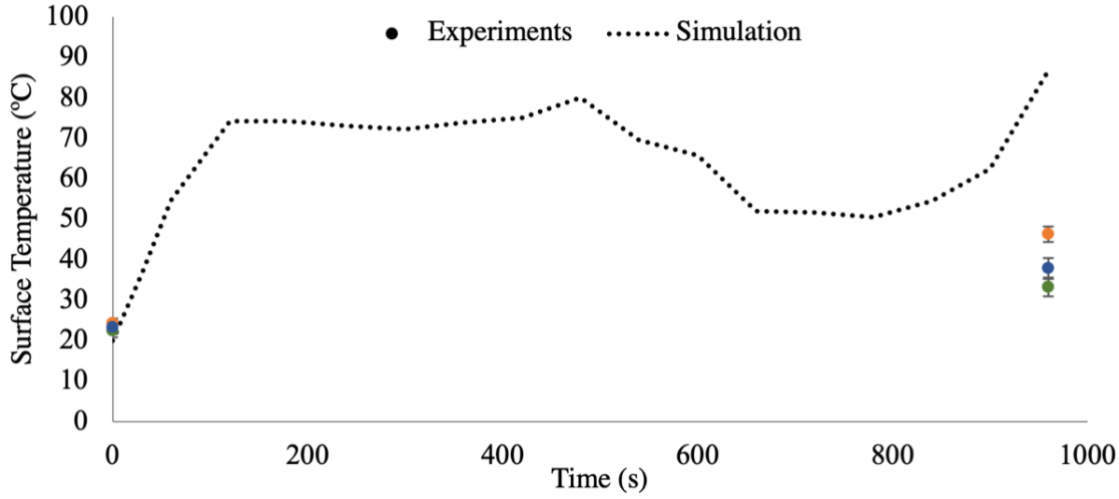

Figure 4.25 shows the average moisture loss during time. Total moisture contents obtained from the computational model as function of time was found to differ from those determined gravimetrically.

Figure 4.25: Experimental moisture curve, Initial and final time moisture for deformation experiments and simulation results.

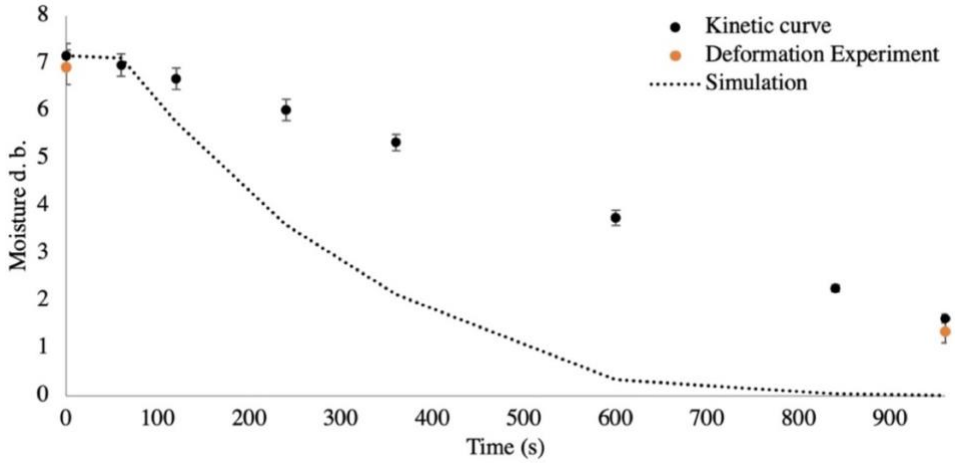

The disparity between the drying curve derived from the simulation and the experimental data can be attributed to two primary factors. Firstly, the experimental data collection process occurred intermittently, necessitating the removal of the sample from the microwave and subsequent restarts to attain data at different time points. During these intervals, the sample was momentarily devoid of heating as it underwent pressurization, reaching atmospheric pressure for weighing. This interruption in the heating process led to a more gradual drying trend in the experimental data compared to the simulations, which did not account for these interruptions. Secondly, a static approach was adopted for energy consideration, as elucidated in the electromagnetic power estimation Section. However, this approach lacks the incorporation of essential updates to the electric field over time. Moreover, the simplification of transforming the 3D model into a 2D representation implies an axisymmetric simulation that overlooks the non-uniform heating characteristic of the actual microwave environment.

It's important to note that there were other unaccounted variables, including starch gelatinization, the occurrence of hot and cold spots, and the transition from the rubbery state to the glassy state of the material. These variables might contribute to the observed disparities between the simulated outcomes and the experimental data.

5. CONCLUSIONS

The proposed coupled model for multiphase transport, deformation, and phase transition during microwave vacuum drying was successfully solved by a numerical approach using finite element methods, which was experimentally validated.

The key points drawn from this study are 1) The microwave power absorbed by the sample decreases throughout the drying process; 2) Square-shaped elements are more suitable for 2D simulations in terms of geometry discretization; 3) Increasing the volumetric shrinkage coefficient leads to greater sample deformation, resulting in larger pressure and water concentration gradients; 4) The samples exhibit larger displacement vectors at the edges compared to the porous medium center; 5) Deformation occurs due to significant pressure gradients and is highly sensitive to water loss; 6) Pressure gradients influence the elastic Jacobian, while the Moisture Jacobian is influenced by water loss; 7) The major change in volume ratio is attributed to water loss; 8) The occurrence of puffing depends on significant pressure gradients; 9) Gas porosity change and mechanical properties increase as the sample loses water during MWVD, contrary to dielectric properties; 10) The choice of boundary condition at the bottom alters the sample's deformation by increasing internal pressure (bottom closed or open) and controlling displacement (fixed or axial displacement); 11) The model effectively represents shrinkage and can be adjusted with heating considerations; 12) The higher the area of a sample exposed to vacuum pressure, the higher the body load in that direction, in the case of MWVD.

A mathematical model was developed that describes the microwave vacuum drying process, including electromagnetic wave propagation and heating, heat and mass transfer phenomena, liquid and vapor flow, and solid mechanical deformation in a porous media based on mechanistic principles. The equations defined in this mathematical model were successfully implemented in the commercial software COMSOL Multiphysics and a numerical solution that describes the trends for microwave vacuum drying of porous media was obtained. The numerical solution was compared with experimental drying results based on the temporal evolution of the moisture content and the before and after drying results of surface temperature and superficial area of a potato. The decrease in the top area aligns with the experimental findings, while the lateral decrease corresponds to shrinkage without the presence of bubbles.

A parametric property study was executed for different values for volumetric shrinkage coefficient, and intrinsic permeability in the numerical solution to evaluate their effects on the microwave vacuum drying process and the profile of moisture, pressure, temperature, evaporation and displacement over space and time. As the shrinkage coefficient increased, both the displacement and internal pressure of the sample also increased, but no alteration was observed on surface temperature.

In summary, these findings provide valuable insights into the behavior of moisture content, temperature, and pressure during the MWVD process. The study highlights the influence of boundary conditions, physical and mechanical properties, and their subsequent effects on the drying dynamics, offering a better understanding of this complex mechanisms.

As recommendations for future work, it is suggested to explore the utilization of an experimental apparatus capable of continuous data collection of moisture and temperature, eliminating the necessity of sample removal from the microwave. In terms of mathematical modeling and numerical solutions, conducting simulations in a fully coupled, transient regime within a 3D system could be advantageous. This is currently underway in parallel studies. Additionally, incorporating the time-varying mechanical properties, as Elastic modulus and Poisson coefficient, of the potato product obtained from MWVD experiments into simulations.

REFERENCES

ACHANTA, S.; OKOS, M. R. Predicting the quality of dehydrated foods and biopolymers - research needs and opportunities. **Drying Technology**, v. 14, n. 6, p. 1329–1368, 1996.

ANDO, Y. et al. Improvements of drying rate and structural quality of microwave-vacuum dried carrot by freeze-thaw pretreatment. **LWT**, v. 100, p. 294–299, 1 fev. 2019a.

ANDO, Y. et al. Effects of prefreezing on the drying characteristics, structural formation and mechanical properties of microwave-vacuum dried apple. **Journal of Food Engineering**, v. 244, p. 170–177, 1 mar. 2019b.

ANTIPOV, S. T.; ARAPOV, V. M.; KAZARTSEV, D. A. Kinetics laws as the base for mathematical simulation of microwave vacuum drying process. **Journal of Physics: Conference Series**, v. 1560, p. 12017, 2020.

ARBALLO, J. R.; GOÑI, S. M.; MASCHERONI, R. H. Modeling of fluid dynamics and water vapor transport in microwave ovens. **Food and Bioproducts Processing**, v. 119, p. 75–87, 1 jan. 2020.

AREGAWI, W. A. et al. Modeling of Coupled Water Transport and Large Deformation During Dehydration of Apple Tissue. **Food and Bioprocess Technology**, v. 6, n. 8, p. 1963–1978, 5 ago. 2013.

AYAPPA, K. G. et al. Microwave heating: an evaluation of power formulations. **Chemical Engineering Science**, v. 46, n. 4, p. 1005–1016, 1 jan. 1991.

BARRETO, I. M. A. et al. Oil–free potato chips produced by microwave multiflash drying. **Journal of Food Engineering**, v. 261, p. 133–139, 1 nov. 2019.

BASAK, T.; BHATTACHARYA, M.; PANDA, S. A generalized approach on microwave processing for the lateral and radial irradiations of various Groups of food materials. **Innovative Food Science and Emerging Technologies**, v. 33, p. 333–347, 1 fev. 2016.

BEAR, JACOB. **Dynamics of fluids in porous media**. Dover Publications Inc, 1972.

BEJAN, A. **Convection Heat Transfer**. 3rd. ed. John Wiley & Sons, 2013.

BELYTSCHKO, T.; LIU, W. K.; MORAN, B. **Nonlinear Finite Elements for Continua and Structures**. [s.l.] Wiley, 2000.

BENCZÉ DI, D.; TOMKA, I.; ESCHER, F. Thermodynamics of Amorphous Starch-Water Systems. 1. Volume Fluctuations. **Macromolecules**, p. 3055–3061, 1998.

BHATTACHARYA, M.; BASAK, T. A comprehensive analysis on the effect of shape on the microwave heating dynamics of food materials. **Innovative Food Science and Emerging Technologies**, v. 39, p. 247–266, 1 fev. 2017.

BLAHOVEC, J.; LAHODOVÁ, M.; ZÁMEČNÍK, J. Potato Tuber Dynamic Mechanical Analysis at Temperatures of Starch Gelatinization. **Food and Bioprocess Technology**, v. 5, n. 3, p. 929–938, 26 abr. 2012.

BONDARUK, J.; MARKOWSKI, M.; BŁASZCZAK, W. Effect of drying conditions on the quality of vacuum-microwave dried potato cubes. **Journal of Food Engineering**, v. 81, n. 2, p. 306–312, 1 jul. 2007.

CHESTER, S. A.; ANAND, L. A coupled theory of fluid permeation and large deformations for elastomeric materials. **Journal of the Mechanics and Physics of Solids**, v. 58, n. 11, p. 1879–1906, 1 nov. 2010.

CHONG, C. H. et al. Combined Drying of Apple Cubes by Using of Heat Pump, Vacuum-Microwave, and Intermittent Techniques. **Food and Bioprocess Technology**, v. 7, n. 4, p. 975–989, 26 abr. 2014.

CLARY, C. D. et al. Improving grape quality using microwave vacuum drying associated with temperature control. **Journal of Food Science**, v. 72, n. 1, p. E023–E028, 2007.

CLARY, C. D.; WANG, S.; PETRUCCI, V. E. Fixed and Incremental Levels of Microwave Power Application on Drying Grapes under Vacuum. **Journal of Food Science**, v. 70, n. 5, p. E344–E349, 1 jun. 2005.

CUI, Z. W. et al. Combined microwave-vacuum and freeze drying of carrot and apple chips. **Drying Technology**, v. 26, n. 12, p. 1517–1523, 2008.

CUI, Z. W.; XU, S. Y.; SUN, D. W. Dehydration of garlic slices by combined microwave-vacuum and air drying. **Drying Technology**, v. 21, n. 7, p. 1173–1184, ago. 2003.

DADMOHAMMADI, Y. et al. Estimating permeability and porosity of plant tissues: Evolution from raw to the processed states of potato. **Journal of Food Engineering**, v. 277, p. 109912, 1 jul. 2020.

DASH, K. K.; CHAKRABORTY, • S; SINGH, • Y R. Modeling of Microwave Vacuum Drying Kinetics of Bael (Aegle marmelos L.) Pulp by Using Artificial Neural Network. [s.d.].
DATTA, A. K. Hydraulic Permeability of Food Tissues. **International Journal of Food Properties**, v. 9, n. 4, p. 767–780, 1 dez. 2006.

DATTA, A. K. Porous media approaches to studying simultaneous heat and mass transfer in food processes. I: Problem formulations. **Journal of Food Engineering**, v. 80, n. 1, p. 80–95, maio 2007.

DATTA, A. K.; NI, H. Infrared and hot-air-assisted microwave heating of foods for control of surface moisture. **Journal of Food Engineering**, v. 51, n. 4, p. 355–364, 1 mar. 2002.

DEFRAEYE, T.; RADU, A. Insights in convective drying of fruit by coupled modeling of fruit drying, deformation, quality evolution and convective exchange with the airflow. **Applied Thermal Engineering**, v. 129, p. 1026–1038, 25 jan. 2018.

DEVAHASTIN, S.; NIAMNUY, C. **Modelling quality changes of fruits and vegetables during drying: A review**. **International Journal of Food Science and Technology**, set. 2010.

DHALL, A.; DATTA, A. K. Transport in deformable food materials: A poromechanics approach. **Chemical Engineering Science**, v. 66, n. 24, p. 6482–6497, 15 dez. 2011.

DONSÌ, G.; FERRARI, G.; NIGRO, R. Experimental determination of thermal conductivity of apple and potato at different moisture contents. **Journal of Food Engineering**, v. 30, n. 3–4, p. 263–268, 1 nov. 1996.

DUDA, F. P.; SOUZA, A. C.; FRIED, E. A theory for species migration in a finitely strained solid with application to polymer network swelling $. **Journal of the Mechanics and Physics of Solids**, v. 58, p. 515–529, 2010.

DUMPLER, J.; MORARU, C. I. A process optimization approach for microwave vacuum drying of concentrated skim milk. **Journal of Dairy Science**, v. 105, n. 11, p. 8765–8781, 1 nov. 2022.

EKEZIE, F. G. C. et al. Microwave-assisted food processing technologies for enhancing product quality and process efficiency: A review of recent developments. **Trends in Food Science and Technology.** Elsevier Ltd, , 1 set. 2017. . Acesso em: 12 maio. 2020.

ELLIOTT, J. RICHARD.; LIRA, C. T. **Introductory chemical engineering thermodynamics**. [s.l.] Prentice Hall, 2011.

ERLE, U.; SCHUBERT, H. Combined osmotic and microwave-vacuum dehydration of apples and strawberries. **Journal of Food Engineering**, v. 49, n. 2–3, p. 193–199, 1 ago. 2001.

ERMOLAEV, V. et al. Analysis of Shrinkage Phenomena in the Process of Cheese Vacuum Drying. **KnE Life Sciences**, 5 abr. 2021.

FANTA, S. W. et al. Microscale modeling of coupled water transport and mechanical deformation of fruit tissue during dehydration. **Journal of Food Engineering**, v. 124, p. 86–96, 1 mar. 2014.

FARKAS, B. E.; SINGH, R. P.; RUMSEY, T. R. Modeling heat and mass transfer in immersion frying. II, model solution and verification. **Journal of Food Engineering**, v. 29, n. 2, p. 227–248, 1 ago. 1996.

FINNEY, E. E.; HALL, J. C. W. Elastic Properties of Potatoes. **Transactions of the ASAE**, v. 10, n. 1, p. 0004–0008, 1967.

FRIÁS, A.; CLEMENTE, G.; MULET, A. Potato Shrinkage During Hot Air Drying. **Food Science and Technology International**, v. 16, n. 4, p. 337–341, 2010.

GAO, X. et al. Numerical analysis and optimization of the microwave inductive heating performance of water film. **International Journal of Heat and Mass Transfer**, v. 139, p. 17–30, 1 ago. 2019.

GEEDIPALLI, S. S. R.; RAKESH, V.; DATTA, A. K. Modeling the heating uniformity contributed by a rotating turntable in microwave ovens. **Journal of Food Engineering**, v. 82, n. 3, p. 359–368, 1 out. 2007.

GIRI, S. K.; PRASAD, S. Modeling Shrinkage and Density Changes During Microwave-Vacuum Drying of Button Mushroom. **http://dx.doi.org/10.1080/10942910600596472**, v. 9, n. 3, p. 409–419, 1 set. 2007.

GULATI, T. et al. Microwave drying of spheres: Coupled electromagnetics-multiphase transport modeling with experimentation. Part II: Model validation and simulation results. **Food and Bioproducts Processing**, v. 96, p. 326–337, 2016.

GULATI, T.; DATTA, A. K. Enabling computer-aided food process engineering: Property estimation equations for transport phenomena-based models. **Journal of Food Engineering**Elsevier Ltd,1 maio 2013.

GULATI, T.; DATTA, A. K. Mechanistic understanding of case-hardening and texture development during drying of food materials. **Journal of Food Engineering**, v. 166, p. 119–138, 10 dez. 2015.

GULATI, T.; DATTA, A. K. Coupled multiphase transport, large deformation and phase transition during rice puffing. **Chemical Engineering Science**, v. 139, p. 75–98, 12 jan. 2016.

GULATI, T.; DATTA, A. K.; RANJBARAN, M. Selective heating and enhanced boiling in microwave heating of multicomponent (solid–liquid) foods. **Journal of Food Process Engineering**, v. 43, n. 2, 1 fev. 2020.

GULATI, T.; ZHU, H.; DATTA, A. K. Coupled electromagnetics, multiphase transport and large deformation model for microwave drying. **Chemical Engineering Science**, v. 156, p. 206–228, 15 dez. 2016.

HALDER, A.; DATTA, A. K. Surface heat and mass transfer coefficients for multiphase porous media transport models with rapid evaporation. **Food and Bioproducts Processing**, v. 90, n. 3, p. 475–490, 1 jul. 2012.

HALDER, A.; DHALL, A.; DATTA, A. K. An improved, easily implementable, porous media based model for deep-fat frying. Part I: Model development and input parameters. **Food and Bioproducts Processing**, v. 85, n. 3 C, p. 209–219, 1 set. 2007a.

HALDER, A.; DHALL, A.; DATTA, A. K. An improved, easily implementable, porous media based model for deep-fat frying. Part II: Results, validation and sensitivity analysis. **Food and Bioproducts Processing**, v. 85, n. 3 C, p. 220–230, 1 set. 2007b.

HALDER, A.; DHALL, A.; DATTA, A. K. Modeling transport in porous media with phase change: Applications to food processing. **Journal of Heat Transfer**, v. 133, n. 3, 2011.

HASSAN, B. H.; ALHAMDAN, A. M.; ELANSARI, A. M. Stress relaxation of dates at khalal and rutab stages of maturity. **Journal of Food Engineering**, v. 66, n. 4, p. 439–445, 1 fev. 2005.

HOLTZ, E. et al. Influence of dielectric and sorption properties on drying behaviour and energy efficiency during microwave convective drying of selected food and non-food inorganic materials. **Journal of Food Engineering**, v. 97, n. 2, p. 144–153, 1 mar. 2010.

HOSSAN, M. R.; BYUN, D.; DUTTA, P. Analysis of microwave heating for cylindrical shaped objects. **International Journal of Heat and Mass Transfer**, v. 53, n. 23–24, p. 5129–5138, 1 nov. 2010.

HOU, L.; ZHOU, X.; WANG, S. Numerical analysis of heat and mass transfer in kiwifruit slices during combined radio frequency and vacuum drying. **International Journal of Heat and Mass Transfer**, v. 154, p. 119704, 1 jun. 2020.

HU, Q. GUO et al. Drying of edamames by hot air and vacuum microwave combination. **Journal of Food Engineering**, v. 77, n. 4, p. 977–982, 1 dez. 2006a.

HU, Q. GUO et al. Drying of edamames by hot air and vacuum microwave combination. **Journal of Food Engineering**, v. 77, n. 4, p. 977–982, 1 dez. 2006b.

HUANG, L. LUE et al. Influence of combination drying methods on composition, texture, aroma and microstructure of apple slices. **LWT - Food Science and Technology**, v. 47, n. 1, p. 183–188, 1 jun. 2012.

ILIC, M.; TURNER, I. W. Convective drying of a consolidated slab of wet porous material. **International Journal of Heat and Mass Transfer**, v. 32, n. 12, p. 2351–2362, 1 dez. 1989.

INCROPERA, F. P. et al. **Fundamentos de transferência de calor e massa**. 7. ed. [s.l.] LTC, 2013.

ISHIBASHI, R. et al. In-situ measurements of drying and shrinkage characteristics during microwave vacuum drying of radish and potato. **Journal of Food Engineering**, v. 323, 1 jun. 2022.

JENI, K.; YAPA, M.; RATTANADECHO, P. Design and analysis of the commercialized drier processing using a combined unsymmetrical double-feed microwave and vacuum system (case study: tea leaves). **Chemical Engineering and Processing: Process Intensification**, v. 49, n. 4, p. 389–395, 1 abr. 2010.

JIANG, N. et al. Evaluation of freeze drying combined with microwave vacuum drying for functional okra snacks: Antioxidant properties, sensory quality, and energy consumption. **LWT - Food Science and Technology**, v. 82, p. 216–226, 1 set. 2017.

JOARDDER, M. U. H. et al. A micro-level investigation of the solid displacement method for porosity determination of dried food. **Journal of Food Engineering**, v. 166, p. 156–164, 10 jun. 2015.

KAENSUP, W.; CHUTIMA, S.; WONGWISES, S. Experimental study on drying of chilli in a combined microwave-vacuum-rotary drum dryer. **Drying Technology**, v. 20, n. 10, p. 2067–2079, 2002.

KATEKAWA, M. E.; SILVA, M. A. **A review of drying models including shrinkage effects**. **Drying Technology**, 2006.

KLAYBORWORN, S. et al. Effects of material properties on heating processes in two-layered porous media subjected to microwave energy. **International Journal of Heat and Mass Transfer**, v. 61, n. 1, p. 397–408, 1 jun. 2013.

KROKIDA, M. K.; MAROULIS, Z. B. Effect of drying method on shrinkage and porosity. **Drying Technology**, v. 15, n. 10, p. 2441–2458, 1997.

KROKIDA, M. K.; MAROULIS, Z. B. Effect of microwave drying on some quality properties of dehydrated products. **Drying Technology**, v. 17, n. 3, p. 449–466, 1999.

KUMAR, C. et al. Investigation of intermittent microwave convective drying (IMCD) of food materials by a coupled 3D electromagnetics and multiphase model. **Drying Technology**, v. 36, n. 6, p. 736–750, 26 abr. 2018.

LAI, W. M.; RUBIN, D.; KREMPL, E. **Introduction to Continuum Mechanics**. Butterworth-Heinemann, 1993.

LI, Z.; THOMAS, C. **Multiscale Biomechanics of Tomato Fruits: A Review**. **Critical Reviews in Food Science and Nutrition**Taylor and Francis Inc., , 18 maio 2016.

LI, Z. Y.; WANG, R. F.; KUDRA, T. Uniformity Issue in Microwave Drying. **Drying Technology**, v. 29, n. 6, p. 652–660, 29 abr. 2011.

LIN, X. et al. Effects of dielectric properties and microstructures on microwave-vacuum drying of mushroom (Agaricus bisporus) caps and stipes evaluated by non-destructive techniques. **Food Chemistry**, v. 367, p. 130698, 15 jan. 2022.

LIN, X.; SUN, D. W. Development of a general model for monitoring moisture distribution of four vegetables undergoing microwave-vacuum drying by hyperspectral imaging. **Drying Technology**, v. 40, n. 7, p. 1478–1492, 2021.

LIU, Y.; TANG, J.; MAO, Z. Analysis of bread dielectric properties using mixture equations. **Journal of Food Engineering**, v. 93, n. 1, p. 72–79, 1 jul. 2009.

LLAVE, Y. et al. Mathematical modeling of shrinkage deformation in eggplant undergoing simultaneous heat and mass transfer during convection-oven roasting. **Journal of Food Engineering**, v. 178, p. 124–136, 1 jun. 2016.

LU, T.; WANG, H. L.; JIANG, P. X. A Thermo-Hydro-Mechanics Bidirectional Coupling Mathematical Model for Drying of Biological Porous Medium. **Drying Technology**, v. 33, n. 4, p. 420–428, 12 mar. 2015.

MCCABE, W. L.; SMITH, J. C.; HARRIOTT, P. **Unit Operation of Chemical Engineering**. 5th. ed. [s.l.] McGraw-Hill, 1993.

MILLINGTON, R. J.; QUIRK, J. P. **Permeability of porous solids**. [s.l: s.n.]. . Acesso em: 19 maio. 2020.

MIRAN, W.; PALAZOĞLU, T. K. Development and experimental validation of a multiphysics model for 915 MHz microwave tempering of frozen food rotating on a turntable. **Biosystems Engineering**, v. 180, p. 191–203, 1 abr. 2019.

MONTEIRO, R. L. et al. How to make a microwave vacuum dryer with turntable. **Journal of Food Engineering**, v. 166, p. 276–284, 29 jun. 2015.

MONTEIRO, R. L. et al. Microwave vacuum drying and multi-flash drying of pumpkin slices. **Journal of Food Engineering**, v. 232, p. 1–10, 1 set. 2018a.

MONTEIRO, R. L. et al. Effect of multi-flash drying and microwave vacuum drying on the microstructure and texture of pumpkin slices. **LWT**, v. 96, p. 612–619, 1 out. 2018b.

MONTEIRO, R. L. et al. Evolution of the physicochemical properties of oil-free sweet potato chips during microwave vacuum drying. **Innovative Food Science & Emerging Technologies**, v. 63, p. 102317, 1 jul. 2020a.

MONTEIRO, R. L. et al. Microwave vacuum drying of foods with temperature control by power modulation. **Innovative Food Science and Emerging Technologies**, v. 65, p. 102473, 1 out. 2020b.

MONTEIRO, R. L. et al. Temperature control for high-quality oil-free sweet potato CHIPS produced by microwave rotary drying under vacuum. **LWT**, v. 157, p. 113047, 1 mar. 2022.

MUDGETT, R. E. et al. Dielectric Behavior of a Semi-Solid Food at Low, Intermediate and High Moisture Contents. **Journal of Microwave Power**, v. 15, n. 1, p. 27–36, jan. 1980.

NAHIMANA, H.; ZHANG, M. Shrinkage and color change during microwave vacuum drying of carrot. **Drying Technology**, v. 29, n. 7, p. 836–847, jan. 2011.

NELSON, S. O. Dielectric properties of agricultural products-measurements and applications. **IEEE Transactions on Electrical Insulation**, v. 26, n. 5, p. 845–869, 1991.

NELSON, S. O.; DATTA, A. K. Dielectric Properties of Food Materials and Electric Field Interactions. Em: **Handbook of Microwave Technology for Food Application**. [s.l.] CRC Press, 2001. p. 69–114.

NI, H. **Multiphase moisture transport in porous media under intensive microwave heating**. Cornell University, 1997.

NI, H.; DATTA, A. K. Heat and moisture transfer in baking of potato slabs. **Drying Technology**, v. 17, n. 10, p. 2069–2092, 1999.

NI, H.; DATTA, A. K.; TORRANCE, K. E. Moisture transport in intensive microwave heating of biomaterials: A multiphase porous media model. **International Journal of Heat and Mass Transfer**, v. 42, n. 8, p. 1501–1512, 1 abr. 1999.

NOWACKA, M. et al. The application of unconventional technologies as pulsed electric field, ultrasound and microwave-vacuum drying in the production of dried cranberry snacks. **Ultrasonics Sonochemistry**, v. 56, p. 1–13, 1 set. 2019.

NOWAK, K. W.; MARKOWSKI, M.; DASZKIEWICZ, T. Ultrasonic determination of mechanical properties of meat products. **Journal of Food Engineering**, v. 147, n. C, p. 49–55, 1 fev. 2015.

OROSZVÁRI, B. K. et al. Permeability and mass transfer as a function of the cooking temperature during the frying of beefburgers. **Journal of Food Engineering**, v. 74, n. 1, p. 1–12, 1 maio 2006.

ORSAT, V. et al. Microwave-assisted drying of biomaterials. **Food and Bioproducts Processing**, v. 85, n. 3 C, p. 255–263, 1 set. 2007.

PANYAWONG, S.; DEVAHASTIN, S. Determination of deformation of a food product undergoing different drying methods and conditions via evolution of a shape factor. **Journal of Food Engineering**, v. 78, n. 1, p. 151–161, 1 jan. 2007.

PAWLAK, T. et al. Application of Machine Learning Using Color and Texture Analysis to Recognize Microwave Vacuum Puffed Pork Snacks. **Applied Sciences**, v. 12, n. 10, 2022.

PERRY, R. H.; GREEN, D. W.; MALONEY, J. O. **Perry's chemical engineers' handbook.** [s.l.] McGraw-Hill, 1997.

PITCHAI, K. et al. Coupled electromagnetic and heat transfer model for microwave heating in domestic ovens. **Journal of Food Engineering**, v. 112, n. 1–2, p. 100–111, 1 set. 2012.

QIAO, M. et al. Effect of moisture, protein, starch, soluble sugar contents and microstructure on mechanical properties of maize kernels. **Food Chemistry**, v. 379, p. 132147, 15 jun. 2022.

RAKESH, V. et al. Microwave combination heating: Coupled electromagnetics - multiphase porous media modeling and MRI experimentation. **AIChE Journal**, v. 58, n. 4, p. 1262–1278, abr. 2012.

RAKESH, V.; DATTA, A. K. Microwave puffing: Determination of optimal conditions using a coupled multiphase porous media - Large deformation model. **Journal of Food Engineering**, v. 107, n. 2, p. 152–163, dez. 2011.

RAKESH, V.; DATTA, A. K. Transport in deformable hygroscopic porous media during microwave puffing. **AIChE Journal**, v. 59, n. 1, p. 33–45, jan. 2013.

RANJBARAN, M.; DATTA, A. K. Pressure-driven infiltration of water and bacteria into plant leaves during vacuum cooling: A mechanistic model. **Journal of Food Engineering**, v. 246, p. 209–223, 1 abr. 2019.

REN, Y.; LEI, T.; SUN, D.-W. In-situ indirect measurements of real-time moisture contents during microwave vacuum drying of beef and carrot slices using terahertz time-domain spectroscopy. **Food Chemistry**, v. 418, p. 135943, 30 ago. 2023.

RENSHAW, R. C. et al. The relationship of dielectric response and water activity in food. **Journal of Food Engineering**, v. 244, p. 80–90, 1 mar. 2019.

RESSING, H.; RESSING, M.; DURANCE, T. Modeling the mechanisms of dough puffing during vacuum microwave drying using the finite element method. **Journal of Food Engineering**, v. 82, n. 4, p. 498–508, out. 2007.

ROOS, Y. H. Mechanical Properties. **Phase Transitions in Foods**, p. 247–270, 1995.
RUSSO, P.; ADILETTA, G.; DI MATTEO, M. The influence of drying air temperature on the physical properties of dried and rehydrated eggplant. **Food and Bioproducts Processing**, v. 91, n. 3, p. 249–256, 1 jul. 2013.

SADIKU, M. N. O. **Elements of electromagnetics**. 7. ed. [s.l.] OXford University Press, 2018.

SAKAI, N.; YANG, H.; WATANABE, M. Theoretical Analysis of the Shrinkage Deformation in Viscoelastic Food during Drying. **Japan Journal of Food Engineering**, p. 105–112, 2002.

SALVADOR, A. A. et al. View of Multiphysics Modeling to Assist Microwave Cavity Design for Food Processing. **International Journal of Electrical and Computer Engineering Research**, v. 2, n. 2, p. 1–10, 2022.

SETIADY, D. et al. Rehydration and sensory properties of dehydrated russet potatoes (Solanum tuberosum) using microwave vacuum, heated air, or freeze dehydration. **Drying Technology**, v. 27, n. 10, p. 1116–1122, out. 2009.

SILVA, E. et al. Influence of swelling of vegetable particles on structure and rheology of starch matrices. **Journal of Food Engineering**, v. 112, n. 3, p. 168–174, 1 out. 2012.
SMITH, J. M.; NESS, H. C. VAN; ABBOTT, M. M. **Introduction to thermodynamics of chemical engineering**, 2007.

SONG, C. et al. Analysis of the heat transfer characteristics of blackberries during microwave vacuum heating. **Journal of Food Engineering**, v. 223, p. 70–78, 1 abr. 2018.

SOUZA, P. G. DE. Aplicação de micro-ondas a vácuo no desenvolvimento de snacks de queijo muçarela. 2021.

SUNJKA, P. S. et al. Microwave-convective and microwave-vacuum drying of cranberries: A comparative study. **Drying Technology**, v. 22, n. 5, p. 1217–1231, maio 2004.

SUTAR, P. P.; PRASAD, S. Modeling microwave vacuum drying kinetics and moisture diffusivity of carrot slices. **Drying Technology**, v. 25, n. 10, p. 1695–1702, out. 2007.

SUVARNAKUTA, P.; DEVAHASTIN, S.; MUJUMDAR, A. S. A mathematical model for low-pressure superheated steam drying of a biomaterial. **Chemical Engineering and Processing: Process Intensification**, v. 46, n. 7, p. 675–683, 1 jul. 2007.

TANG, J.; LIANG, L. Moisture distribution in spherical foods in microwave drying. **Drying Technology**, v. 16, n. 3–5, p. 503–524, 1998.

TANIKAWA, W.; SHIMAMOTO, T. Comparison of Klinkenberg-corrected gas permeability and water permeability in sedimentary rocks. **International Journal of Rock Mechanics and Mining Sciences**, v. 46, n. 2, p. 229–238, 1 fev. 2009.

TELEKEN, J. T. et al. Mechanistic understanding of microwave-vacuum drying of non-deformable porous media. **Drying Technology**, p. 1–18, 19 fev. 2020.

TOPCAM, H.; ERDOGDU, F. Designing system cavity geometry and optimizing process variables for continuous flow microwave processing. **Food and Bioproducts Processing**, v. 127, p. 295–308, 1 maio 2021.

TOUJANI, M. et al. Hydro-thermo-viscoelastic Based Finite Element Modeling of Apple Convective Drying Process G Shear modulus (MPa) h Heat transfer coefficient (W/m 2 /K) K Bulk modulus (MPa) k Mass transfer coefficient (Kg/m. **Tunisia. CMES**, v. 98, n. 5, p. 469–485, 2014.

TSURUTA, T.; TANIGAWA, H.; SASHI, H. Study on shrinkage deformation of food in microwave–vacuum drying. **Drying Technology**, v. 33, n. 15–16, p. 1830–1836, 1 maio 2015.

TULASIDAS, T. N.; RATTI, C.; RAGHA VAN, G. S. V. Modelling of microwave drying of grapes. **Canadian Agricultural Engineering**, p. 57–67, 1997.

VERBOVEN, P. et al. Computation of airflow effects on heat and mass transfer in a microwave oven. **Journal of Food Engineering**, v. 59, n. 2–3, p. 181–190, 1 set. 2003.

WANG, N.; BRENNAN, J. G. Moisture sorption isotherm characteristics of potatoes at four temperatures. **Journal of Food Engineering**, v. 14, n. 4, p. 269–287, 1 jan. 1991.

WANG, N.; BRENNAN, J. G. Changes in structure, density and porosity of potato during dehydration. **Journal of Food Engineering**, v. 24, n. 1, p. 61–76, 1 jan. 1995.

WARNING, A. et al. Porous media based model for deep-fat vacuum frying potato chips. **Journal of Food Engineering**, v. 110, n. 3, p. 428–440, 1 jun. 2012.

WARNING, A. D.; ARQUIZA, J. M. R.; DATTA, A. K. A multiphase porous medium transport model with distributed sublimation front to simulate vacuum freeze drying. **Food and Bioproducts Processing**, v. 94, p. 637–648, 1 abr. 2015.

WHITAKER, S. A Theory of Drying. **Advances in Heat Transfer**, v. 13, p. 119–203, 1977.

WRAY, D.; RAMASWAMY, H. S. Development of a Microwave–Vacuum-Based Dehydration Technique for Fresh and Microwave–Osmotic (MWODS) Pretreated Whole Cranberries (Vaccinium macrocarpon). **Drying Technology**, v. 33, n. 7, p. 796–807, 19 maio 2015.

YANG, H.; SAKAI, N. Shrinkage and Mechanical Characteristics of potato Undergoing Air Convection Drying. **Japan Journal of Food Engineering**, v. 2, n. 2, p. 1441–1460, 31 jul. 2001.

YANYANG, X. et al. Studies on hot air and microwave vacuum drying of wild cabbage. **Drying Technology**, v. 22, n. 9, p. 2201–2209, 2004.

YUAN, Y. et al. Numerical and experimental study on drying shrinkage-deformation of apple slices during process of heat-mass transfer. **International Journal of Thermal Sciences**, v. 136, p. 539–548, 1 fev. 2019.

ZANG, Z. et al. Improving Drying Characteristics and Physicochemical Quality of Angelica sinensis by Novel Tray Rotation Microwave Vacuum Drying. **Foods 2023, Vol. 12, Page 1202**, v. 12, n. 6, p. 1202, 12 mar. 2023.

ZHANG, H.; DATTA, A. K. Microwave power absorption in single- and multiple-item foods. **Food and Bioproducts Processing: Transactions of the Institution of of Chemical Engineers, Part C**, v. 81, n. 3, p. 257–265, 1 set. 2003.

ZHOU, J.; WANG, Y.; YANG, X.-Q. Shape Optimization of Microwave Cavity Using Arbitrary Lagrangian-Euler Method to Improve the Heating Uniformity. **IEEE transactions on microwave theory and techniques**, v. 70, n. 3, 2022.

ZHOU, Y. et al. Drying kinetics and heat mass transfer characteristics of thin layer pineapple during microwave vacuum drying. **Journal of Computational Methods in Sciences and Engineering**, v. 23, n. 3, p. 1165–1178, 1 jan. 2023.

ZHOU, Y.-H. et al. Microwave-vacuum-assisted drying of pretreated cranberries: Drying kinetics, bioactive compounds and antioxidant activity. **LWT**, v. 146, p. 111464, 1 jul. 2021.

ZHU, H. et al. Microwave drying of spheres: Coupled electromagnetics-multiphase transport modeling with experimentation. Part I: Model development and experimental methodology. **Food and Bioproducts Processing**, v. 96, p. 314–325, 1 out. 2015.

ZIELINSKA, M.; MARKOWSKI, M.; ZIELINSKA, D. The effect of freezing on the hot air and microwave vacuum drying kinetics and texture of whole cranberries. **Drying Technology**, v. 37, n. 13, p. 1714–1730, 3 out. 2019.

APPENDICES

A-1 HEAT SOURCE STUDY

There are different forms to calculate the heat provided, and all are in the heat source term of heat transfer in fluids physics. The **Figure A-1.1** below presents the results for simulation with 3 types of heat source.

The first equation provides a constant value as heat source. In this case, the heat source was estimated by manual calculations in Excel considering each term of energy conservation equation and by the study of Real power in the microwave cavity during experiments. When the magnetron was kept in 100% power, without cyclins of turning ON/OFF the power was 767 ± 26 W, and when in 50% power with duty cycle the result was 337 ± 4 W.

In the second (Q_{mw}) and the third heat equation ($Poynting$), the amount of heat is decreasing with time, because the amount of water in the sample is also decreasing. In the third form is possible to provide the frequency used in the microwave and the dielectric loss of the sample.

$$Q_{mw}\left[\frac{W}{m^3}\right] = 5.92 \times 10^5 \left(\frac{M_0}{M}\right)^{-1.17} \qquad Poynting\left[\frac{W}{m^3}\right] = \frac{1}{2}\omega\varepsilon_0\varepsilon''\boldsymbol{E}^2$$

Figure A-1.1: Moisture loss over time according to different power source determination.

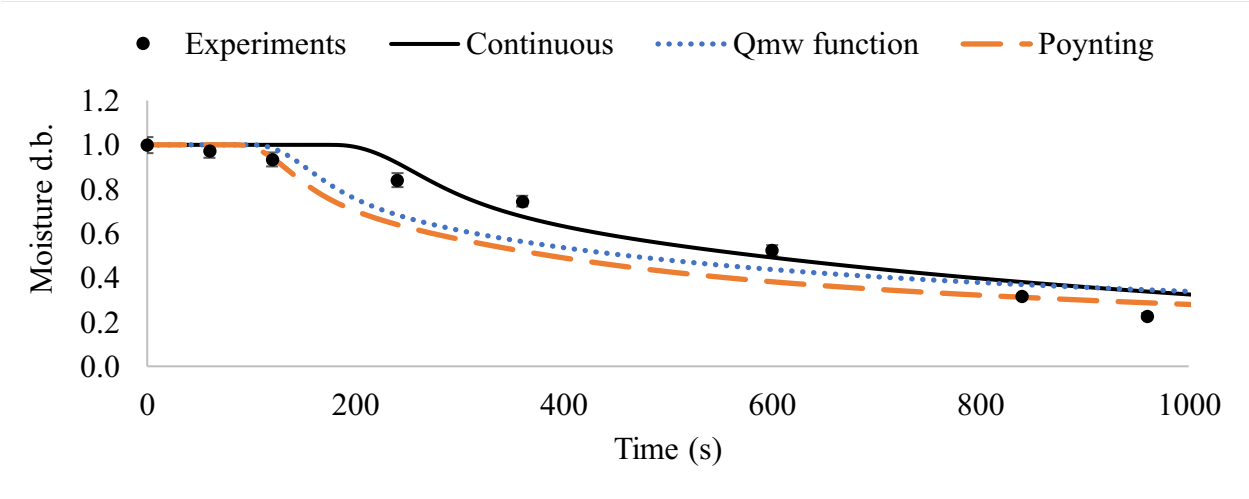

A-2: SIMULATION FULLY COUPLED

The preliminary results of the simulation incorporating fully coupled physics, including electromagnetism, vapor generation and transport, water transport, and heat transfer, are presented as follows. **Figure A-2.1** shows the variation of moisture of the sample over time, compared to experimental data. In **Figure A-2.2**, the temperature of top surface and the average power absorbed for the sample are displayed. Finally, **Figure A-2.3** presents a representation of the temperature distribution in the sample at two different time points, 360s and 600s.

Figure A-2.1: Variation of moisture over time, compared to experimental data

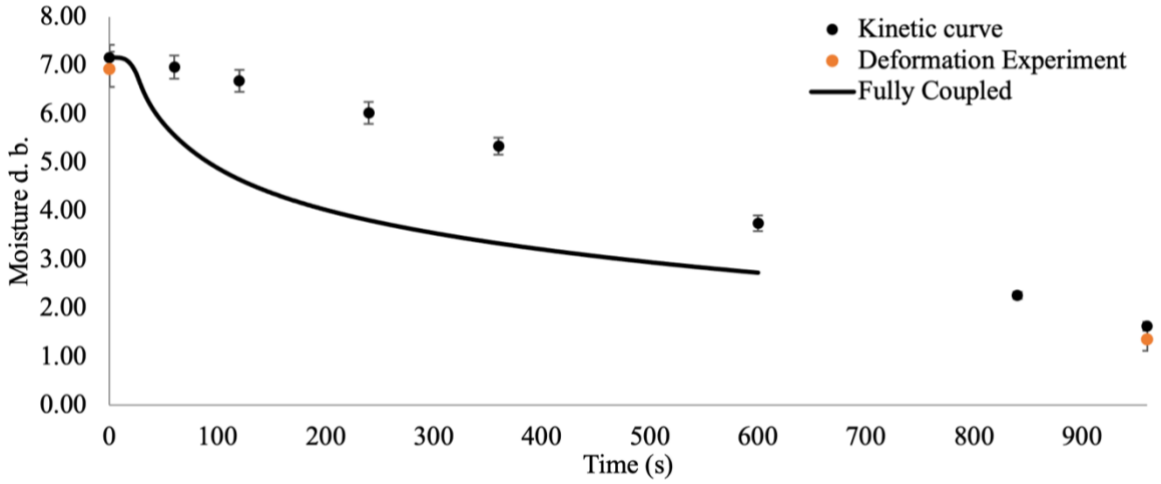

Figure A-2.2: The temperature of top surface (left) and the average power absorbed by the sample (right) over time, compared with the Two-stage solution.

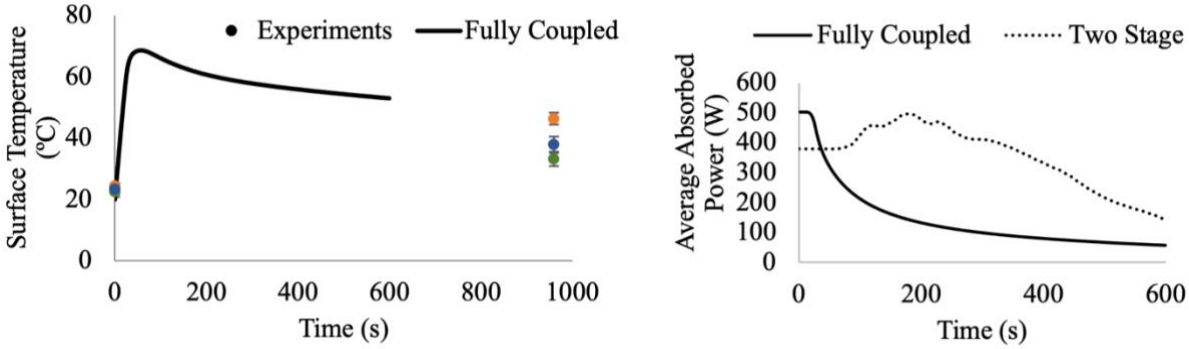

Figure A-2.3: Representation of the surface temperature distribution in the sample at 360s and 600s.

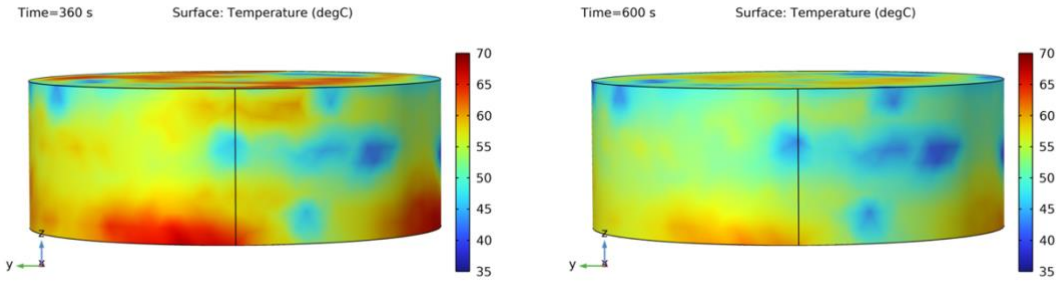

In **Figure A-2.1**, it is evident that the rate of moisture decreases in the fully coupled model is comparatively slower than that observed in the two-stage model. This divergence can be attributed to the discrepancy in power absorption by the sample between the two approaches.

Figure A-2.2 presents a contrast in the power absorbed by the sample between the two-stage solution strategy and the fully coupled model. Throughout the drying process, the power absorbed in the two-stage model consistently surpasses that of the fully coupled model, particularly during the initial stages. Consequently, this dissimilarity in power absorption contributes to a reduction in the surface temperature of the sample, as clearly illustrated in the first graph of **Figure A-2.2** and the visual representations in **Figure A-2.3**.

A-3: STRESS STUDY

A study was conducted to investigate the fracture stress and pressure in potatoes during the microwave drying process to determine typical values of these variables. The results of this study are presented in **Figure A-3.1**, which provides insights into the magnitude of stress and pressure within the potato sample.

Figure A-3.1: Magnitude of fracture stress and pressure within the potato sample.

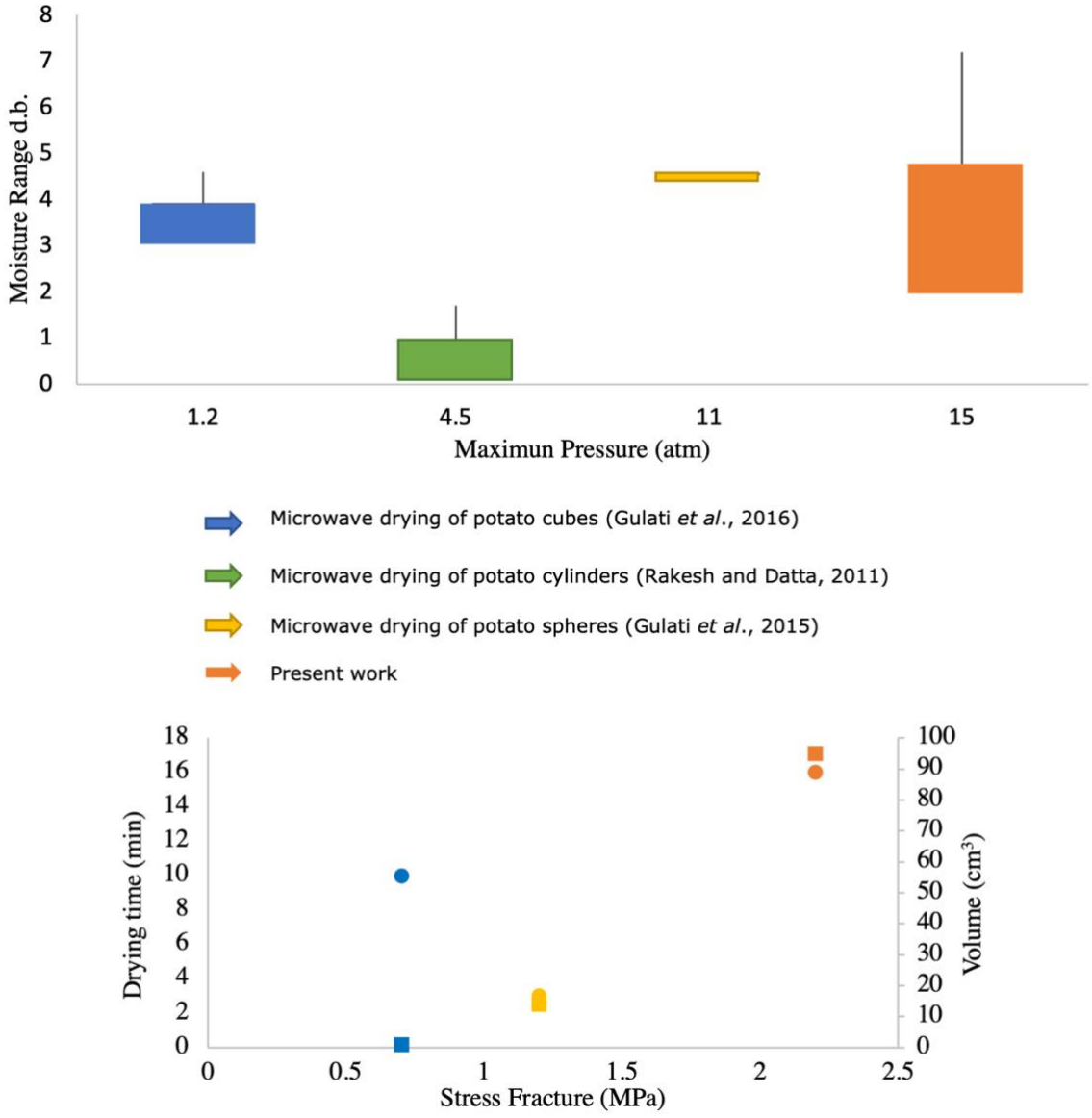

Furthermore, an analysis was performed to examine the stress balance that would occur in a potato with the same dimensions as those used in this study if it underwent linear deformation. The findings of this analysis are illustrated in **Figure A-3.2**, which demonstrates the stress over strain in the sample at z direction.

Figure A-3.2: Stress over strain in the sample in z direction

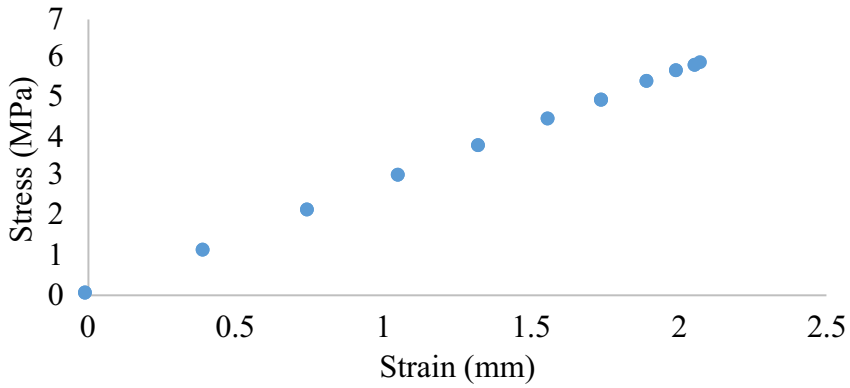

It is important to note that these results are specific to the sample dimensions used in this study and may vary for different potato sizes or drying conditions. Nevertheless, they contribute to the overall understanding of the mechanical response of potatoes to microwave drying and serve as a foundation for further investigations.